

NMP4 RESTRICTS BONE MARROW OSTEOPROGENITORS AND
PARATHYROID HORMONE INDUCED BONE FORMATION IN HEALTHY AND
ESTROGEN DEPLETED FEMALE MICE

Paul Jeffrey Childress

Submitted to the faculty of the University Graduate School
in partial fulfillment of the requirements
for the degree
Doctor of Philosophy
in the Department of Anatomy and Cell Biology
December 2014

Accepted by the Graduate Faculty, Indiana University, in partial fulfillment of the requirements for the degree of Doctor of Philosophy.

Joseph P. Bidwell, PhD. Chair

Doctoral Committee

Frederick Pavalko, PhD.

Teresita Bellido, PhD.

Alexander Robling, PhD.

Melissa Kacena, PhD.

September 25, 2014

Dedication

This thesis is dedicated to many special people in my life – first and foremost my boys, Mason and Joshua. I would like to thank them for sacrificing with me as I pursued this PhD. Of the many lessons to be drawn from academic work, I hope they appreciate the value of chasing a dream most of all. My family and friends have been patient and understanding through the long nights and missed holidays; this thesis is dedicated to thanking them. Finally, I would like to dedicate this work to my mother. Everything good that I am I owe, in whole or in part, to her. Thank you for the love, support, laughter and friendship that have sustained me.

Acknowledgements

The work presented in this thesis represents years of collective efforts by many. In particular Dr. Joseph Bidwell has been tirelessly supportive and encouraging. As a mentor he has always known the value of teaching me, challenging me, and congratulating me every step along the way. As a scientist, I have learned from him that the work of being a scientist does not have to diminish the joy of doing science. And, most importantly, the questions we ask, determine the directions we take – choose wisely. The work presented here would not have been possible without the help of Dr. Marta Alvarez. She is at once a teacher, colleague and friend; and I cannot thank her enough. I would also like to thank my committee, Drs. Pavalko, Kacena, Bellido, and Robling, for their support and friendship over the years. Their advice and input was critical to the success of this project, and my development as a researcher. I appreciate the entire Anatomy and Cell Biology department for their help along the way. Lastly, I would like to send a special thanks to the Indiana Clinical and Translational Science Institute and Dr. Kathryn Jones and Dr. Bruce Mitlak for funding and advice to support this work and my growth as a scientist.

Paul Jeffrey Childress

NMP4 RESTRICTS BONE MARROW OSTEOPROGENITORS AND PARATHYROID
HORMONE INDUCED BONE FORMATION IN HEALTHY AND ESTROGEN
DEPLETED FEMALE MICE

We have shown that nuclear matrix protein 4 (Nmp4) attenuates the response to intermittent parathyroid hormone (PTH) in healthy and ovariectomized (OVX) female mice using a global knockout of the Nmp4 gene. Additionally, these mice have increased bone marrow osteoprogenitors and CD8⁺ T-cells which support osteoblast differentiation. The animals were not protected from bone loss following OVX, but retained the hypersensitivity seen in the intact mice. Mesenchymal stem/progenitor cells (osteoprogenitors) demonstrated increased growth rate in culture and showed more robust differentiation into mineralizing bone cells. Chromosome precipitation followed by next generation sequencing and bioinformatics analysis characterized Nmp4 as a negative regulator of synthetic processes and suggested the IGF1/Akt and BMP2/Smad biochemical pathways which are likely targets for Nmp4 regulation. We have experimentally verified these pathways in immortalized bone marrow mesenchymal cells from wild type and *Nmp4*-KO mice.

Joseph P. Bidwell, PhD., Chair

Table of Contents

Chapter 1	1
Chapter 2	14
Abstract.....	15
Introduction.....	16
Materials and Methods	16
Results	21
Discussion.....	26
Chapter 3	45
Abstract.....	46
Introduction.....	47
Materials and Methods	49
Results	51
Discussion.....	53
Chapter 4	64
Abstract.....	65
Introduction.....	66
Materials and Methods	69
Results	74
Discussion.....	79
Chapter 5	100
Appendix	106
References	127
Curriculum Vitae	

CHAPTER 1

INTRODUCTION

Osteoporosis disease burden and treatment approaches

Osteoporosis (OP) is a chronic skeletal disorder characterized by loss of bone mineral density (BMD) and increased risk of fracture. Although OP is a multifactorial disease, major risk factors include ethnicity, sex steroid deficiency, age and chronic steroid use. Likely, these factors work in combination with the end result being declining bone mass and weaker bone strength (Bidwell, Alvarez et al. 2013). Diagnosis of OP has traditionally relied on BMD measurements and/or presence of a non-traumatic (fragility) fracture with 10 million Americans currently diagnosed as osteoporotic and another 40 million at risk. These numbers will not likely decline as the US population ages, which it is expected to do until 2050. The economic burden imposed by OP, most accounted for by fractures, is approximately \$20 billion annually (Burge, Dawson-Hughes et al. 2007). Despite this prevalence, treatment modalities are limited and largely focus on decreasing bone resorption. Bisphosphonates and newer generation anti-resorptives such as anti-RANKL antibodies have led to improved risk for fractures, but are not effective at stimulating bone formation (Boonen, Ferrari et al. 2012). Currently only intermittent parathyroid hormone, or teriparatide (PTH 1-34), is FDA approved as an anabolic therapy for OP. Intermittent treatment with PTH results in a rapid increase in bone formation in the osteoporotic skeleton followed by a delayed increase in bone resorption. The molecular actions of PTH are not fully known, but hormone treatment is known to increase bone turnover with a positive bone balance. Unfortunately, effectiveness is time restricted and the drug carries a black box warning limiting use to 2 years due to a slight increase in cancer reported in animal studies (Tella and Gallagher 2014). This thesis will explore the role that Nmp4 plays in restricting the anabolic actions of intermittent PTH in mice including some of the cellular and molecular actions that are involved.

Nmp4 characteristics

Nuclear matrix protein 4 (Cas interacting zinc finger protein - CIZ, Zfp384) was independently cloned as a PTH-responsive architectural transcription factor in the nuclear matrix and a cytosolic protein that was shown to bind p130Cas by far western analysis. Interspecies heterokaryon formation assays showed Nmp4 to be a nucleocytoplasmic shuttling protein. Nmp4 binds to the minor groove of AT-rich DNA and bends DNA, as is characteristic of architectural transcription factors (Nakamoto, Yamagata et al. 2000, Thunyakitpisal, Alvarez et al. 2001). Sub-cellular localization studies show the protein to largely localize in the nucleus, however a punctate distribution was also observed in the cytoplasm (Feister, Torrungruang et al. 2000). This punctate distribution is consistent with binding to p130Cas, an adaptor protein which localizes near focal adhesions (Cary, Han et al. 1998). The protein is highly conserved at the nucleotide and amino acid level from yeast to humans with mouse and humans sharing about 92% amino acid identity. There are known isoforms of Nmp4 which are the result of alternately spliced variants from a full length transcript in mouse, rats, and humans. Surprisingly, despite the high sequence homology Nmp4 appears to be dispensable in mouse gestation, growth, and longevity. Its absence is not associated with reported pathological changes except for a spermatogenic abnormality which leads to sporadic infertility (Nakamoto, Shiratsuchi et al. 2004). At the genetic level Nmp4 is controlled by two independent promoters and EMSA and ChIP-seq analysis suggests that it binds its own promoter and contributes to its own expression regulation (Alvarez, Shah et al. 2005).

Knockout Phenotype

Two labs have independently generated mice with a global genetic deletion of Nmp4/CIZ. Studies using this mice have revealed that despite the protein's strong conservation across species and phyla the protein is dispensable for development and growth. In 2005 work from the Noda lab in Japan revealed that *Nmp4* (*CIZ*) deletion resulted in a defect in spermatogenic development which left male mice sporadically infertile. In addition the mice were noted to have a slightly higher mineral apposition rate (MAR) and bone formation rate with normal osteoclast activity resulting in a modestly enhanced skeleton (Morinobu, Nakamoto et al. 2005). These comparisons were made between F2 generation KO and WT mice. In our lab comparisons made in mice backcrossed 6 or 7 generations with C57/B6 mice differed slightly. We have observed

increases in cancellous bone, but these increases are modest and not consistently found (Robling, Childress et al. 2009, Childress, Philip et al. 2011, He, Childress et al. 2013). Additionally clonogenic assays, histomorphometry, serum analysis, and in vitro studies suggest a mild increase in osteoclast numbers and activity in healthy mice. Osteoclast enriched cultures stimulated with receptor activator of nuclear factor κ B ligand (RANKL) and macrophage colony stimulating factor (M-CSF) yielded more multinucleated osteoclasts in *Nmp4*-KO mice compared to WT. Also, pit formation assay showed these osteoclasts to be more effective at resorption on dentin slices (Childress, Philip et al. 2011). Histomorphometric analysis of WT and KO mice treated with PTH or vehicle control revealed an increase in tartrate-resistant acid phosphatase (TRAP) positive osteoclasts and TRAP stained surface in vehicle treated knockout animals which was statistically significant by 2-way ANOVA and Tukey's HSD post-hoc test (Childress, Philip et al. 2011). Finally, these *Nmp4*-KO mice had higher serum levels of c-terminal telopeptide (CTX), a marker for bone resorption, in both vehicle treated and PTH treated groups. This comparison of serum CTX was made in *Nmp4*-KO mice backcrossed 6 generations with C57/B6 mice and wildtype C57/B6 mice from Jackson Laboratories so there remains a formal possibility that the differences noted were due to genetic background differences despite the extensive backcrossing (Robling, Childress et al. 2009). Nonetheless, taken together the evidence points to a modest, but significant increase in bone resorption in *Nmp4*-KO mice compared to wildtype (Bidwell, Childress et al. 2012). Because the mice are not osteopenic, and the KO mice have been reported to have a modestly enhanced skeleton the evidence suggests a skeletal phenotype where *Nmp4*-KO mice have increased bone formation and bone resorption which result in a net (albeit small) increase in bone mass. This likely results from increases in both the osteoblast and osteoclast progenitor populations. However, it is not clear if the same cellular mechanism is responsible for the increases in each population.

Mice with a global deletion of *Nmp4*/*CIZ* are hyper-responsive to multiple anabolic bone signals. In 2005 it was reported that mice these mice respond to local delivery of BMP2 with about a 2 fold increase in calvarial bone growth over WT controls as seen on soft x-ray (Morinobu, Nakamoto et al. 2005). Our previous work has characterized the increased anabolic response healthy *Nmp4*-KO mice have compared to healthy WT animals. After 2 weeks of intermittent PTH (30ug/kg/day), KO and WT mice had a similar increase in distal femur trabecular bone accrual. However, by 3 weeks of treatment, the KO mice accrual had begun to pace the WT significantly (Childress, Philip et al. 2011).

The enhanced bone growth was even more exaggerated after 7 weeks of treatment when the KO mice gained over 2 fold more bone in the trabecular compartment (Robling, Childress et al. 2009). Consistent with this, *Nmp4*-KO mice had a larger percent increase in serum osteocalcin (OCN, marker for bone formation) after 3 weeks of PTH than WT mice. By 7 weeks of treatment, the disparity in serum OCN was again more exaggerated; the percent change of osteocalcin in WT mice had plateaued, but the KO mice showed a marked increase in concentration of this serum marker for bone formation. Interestingly, bone histomorphometry after 7 weeks of hormone did not reveal any differences in mineral apposition rate (MAR) or bone formation rate (BFR). The amount of mineralizing surface was much greater in the *Nmp4*-KO animals, but the proportion to bone surface was not different (Childress, Philip et al. 2011).

We also examined the marrow of these mice by FACS and clonogenic assay which revealed changes in the *Nmp4*-KO mice which were independent of PTH treatment. The number of CD45⁻/CD146⁺/Nestin⁺ osteoprogenitors was approximately 4 fold higher in the KO mice. Though some controversy exists regarding how to define an osteoprogenitor in the field, the cell surface markers CD146 and the intermediate filament nestin are generally accepted to define a large percentage of the osteogenic activity in the mouse (Sacchetti, Funari et al. 2007, Méndez-Ferrer, Michurina et al. 2010, Park, Spencer et al. 2012). Interestingly, this difference may arise from expansion of specific subset of mesenchymal stem/progenitor cells because a different set of osteoprogenitor markers (Lin⁻ CD45⁻ CD105⁺ CD29⁺) did not show any differences with control animals (unpublished data). These FACS analyses agree with results of our CFU-F^{alk phos} clonogenic assay, as well as CFU-Ob assays in the *Ciz*-KO mice (Hino, Nakamoto et al. 2007). Additionally, *Nmp4*-KO mice have a statistically significantly higher ratio of CFU-F^{alk phos} to total CFU-F colonies suggestive of a greater commitment to the osteoblast lineage, but will require further work to confirm (He, Childress et al. 2013).

The osteoclast lineage cells also showed an increase in the bone marrow of *Nmp4*-KO mice. This increase was to a lesser magnitude than what has been shown in the osteoblast progenitor population, however. The number of CFU-GM cells was shown to be ~2 fold higher in *Nmp4*-KO marrow compared to WT marrow. CFU-GM have previously been reported to be a rich source of osteoclast progenitors (Menea, Kurihara et al. 2000). Consistent with these results the marrow from KO animals yielded more multinucleated osteoclasts in vitro after stimulation with MCSF and RANKL, a standard osteoclastogenic protocol. Moreover, osteoclasts generated from the *Nmp4*-KO marrow have an increased

capacity for resorption on dentin slices. Consistent with these *ex vivo* and *in vitro* results, serum from KO mice treated with PTH or vehicle for 7 weeks had a higher CTX concentration at the beginning of the experiment (age 10 weeks), after 3 week of treatment and after 7 weeks. The increase was seen in both vehicle and PTH treated groups. It should be mentioned however, that this comparison was made between WT C57/B6 mice obtained from Jackson labs and Nmp4-KO mice which had been backcrossed for 6 generations on a C57/B6 background.

Spermatogenesis provides another example of Nmp4 (aka CIZ) having a role in developing progenitors. This case, unlike that of osteoblastogenesis and osteoclastogenesis however, is one in which the end result is a reduction in the number of differentiated progeny. Nakamoto and co-workers examined the testis and found degenerated tissue and increased apoptosis in dividing secondary spermatocytes in tissue from the KO mice. Both of these phenomenon showed heterogeneity in the KO population which corresponds to a phenotype of sporadic infertility in these mice. Although the mechanisms involved were not fully described, SMAD1 signaling was suggested a playing a role (Nakamoto, Shiratsuchi et al. 2004). What is clear from these studies is that null mice are largely phenotypically normal, but do have differences which manifests during differentiation from progenitor populations in the adult animal. Thus far there have been no reports of other defects in development.

In addition to the enhanced response to various anabolic agonists, null mice also are resistant to bone loss associated with disuse from hind limb unloading. The molecular mechanisms of bone loss in this model are not known, however increased osteocyte apoptosis which proceeds osteoclast recruitment is believed to be important and may direct resorption at the endosteal surface in rats (Aguirre, Plotkin et al. 2006). Male mice without a functional copy of Nmp4 are protected from bone loss in this model by a mechanisms which does not involve reduced bone resorption. However, these mice are also resistant to the loss of osteoprogenitors associated with HLU as measured by the number of mineralized nodules obtained from bone marrow cultures. Given the role that mechanical stimulation plays in maintaining osteoprogenitors and osteocytes through reduced apoptosis (Aguirre, Plotkin et al. 2006) and the involvement of Nmp4 deficiency in the apoptotic response in secondary spermatozoa, it is tempting to speculate that osteocytes in the null mice are protected from apoptosis. Further work is needed to clarify the cellular and molecular pathways involved.

Parathyroid hormone - anabolic, but why?

Endogenous PTH is synthesized as a 115 amino acid pre-pro-hormone which is cleaved to an active 84 amino acid peptide and maintains serum calcium levels through 3 main mechanisms. The first is increased calcium reuptake in the renal tubular system (Murray, Rao et al. 2005). Also in the renal tubular system the hormone stimulates production of 1,25-dihydroxyvitamin D₃, which increases calcium uptake in the small intestine and distal convoluted tubule of the kidney (Christakos 2012). PTH also works to increase bone resorption by stimulating osteoclastogenesis through osteoblastic release of receptor activator of NF-κB ligand (RANKL). In this manner PTH stimulates calcium release, and ultimately bone loss. The paradoxical effect PTH (Yasuda, Shima et al. 1998, Udagawa, Takahashi et al. 1999) as an anabolic agent to treat osteoporosis remains incompletely understood.

The anabolic actions of intermittent parathyroid hormone are well-documented and it remains the only FDA- approved treatment for osteoporosis which adds bone to the aged skeleton. The cellular, molecular, and tissue level mechanisms are not completely understood, but do include direct effects on osteoblasts, indirect effects on osteoclasts, and encompass several molecular pathways highlighting the pleiotropic nature of this hormone. The PTH receptor, PTHR1, is a 7-transmembrane receptor which stimulates both the PKA/cAMP and PKC/phospholipase C pathways, among others (Hruska, Moskowitz et al. 1987, Juppner, Abou-Samra et al. 1991). Receptor internalization limits the response to hormone, and as will be described, may also contribute to sensitizing the BMP2 response (Goltzman 2008).

Perhaps the most fundamental aspect of anabolic PTH is its mode of delivery. Continuously elevated and intermittently elevated levels of PTH have distinct and paradoxical effects on bone mass. Chronic elevation such as is seen with hyperparathyroidism is typified by hyperkalemia and loss bone mass. This phenotype is consistent with the primary action of endogenous PTH which is to increase serum calcium concentration, in part by mobilizing osteoclasts to differentiate and increase bone resorption thereby releasing Ca²⁺ stores in the skeleton. Seminal work by Walter Bauer, Joseph Aub, and Fuller Albright in 1929 demonstrated that parathyroid hormone could lead to bone resorption or apposition if given continuously vs a daily injection (Bauer, Aub et al. 1929). This work was confirmed by Hans Selye a few years later (Selye 1932).

Direct effects of PTH on osteoblasts involve increasing life span via decreasing apoptosis (Jilka, Weinstein et al. 1999). Because apoptosis is the eventual fate for most osteoblasts, this increases the number of bone-forming cells and a concomitant increase in osteocyte density. Osteocytes are a major source for RANKL-driven osteoclastogenesis and whether the increases in osteocyte density contributes to the increases in resorption seen after extended PTH treatment is not known. However, in mice osteocytic PTH signaling is required for hormone-induced RANKL expression and anabolic action from intermittent PTH, suggesting active bone remodeling is required for bone gain (Saini, Marengi et al. 2013). Intermittent PTH also has direct effects on matrix-forming osteoblasts by increasing the rate of bone formation. This can be seen clinically by rapid increases in serum bone formation markers within weeks of starting treatment and by measuring bone formation rates (BFR) in both humans and rodents (Hodsman 2005, Delmas, Licata et al. 2006). Associated with increased bone formation are increases in many genes involved in the process such as *Col1a1*, *Runx2*, MMPs, BMPs, and others. Importantly, PTH causes a marked increase in RANKL expression in vitro and in vivo. RANKL stimulated osteoclastogenesis via PTH-stimulated osteoblast expression has been a long held paradigm in osteobiology; however, this has recently come under question. Mice depleted for osteoblasts do not have a significant reduction in RANKL production and mice null for *Runx2* (required for osteolineage commitment) maintain a significant PTH-stimulated RANKL increase in stromal fibroblastic cells (Galli, Fu et al. 2009). On the other hand, osteocytic suppression of *Sost* has been suggested as a critical component of the intermittent PTH response, suggesting that terminally differentiated osteolineage cells are indeed important for PTH action (similar to RANKL production above). Sclerostin (product of the *Sost* gene) is a potent inhibitor of osteoblastic bone formation ostensibly down regulation of Wnt signaling. PTH decreases sclerostin expression and this action potentially contributes to bone gain seen with hormone therapy (Bellido 2006). Additionally, the dependence of PTH anabolic action on *Sost* inhibition in mice has been shown by genetic deletion and over-expression: in both cases bone gain was blocked due to PTH was blunted (Kramer, Loots et al. 2010). A possible confounding factor with the *Sost*-Tg mice in this study was the use of the endogenous *SOST* promoter, which is directly responsive to PTH-stimulated cAMP signaling. Additionally, these mice were osteopenic and the effect of the transgene on osteoprogenitor pools was not evaluated. Similarly, the *Sost*-KO mice started with a high bone mass phenotype, which may have affected the amount of bone gain possible with PTH. Finally, multiple studies have

documented a decrease in *Sost* expression with PTH (Keller and Kneissel 2005). As mentioned previously PTH decreases OB apoptosis, and this phenomenon was shown to be dependent on proteasomal degradation of pro-apoptotic Bad. Also, the master bone transcription factor Runx2 is stimulated for degradation by PTH in a Smurf1 in an apparent self-limiting feedback mechanism. The kinetics of intermittent hormone administration may favor then a reduction in apoptosis while avoiding the full effect of the self-limiting nature of PTH by Runx2 degradation (Bellido, Ali et al. 2003) Consistent with this proteasomal inhibitors have been shown to be bone anabolic in patients with multiple myeloma. These drugs also stabilized β -catenin and Runx2 (Zangari, Terpos et al. 2012). The story is complex however as Runx2 is necessary for mesenchymal differentiation to osteoblasts, but may inhibit proliferation and differentiation at later stages (Marie 2008). Therefore, the role Runx2 plays in osteoblast differentiation in vivo and in cultured osteoblasts may not be straightforward.

At the tissue level the pleiotropic nature of anabolic PTH action is complex and involves many cell types beyond those direct effects discussed previously on osteoblasts. This is due at least in part various growth factors and anabolic factors such as BMPs, IGF1, and RANKL which are target genes of PTH stimulation. An example of the dependence on these factors is highlighted by osteoblastic IGF1 signaling which is required for bone gain from intermittent PTH (Bikle, Sakata et al. 2002). Similarly, Wnt10b secreted by bone marrow CD8+ T-cells in response to intermittent hormone treatment is necessary for bone gain in mice. This was shown by both depletion of PTH receptors from T-cells and selective deletion of Wnt10b from these cells (Bedi, Li et al. 2012, Li, Walker et al. 2014). Wnt10b functions to promote differentiation of mesenchymal precursors along the osteogenic pathway (Bennett, Ouyang et al. 2007). Additionally, work in Tg mice expressing constitutively active PTHr1 in osteocytes demonstrated the increased bone mass in these animals was dependent on Wnt signaling on the periosteal surface and Wnt signaling along with osteoclastic bone resorption on the endocortical surface (Rhee, Lee et al. 2013). PTH is primarily responsible for trabecular bone formation as shown in mice null for the *Pth* gene. This was coincident with decreases in both osteoblasts and osteoclasts (Goltzman 2008). The *pth*-KO mice also revealed a defect in vascular invasion in the chondro-osseous junction of developing fetus. That PTH stimulates vasculogenesis is also seen in the adult where intermittent PTH preferentially stimulates small arteriole formation over larger arteriogenesis in the context of allograft transplant healing. The former being mediated by an induction of Angiopoietin-1 and the latter being mediated by

a large decrease in angiopoietin-2 (Dhillon, Xie et al. 2013). These data are complemented by work by Kusumbe and colleagues who showed that osteogenesis is coupled to specific types of capillaries. They suggest this network at the distal end of the arterial network in bone represents a specialized location with increased oxygen and nutrients for osteoblasts (Kusumbe, Ramasamy et al. 2014).

Anabolic PTH increases bone volume in the cortical and cancellous envelopes and increases mineral apposition rate in animal models as well as patients (Mitlak 2002). Though, capturing these rate increases depends on time of analysis and is confounded by ongoing treatments for osteoporosis (i.e. previous anti-resorptives), leading to discrepancies in the literature (Jiang, Zhao et al. 2003, Ma, Zeng et al. 2014). Special consideration has been given to the effect of PTH on the hip because differences have been shown at the cortical and cancellous sites in the femoral neck; specifically PTH decreases volumetric BMD at the femoral neck – at least for the first half of treatment. Employing finite element analysis to evaluate strength after a simulated sideways fall, Keaveny *et. al.* showed that that despite loss of BMD, predicted strength did not change. This was hypothesized to result from improved trabecular architecture which took place over the 18 months of the study (Keaveny, Hoffmann et al. 2008). The apparent inconsistency between decreased cortical bone at the femoral neck compared to other sites in the skeleton might be explained by the timing of measurements. Most human studies are conducted from 6-18 months, and during this time the femoral neck cortical shell might be especially vulnerable to increases in bone resorption which PTH causes. However, in a study of patients with glucocorticoid induced osteoporosis (GIOP) which tracked patients 36 months, there was a 6.3% increase in femoral neck BMD (Saag, Zanchetta et al. 2009). This study is not directly comparable to the work by Keavney. Though the doses were similar (20µg/day), the first evaluated female patients only with post-menopausal osteoporosis, while the second group suffered from GIOP. Still the suggestion is that the site specific dynamics of PTH action are complex and may depend greatly on the timing of experimental endpoints.

The mechanism(s) which limit PTH anabolism are unknown but may be the result of increased osteoclastogenesis, proteosomal degradation of Runx2 as suggested above, depletion of the progenitor pool, as well as thus far unknown phenomenon. Of course these need not be mutually exclusive and multiple overlapping pathways likely contribute to negative regulation of the bone gains seen with PTH. Work in Xu Cao's lab provides support for depletion of progenitor cells as central to the endogenous restriction of bone

gain with PTH. Working in mice these researchers showed that Sca-1⁺ bone marrow stromal cells (an osteoprogenitor) are recruited to remodeling sites by release of matrix TGF β following bone resorption. The bisphosphonate alendronate decreased osteoclast activity and the intermittent PTH response. Also, TGF β ^{-/-} mice had a decreased response to PTH (Wu, Pang et al. 2010). This study suggests that exhaustion of the osteoprogenitor pool can limit the PTH response, also osteoclast activity is shown to be a critical component of that that response. However, this work does not provide evidence that bone forming progenitors are exhausted with hormone therapy. Studies evaluating the numbers, proliferation and bone forming potential of osteoprogenitors is compromised with increasing age. Combined, these mechanisms support the hypothesis that once aged marrow is exposed to PTH, its ability to respond with new bone would be attenuated (Bergman, Gazit et al. 1996, Nishida, Endo et al. 1999, Chen 2004). Interestingly, recent work in the Marie lab describes N-cadherin mediating an age-dependent decrease in osteoprogenitor number in favor of adipogenesis in a BMSC-derived Wnt5a and Wnt10b dependent manner (Haÿ E 2013). This suggests possible mechanistic clues to the osteoprogenitor pool decrease. Wnt10b is a crucial component of the anabolic PTH response, and it is possible that a restricted osteoprogenitor pool is less responsive to PTH, in part, due to lower Wnt10b levels. Other studies show that bone lining cells are rapidly differentiated into bone forming osteoblasts in response to PTH, and that depletion of this population restricts the anabolic effect (Dobnig and Turner 1995)

The Role of Estrogen

Osteoporosis has multiple contributing factors including significant genetic and environmental components. The complex nature of the disease leads to a varied patient population. However, the prototypical patient is that of postmenopausal women of American or Japanese descent (Bidwell, Alvarez et al. 2013). This profile suggests a strong role for estrogen in determining bone mass and indeed estrogen effects both osteoblasts and osteoclasts are profound. Evidence supports both direct effects as a classical sex steroid binding nuclear receptors which affect gene expression and indirect, or non-genotropic, effects which affect signal transduction. This section will consider first estrogen's effect on osteoblasts (or formation) and then effects on osteoclasts (or resorption).

Formation

Post-menopausal accumulation of adipocytes in the marrow cavity has been proposed as a cellular mechanism for decreased bone formation with age (Syed, Oursler et al. 2008). Syed et al tested this hypothesis directly in post-menopausal women in placebo controlled trial. They reported women receiving estrogen replacement for 1 year experienced no change in marrow adipocyte number compared to a 20% increase in the placebo group. At the same time hormone treatment decreased adipocyte volume/tissue volume approximately 24%, while placebo group experience a nearly equal increase in this parameter (Syed, Oursler et al. 2008). The mechanism(s) involved are not fully described, but many of the details have been reported. Estrogen binding to ER α or ER β in osteoprogenitors directs differentiation into osteoblasts *in vitro* while antagonizing adipocyte development. This was shown in ST-2 cells, an incompletely differentiated stromal line which can be driven to both osteogenic and adipogenic fates by BMP2. Osteogenic potential was shown to be positively mediated by estrogen receptors α and β . While adipocyte differentiation was inhibited by lines carrying only ER α and ER β individually (Okazaki, Inoue et al. 2002).

Transdifferentiation of osteoprogenitors into adipocytes may contribute to the increase in marrow adiposity as well. Gao et al recently showed a dose dependent suppression of osteolineage to adipocyte transdifferentiation using MC3T3 and primary murine BMMNCs cells grown in osteogenic media for 14 days and subsequently grown in adipogenic media (Gao, Huang et al. 2014). Although this needs to be verified *in vivo*, the results might contribute to understanding the paradox of decreased bone formation and increased adipocyte formation despite multiple studies reporting no decrease of osteoblast producing MSCs with age (Sethe, Scutt et al. 2006).

Estrogen negatively impacts osteoblast progenitor numbers through direct action involving ER α by decreasing their self-renewal. This population of cells characterized by CFU-Ob activity has limited capacity for self-renewal, which is decreased by 17 β -estradiol *in vitro* and *in vivo* (Di Gregorio, Yamamoto et al. 2001). This effect is seemingly paradoxical to the overall anabolic effect of estrogen. However, the authors of this study suggest the action of suppressing osteoblast numbers ultimately suppressed osteoclast numbers because the latter rely on the former for developmental cues. In this regard, estrogen can be viewed as a coupling factor in bone formation and resorption. Consistent with this notion is the fact that post-menopausal osteoporosis is described as a high turnover disease state in which resorption is uncoupled from and outpaces formation

(Pacifci 1996). Curiously, bone formation increases in the post-menopausal woman, but not as much as resorption based on systemic markers of bone turnover. Serum osteocalcin, bone specific alkaline phosphatase and C-propeptide of type I collagen in the case of formation, and urinary N-terminal & C-terminal telopeptides in the case of resorption (Garnero, Sornay-Rendu et al. 1996) which suggests that estrogen restricting the number of osteoblasts is not the only mechanism for restricting the number of osteoclasts. Indeed as described below, estrogen simulated cytokine production which increase osteoclast apoptosis. Similar results showing increases in the formation an resorption arms of bone homeostasis were noted in animals models as early as 1987 (Turner, Vandersteenhoven et al. 1987). It should be noted as well that reports of bone formation and aging are inconsistent. The issue of bone formation with aging is confused by sex steroid independent declines in bone formation related to senile osteoporosis, seen in both men and women, which are separate from post-menopausal (or sex steroid deficiency) osteoporosis. Some studies indicated normal osteoblast progenitor numbers and bone formation parameters is study populations, while other studies indicate decreases in one or both of these parameters (Pei, Bellows et al. 2006, Bidwell, Alvarez et al. 2013).

Finally, recently it has become clear that estrogen has differential effects in the cortical and trabecular bone components. This differences likely arises from the expression patterns of ER β , which is more highly expressed in osteoblasts and osteocytes in the trabecular compartment (Bord, Horner et al. 2001). ER β can form heterodimers with ER α which are less responsive to transcriptional activation upon binding with E2. These heterodimers therefore require more circulating estrogen to realize the overall anabolic response estrogen has on bone formation (Hall and McDonnell 1999).

Resorption

As mentioned previously, estrogen attenuates osteoblastic production of cytokines which contribute to bone loss. In particular, IL6, TNF α , and FASL. In 1992 Girasole and coworkers showed using multiple in vitro systems that 17beta-estradiol attenuated IL-6 production and induction of IL-6 by TNF α . Mixed-cell calvarial cultures demonstrated that IL-6 regulates, in part, osteoclastogenesis. This work suggested for the first time a potential mechanism for cytokine-mediated bone loss with estrogen depletion (Girasole, Jilka et al. 1992). This effect was later shown to be dependent on NF-kB and C/EBP

interactions with the estrogen receptor (ER), but *not* on an ER-binding *cis* element (Stein and Yang 1995).

Estrogen control of osteoclast apoptosis has been long understood (Kameda, Mano et al. 1997, Kousteni, Chen et al. 2002). This control of osteoclast life span by estrogen is through direct action of ER α receptor binding to a FAS Ligand enhancer element in osteoblasts to induce pre-osteoclastic apoptosis. The canonical action of estrogen binding ER α and causing transcriptional changes was shown *in vitro* and genetically *in vivo* (Krum, Miranda-Carboni et al. 2008). However, the effects of estrogen on osteoclast apoptosis are not restricted to those induced by changing genetic expression. Kousteni and co-workers showed *in vitro* with pharmacological agents capable of binding ER α , but not inducing transcriptional changes, that non-genotropic effects of the estrogen receptor are sufficient to induce osteoclasts apoptosis. Interestingly, this same group demonstrated that non-genotropic effects of estrogen are capable of decreasing osteoblast apoptosis placing this activity at a junction potentially convenient to pharmacological intervention to affect formation and resorption (Kousteni, Bellido et al. 2001, Kousteni, Chen et al. 2002).

T-cells also contribute to bone resorption in estrogen deficiency by increasing production of the pro-osteoclastogenic cytokine TNF- α . This phenomenon was first described in mice (Cenci, Weitzmann et al. 2000) and has since been accepted as part of the pathophysiology of post-menopausal osteoporosis (Pacifci 2010).

Working with murine osteoclasts *in vitro* Jimi and co-workers showed that osteoclasts spontaneously apoptose in culture and addition of IL-1 protected cells from this fate. Furthermore, the researchers showed this protection was NF- κ B dependent (Jimi, Nakamura et al. 1998). Consistent with the role of estrogen in protecting bone mass, stimulation of IL-1 by stromal cells, osteoblasts and lymphocytes is under direct control by estrogen acting through its classical transactivation capacity. Estrogen also affects osteoclast formation by stimulating osteoblastic production of osteoprotegrin (OPG). This decoy receptor for RANKL binds the RANK receptor on osteoclast progenitors, but does not result in maturation. As such, soluble OPG serves as an inhibitor of bone resorption (Hofbauer, Khosla et al. 1999).

CHAPTER 2

NMP4 SUPPRESSES BONE FORMATION AND RESORPTION FOLLOWING INTERMITTENT PARATHYROID HORMONE RESULTING IN NET POSITIVE BONE FORMATION

Childress P¹, Philip BK¹, Robling AG¹, Bruzzaniti A², Kacena MA³, Bivi N¹, Plotkin LI¹, Heller A¹, Bidwell, JP¹.

1. Department of Anatomy and Cell Biology, Indiana University School of Medicine (IUSM), Indianapolis, IN 46202.
2. Indiana University School of Dentistry, Indianapolis, IN 46202.
3. Department of Orthopaedic Surgery, IUSM.

Key Words: c-fos, Fra-2, Ephrin, Osteoclastogenesis, Osteocalcin, Osteoporosis

**Material in this Chapter was published in:
Calcified Tissue International. July 2011; 89(1)74-89.**

Abstract

How parathyroid hormone (PTH) increases bone mass is unclear, but understanding this phenomenon is significant to the improvement of osteoporosis therapy. Nmp4/CIZ is a nucleocytoplasmic shuttling transcriptional repressor that suppresses PTH-induced osteoblast gene expression and hormone-stimulated gains in murine femoral trabecular bone. To further characterize Nmp4/CIZ suppression of hormone-mediated bone growth, we treated 10-week-old Nmp4-knockout (KO) and wild-type (WT) mice with intermittent human PTH(1-34) at 30 µg/kg daily or vehicle, 7 days/week, for 2, 3, or 7 weeks. Null mice treated with hormone (7 weeks) gained more vertebral and tibial cancellous bone than WT animals, paralleling the exaggerated response in the femur. Interestingly, Nmp4/CIZ suppression of this hormone-stimulated bone formation was not apparent during the first 2 weeks of treatment. Consistent with the null mice enhanced PTH-stimulated addition of trabecular bone, these animals exhibited an augmented hormone-induced increase in serum osteocalcin 3 weeks into treatment. Unexpectedly, the Nmp4-KO mice displayed an osteoclast phenotype. Serum C-terminal telopeptide, a marker for bone resorption, was elevated in the null mice, irrespective of treatment. Nmp4-KO bone marrow cultures produced more osteoclasts, which exhibited elevated resorbing activity, compared to WT cultures. The expression of several genes critical to the development of both osteoblasts and osteoclasts was elevated in Nmp4-KO mice at 2 weeks, but not 3 weeks, of hormone exposure. We propose that Nmp4/CIZ dampens PTH-induced improvement of trabecular bone throughout the skeleton by transiently suppressing hormone-stimulated increases in the expression of proteins key to the required enhanced activity and number of both osteoblasts and osteoclasts.

INTRODUCTION:

Parathyroid hormone (PTH) therapy is the only osteoporosis treatment that restores bone to the aged skeleton, however its expense makes it the least cost-effective (Liu, Michaud et al. 2006, Stroup, Kane et al. 2008). The development of shorter PTH-based treatments yielding similar efficacy as the longer-term therapy will improve its cost-benefit ratio (Liu, Michaud et al. 2006) but this requires a better understanding of the mechanisms underlying the PTH anabolic response.

Data on the self-limiting pathways to PTH action, inherent to all endocrine response loops, are lacking and it is these molecules that may provide the best pharmaceutical targets for improving hormone efficacy and cost-effectiveness (Childress, Robling et al.). For example, as PTH activates the osteoblast generation of cAMP and the enhanced expression of RUNX2 it simultaneously stimulates phosphodiesterase activity (Ahlstrom and Lamberg-Allardt 1997) and Smurf1-mediated RUNX2 proteasomal degradation (Bellido, Ali et al. 2003).

We recently demonstrated that disabling the nucleocytoplasmic shuttling transcription factor Nmp4/CIZ (nuclear matrix protein 4/cas interacting zinc finger protein) in mice enhances the skeletal response to anabolic PTH (Robling, Childress et al. 2009) suggestive of a significant role in the hormone's self-limiting pathways. Ten wk-old *Nmp4*-knockout (KO) mice treated with intermittent PTH for 7 wks exhibited an augmented increase in femoral trabecular bone compared to wild-type (WT) mice without compromising the hormone-stimulated increases in bone mineral density and content throughout the skeleton (Robling, Childress et al. 2009).

The ubiquitously expressed Nmp4/CIZ appears to act as a general repressor of anabolic bone growth, in part, by suppressing the transcription of genes that support the development of the osteoblast phenotype, including the pro-alpha1(I) chain (*Col1a1*) and the *Mmp-13* promoters (Childress, Robling et al. , Thunyakitpisal, Alvarez et al. 2001, Shah, Alvarez et al. 2004). This trans-acting protein suppressed the PTH induction of rat *Mmp-13* transcription in UMR-106-01 osteoblast-like cells via its binding to a PTH-responsive element in the 5' regulatory region of the gene (Shah, Alvarez et al. 2004) but whether Nmp4 represses the hormone responsiveness of other tissues has not been reported.

In the present study we determined that Nmp4/CIZ suppressed the PTH-stimulated improvement of trabecular bone throughout the mouse skeleton and was not site-specific as is common in other mouse models (Chung, Castro et al. 2006, Philip, Childress et al.

2010). Most surprisingly, we discovered that the null mice have an osteoclast phenotype. The analysis of serum biochemistry, bone histomorphometry, bone mRNA expression profiles, and osteoclast cell culture, suggest that the numbers and activities of both osteoblasts and osteoclasts are enhanced in the *Nmp4*-KO mice due, in part, to a transient de-repression of key transcription factors and signaling proteins common to pathways critical for the development and hormone-responsiveness of both cell types.

MATERIALS AND METHODS:

Mice

Construction of the *Nmp4*-KO mouse, its backcrossing six generations onto a C57BL/6J background, and the baseline phenotype, has been described (Robling, Childress et al. 2009). As in our previous study wild-type C57BL/6J mice from The Jackson Laboratories (Bar Harbor, ME) were used as controls (6). Experiments designed to compare the response of WT and *Nmp4*-KO mice to PTH compensated for any differences in genetic and environmental factors (see Statistical Analyses). Our local Institutional Animal Care and Use Committee approved all experiments and procedures involving the production and use of the experimental mice described in this study.

PTH treatment regimen:

Prior to the start of an experiment 8 wk-old female WT and *Nmp4*-KO mice were given 100µl sterile saline by subcutaneous (sc) injection once daily to acclimatize them to handling. At 10 wks of age, mice were sorted into four groups based on equivalent mean-group-body weight. The four treatment groups included 1) vehicle-treated WT; 2) PTH-treated WT; 3) vehicle-treated *Nmp4*-KO and 4) PTH-treated *Nmp4*-KO. Mice were injected sc with human PTH 1-34 (hPTH(1-34), Bachem Bioscience Inc, PA) at 30µg/kg/day, daily or vehicle control (0.2% BSA/0.1% 1.0 mN HCl in saline, Abbott Laboratory, North Chicago, IL) for the times specified in the Results. Additionally, animals were administered by intraperitoneal injection calcein green (20 mg/kg, Sigma-Aldrich, St Louis, MO) and alizarin red (25 mg/kg, Sigma-Aldrich) 6 days and 3 days before euthanasia, respectively.

Dual energy x-ray absorptiometry (DEXA)

Bone mineral content (BMC; g), areal bone mineral density (aBMD; mg/cm²), and body weight were measured weekly (8 wks to 12 wks of age). The BMC and aBMD were

obtained for the post-cranial skeleton by dual-energy X-ray absorptiometry (DEXA) using an X-ray PIXImus mouse densitometer (PIXImus II; GE-Lunar Corp., Madison, WI) as previously described (Robling, Childress et al. 2009). We report whole body (WB), femur, tibia, and spine BMD and BMC.

Micro computed tomography (μ CT)

Vertebrae, femurs, and tibiae were dissected from the WT and *Nmp4*-KO animals after euthanasia, the connective tissue and muscle removed, and the bones stored in 10% buffered formalin at 4°C. After 48 hr the bones were transferred to 70% ethanol and stored at 4°C until analyzed. We have previously described our methodology for assessing the trabecular microarchitecture at the distal femoral metaphysis and within the 5th lumbar vertebra using the desktop micro-computed μ CT 20 tomographer (Scanco Medical AG, Bassersdorf, Switzerland; [6, 9]). Cancellous bone of the tibia was evaluated by scanning the proximal 20% of each tibia at 9 μ m resolution. A microfocus X-ray tube with a focal spot of 10 μ m was used as a source. Precisely 90 micro-tomograph slices were acquired per bone beginning 1 mm from the epiphysis and extending distally 1.53 mm using a slice increment of 17 μ m. For each slice, 600 projections were taken over 216° (180° plus half of the fan angle on either side). Proximal tibia stacks were reconstructed to the 3rd dimension using a standard convolution-backprojection procedure with a Shepp-Logan filter using a threshold value of 275. The Scanco software permitted evaluation of tibial, femoral and vertebral trabecular bone volume per total volume (BV/TV, %), connectivity density (Conn.D, mm^{-3}), structure model index (SMI), trabecular number (Tb.N, mm^{-1}), trabecular thickness (Tb.Th, mm), and spacing (Tb.Sp, mm) from the 3D constructs. To evaluate cortical architecture, a single slice was taken through the midshaft femur (simply by measuring the number of slices for the whole femur and dividing by 2), and the cortical area (CA, mm^2), marrow area (MA, mm^2), and the total area (TA, mm^2) were calculated (6). Additionally, the moments of inertia, the resistance of the bone to a bending load, were derived from these data. These parameters included the greatest (I_{MAX} , mm^4) and smallest (I_{MIN} , mm^4) flexural rigidity as well as the polar moment of inertia (J, mm^4), which is the torsional and bending rigidity around the neutral axis of the bone and perpendicular to the x- and y-axes passing through the center of mass (Cheng, Sipilä et al. 2002).

Quantitative real-time PCR (qRT-PCR) analysis:

Femoral or tibial RNA from mice that had been treated with intermittent PTH or vehicle for 2 wks or 3 wks was harvested either 1 hr or 24 hrs after the last injection. The harvesting, processing, and analysis protocols for qRT-PCR analysis have been described (6, 9). Real-time PCR primers and probes were obtained from Assays-on-Demand™ (Applied Biosystem, Foster City CA, see Table 1). The $\Delta\Delta$ CT method was used to evaluate gene expression between WT and KO animals using *Rplp2* as the normalizer after screening several housekeeping gene candidates. The coefficient of variation of *Rplp2* was typically 2-3% between all samples. Normalization against internal control genes is most frequently used because it can control all variables including cell number (Goossens, Van Poucke et al. 2005, Zhang, Ding et al. 2005). The data represent the mean \pm standard deviation from at least 6 mice per genotype.

Bone histomorphometry:

Femurs were removed from the WT and *Nmp4*-KO animals after euthanasia and fixed as described above. The anterior face of the epiphyseal plate was cut to expose the marrow cavity. Samples were then dehydrated with graded alcohols, embedded in methyl-methacrylate, sectioned (4 μ m) with a Leica RM2255 microtome (Leica Microsystems, Wetzlar, Germany), and mounted on standard microscope slides. All histomorphometric parameters were obtained following ASBMR guidelines (14). Mineral apposition rate (MAR), mineralizing surface (MS/BS) and bone formation rate (BFR), were obtained from a 0.03mm² metaphyseal region of interest from 250 μ m to 1750 μ m below the growth plate using ImagePro 3.1 software (Media Cybernetics, Bethesda, MD, USA). Some sections were stained for tartarate resistant acid-phosphatase (TRAP). The number of TRAP-positive (TRAP+) cells on the bone surface (TRAP+ cell N/BS) and the TRAP-stained surface to bone surface (TRAP+ S/BS) were determined.

Serum biochemistry:

Intact serum osteocalcin was measured using the sandwich ELISA BTI Mouse Osteocalcin EIA Kit (Biomedical Technologies, Inc., Stoughton MA; [15]). Serum C-terminal telopeptides (CTX) were determined using the RatLaps™ ELISA (Immunodiagnostic Systems Inc., Scottsdale, AZ; (O'Brien, Plotkin et al. 2008)).

Osteoclast culture and activity:

To compare the number of osteoclasts derived from *Nmp4*-KO and WT mice, bone marrow was flushed from the long bones of 6-8 week-old animals. Cells were seeded into 24-well culture dishes at an initial density of 2.1×10^5 cells/mm² and cultured in alpha-MEM (Invitrogen, Carlsbad, CA) supplemented with 10% FBS (FBS, Hyclone, Logan Utah) and 20 ng/ml of recombinant human M-CSF (Peprotech, Rocky Hill, NJ) for 2 days and then supplemented with 20 ng/ml of recombinant human M-CSF and 80 ng/ml of recombinant human RANKL (Peprotech) for the duration of the experiment. The cell culture medium was changed every third day until osteoclasts were visible. Once osteoclasts had formed, the cells were fixed with 2.5% glutaraldehyde in phosphate buffered saline for 30 minutes at room temperature, stained for TRAP (Sigma-Aldrich), and TRAP+, multinucleated (≥ 3) cells were counted.

The osteoclast resorption activity of cells derived from the KO and WT mice was evaluated using a standard pit assay (Tanaka, Amling et al. 1996). Bone marrow was isolated as above and plated into 6-well culture dishes at 2×10^6 cells/well (2.1×10^5 cells/mm²). As detailed above, cells were incubated in alpha-MEM containing 10% FBS and 20 ng/ml M-CSF for 2 days. The media was removed and replaced with fresh media containing 20 ng/ml M-CSF and 80 ng/ml RANKL for an additional 2-3 days. Mature osteoclasts were detached by trypsinization, washed once, re-plated onto dentin slices (Immunodiagnosics Systems Inc, Fountain Hills, AZ) and cultured for an additional 48 hrs in media containing 20 ng/ml M-CSF and 80 ng/ml RANKL. Dentin slices were washed, incubated in 6% NaOCl for 5 min, and sonicated for 20 s to remove cells. Resorption pits were stained with a solution containing 1% toluidine blue and 1% sodium borate for 1 min, washed with water and air-dried. Pit surface area was quantified using the ImagePro 7.0 on a Leica DMI4000 with a 10X objective. Results were normalized for osteoclast number, as determined by counting TRAP+ cells containing 3 or more nuclei. Experiments were performed in triplicate and results represent average pit area per dentin slice/OC number.

Statistical analyses:

Statistical analysis was processed using JMP Version 7.0.1 (SAS Institute, Cary, NC). Experiments designed to compare the response of WT and *Nmp4*-KO mice to PTH compensated for any differences in genetic and environmental factors, i.e. the fact that WT mice were not bred in-house was accounted for by our analyses. For example, the raw BMD and BMC data were converted to % change (between 8 and 12 wks of age). Comparing hormone-treated to vehicle-treated within each genotype for all the endpoint

analyses removed baseline differences from those factors and permitted analysis for genotype x treatment interactions, i.e. whether the WT and *Nmp4*-KO mice responded differently to hormone for the parameter under consideration. We employed a two-factor ANOVA for these analyses. If a genotype x treatment interaction was indicated the data were then analyzed by a Tukey's HSD post hoc test to determine significant differences between the experimental groups. For the serum analysis experiment we used a repeated-measures multivariate analysis of variance (MANOVA) to evaluate the raw longitudinal serum osteocalcin and CTX levels over the 7 wk hormone treatment period. Additionally, we converted the serum data to % change and analyzed with the two-factor ANOVA. The genotype x time term for the raw longitudinal serum data is equivalent to the genotype term for the % change data i.e. both terms indicate a difference in the rate of either osteocalcin/CTX increase or bone accrual (for the BMD/BMC study) between the WT and null mice. For some experiments, unpaired t-tests were employed as indicated. Data are presented as mean \pm SD unless otherwise indicated. Statistical significance was taken at $p < 0.05$.

RESULTS:

Nmp4-KO mice exhibited an enhanced PTH-induced acquisition of trabecular bone throughout the skeleton compared to WT mice after 7 wks but not 2 wks of treatment.

We previously showed that *Nmp4*-KO mice exhibited a significantly exaggerated PTH-stimulated increase in femoral trabecular bone compared to WT mice after 7 wks of hormone challenge (6); here we addressed whether *Nmp4*/CIZ represses PTH-induced improvement in other parts of the skeleton and if this suppression is evident from the start of the treatment regimen. Animals were treated with intermittent hPTH(1-34) 30 μ g/kg/day or vehicle for 7 wks from 10 wks of age. Mice were sorted in the four treatment groups and the cancellous architecture characterized as described in the Material and Methods. The *Nmp4*-KO L5 vertebra BV/TV exhibited a more robust increase in response to 7 wks of PTH than the WT BV/TV as demonstrated by a strong treatment effect and significant genotype x treatment interaction (Figure 2-1A). The PTH-induced change in vertebral morphology from a rod-like to plate-like form was more pronounced in the null mice (SMI, Figure 1C). Vertebral Tb Th was significantly enhanced in response to 7 wks of hormone in the null mice but not in the WT animals (Figure 1E), whereas PTH had an equivalent impact on Tb Sp (Figure 1F); a consequence of the fact that these parameters do not have a simple reciprocal relationship (14). PTH had an equivalent impact on Conn D (Figure 2-

1B) in the genotypes. Finally, there was a strong genotype effect for all the measured vertebral parameters consistent with the more robust trabecular architecture in the null mice (Figures 2-1 A-F). Typical μ CT scans of L5 vertebra from mice treated with intermittent hormone or vehicle for 7 wks are shown in Figure 2-1G.

To evaluate the early hormone response of the L5 vertebra we compared bones from WT and *Nmp4*-KO mice that had been treated with PTH or vehicle for 2 wks. The L5 vertebra trabecular bone showed no improvement after 2 wks of hormone in either the WT or null animals (Figure 2-1A-F). However, there was a genotype effect for BV/TV, Conn D, SMI, and Tb Th (Figures 2-1A, B, C, and E, respectively), thus the enhanced vertebral trabecular architecture observed in the 17 wk-old null mice irrespective of treatment, was apparent in these mice at 12 wks of age.

Nmp4/CIZ also repressed the hormone-induced increase in tibial cancellous bone (Figure 2). The PTH-stimulated increase in tibial BV/TV after 7 wks of hormone was greater in the null than the WT mice (Figure 2-2A). PTH increased tibial Tb N in both genotypes but significantly more so in the null mice (Figure 2-2D) and the hormone-stimulated change in tibial SMI was more pronounced in the null mice (Figure 2-2C). PTH had a comparable positive effect on Conn D (Figure 2-2B), Tb Th, (Figure 2-2E), and Tb Sp (Figure 2-2F) in the WT and null mice with 7 wks of treatment. Typical μ CT scans of tibia from mice treated with hormone or vehicle for 7 wks are shown in Figure 2-2G.

To evaluate the early hormone response of the tibia we compared bones from WT and *Nmp4*-KO mice that had been treated with PTH or vehicle for 2 wks. Both genotypes showed equal hormone-induced improvement of tibial BV/TV, Conn D, SMI, and Tb Th during the initial 2 wks of treatment (Figures 2-2A, B, C, and E). PTH failed to improve Tb N and Tb Sp in both WT and null mice during this period of the regimen, however there was a genotype effect for these two parameters indicating enhanced aspects of tibial architecture in the null mice at 12 wks of age (Figure 2-2D & F).

Disabling *Nmp4* had no impact on any aspect of the skeletal response to PTH (no genotype x treatment interaction) during the first 2 wks of treatment including femoral cancellous architecture (Table 2-2A), midshaft cortical architecture (Table 2-2B) and the percent change skeletal BMD and BMC (Table 2-2C). Consistent with *Nmp4* repressive action on bone growth (Robling, Childress et al. 2009) genotype effects were observed for some of these parameters indicative of the modestly enhanced skeletal phenotype of the null animals. Interestingly, the genotype effects for WB BMC and femur and tibia BMD and

BMC (Table 2-2C) indicated that the rate of bone accrual was lower in the null mice over the four-week period of measurement irrespective of treatment.

The enhanced PTH-stimulated increase in femoral trabecular bone observed in Nmp4-KO mice occurred after 2 wks and before 7 wks of hormone exposure.

Histological sections of the femoral spongiosa prepared for histomorphometry (Figure 2-3A) confirmed our previous analysis using μ CT (Robling, Childress et al. 2009) that the *Nmp4*-KO mice added more cancellous bone in response to 7 wks of hormone treatment than WT mice. However, bone formation rate parameters were not different between the null and WT mice at the end of treatment and in fact were declining suggesting that PTH response was beginning to plateau in both genotypes. MS/BS, *proportion of bone surface undergoing mineralization*, was significantly decreased in both genotype treatment groups consistent with the declining PTH-responsiveness (Table 2-2D). Additionally, we did not observe a significant hormone-induced increase in bone formation rate (BFR) in either of the genotypes at this point in treatment (Table 2-2D). Nevertheless, PTH equally enhanced the mineral apposition rate (MAR) in both genotypes at this time point (Table 2-2D).

Our histomorphometric analysis of mice treated with PTH or vehicle for 7 wks included the parameters of TRAP+ S/BS and TRAP+ N/BS, which provide an estimate of the size and number of osteoclast precursors and mature osteoclasts normalized to bone surface. Clearly the anabolic hormone treatment enhanced the absolute number of osteoclasts and the total osteoclast surface over bone in both genotypes as evident from the histological sections (Figure 2-3B); normalizing these parameters to bone surface reveals that although both parameters are elevated in the null mice the differences are not statistically significant (Table 2-2D). However there were strong treatment effects, i.e. PTH significantly attenuated the percent bone surface covered by TRAP+ cells and their number/surface (Table 2-2D). Interestingly there was a genotype x treatment interaction for TRAP+ S/BS indicating that hormone had a larger impact on the reduction of bone surface covered by osteoclasts in the null mice than in the WT animals (Table 2-2D).

Nmp4-KO mice exhibited strikingly different serum osteocalcin and CTX profiles compared to WT animals.

Whole blood was collected and serum separated from the mice of the four treatment groups at 10 wks of age (before initiation of treatment), 13 wks of age (3 wks of

PTH/vehicle treatment), and 17 wks of age (7 wks of PTH/vehicle treatment). The raw longitudinal data and the % change data for osteocalcin, a standard marker for bone formation and osteoblast number, revealed that null and WT mice had equivalent serum levels just prior to hormone treatment but the *Nmp4*-KO mice exhibited a higher rate of increase over the hormone treatment period (genotype x time interaction, longitudinal data; genotype interaction, % change data) and exhibited an enhanced response to hormone (genotype x treatment interaction, Figures 2-4A & B). Specifically, the null mice showed an enhanced and sustained increase in osteocalcin after 3 wks of treatment while the WT animals showed a peak at 3 wks of treatment followed by a decline by 7 wks of treatment (Figure 2-4A & B).

Serum C-terminal telopeptides (CTX), a marker for bone resorption, was significantly elevated in the *Nmp4*-KO mice compared to the WT animals before and during the hormone treatment period. CTX was elevated with PTH treatment in both genotypes but this increase was not statistically significant (Figure 2-4C & D).

Bone marrow from Nmp4-KO mice yields more osteoclasts than marrow from WT mice and the null osteoclasts exhibit an enhanced resorbing activity.

To confirm our serum data indicating an increased activity of osteoclasts in the *Nmp4*-KO mice we compared the number of these cells derived from the bone marrow cultures of the untreated null and WT animals at 7-8 wks of age. Bone marrow preparations from 3 null mice and 4 WT mice were cultured in 6-well plates and treated with M-CSF and RANKL as described in the Materials and Methods section. On average, the *Nmp4*-KO bone marrow cultures produced 2-fold more osteoclasts than the WT marrow (null = 1608 ± 87 OC/well; WT = 877 ± 243 OC/well; $p < 0.05$, data presented as average \pm SD). This experiment was performed twice yielding similar results.

Next we compared the dentin-resorbing activities of the *Nmp4*-KO and WT osteoclasts. Mature osteoclasts were obtained from the bone marrow of WT and null mice (n=2-3 mice per group) as described in the Materials and Methods section. Fully differentiated bone marrow-derived osteoclasts were re-plated on dentin slices for 48 hrs. The area resorbed was quantified and normalized for TRAP+ osteoclasts. The *Nmp4*-KO osteoclasts exhibited a 50% increase in the area resorbed on dentin compared to the WT osteoclasts (null = 154 ± 4.6 % area resorbed/Trap+ cells; WT = 100 ± 13.3 % area resorbed/Trap+ cells; $p < 0.05$, data presented as average \pm SD).

Nmp4-KO mice exhibit a transiently enhanced basal or PTH-stimulated expression of genes common to osteoblast and osteoclast development.

To follow up on our observation that both osteoblast and osteoclast numbers were enhanced in the null mice, we analyzed femoral RNA harvested during the early phase of PTH treatment to evaluate the expression of genes that support the development of both cells. Animals were treated with intermittent PTH or vehicle for 2 or 3 wks and RNA harvested 1 hr after the last injection. The AP-1 transcription factors *c-fos* and *Fra-2* both exhibited a significantly enhanced PTH-stimulated increase in the *Nmp4-KO* mice (genotype x treatment interaction) after 2 wks of treatment but these differences were absent after 3 wks of PTH (Table 2-3A). Additionally, the transcription factor *Nfatc1* was significantly elevated in the femur of null mice (genotype effect) at the 2 wk time point but was equivalent to the WT expression at 3 wks of treatment (Table 2-3A). We also examined the expression of several genes that mediate osteoblast-osteoclast signaling. Interestingly, the *Nmp4-KO* mice showed a significant increase in the expression of *EphB4* the receptor for *EphrinB2*, its transmembrane ligand, which also showed an elevation in expression that approached significance but again these differences between the genotypes disappeared at the 3 wk time point (Table 2-3A). Both *EphB4* and *EphrinB2* were responsive to PTH in the null and WT mice (Table 2-3A). Interestingly, the *Rankl/Opg* ratio was diminished in the null mice compared to WT animals at 2 and 3 wks of treatment, which was significant at the latter time point (Figure 2-3A).

Further comparative analysis of femoral gene expression profiles between WT and null mice at the 2 wk time period failed to show any significant differences between the two genotypes with one exception (Table 2-3B). The expression of the pro-survival gene *Bcl2* was not different in WT and null mice and did not respond to hormone in either genotype at this point in the treatment regimen, however, the expression of *Bax*, the pro-apoptotic gene was significantly attenuated in the *Nmp4-KO* mice (Table 2-3B). *M-csf*, its receptor *c-fms*, and the osteoclast recruitment cytokine *Mcp-1* showed no difference in their expression or PTH-responsiveness between WT and *Nmp4-KO* animals (Table 2-3B). Hormone induced over a 25-fold increase in *Nurr1* expression in both WT and null mice (Table 2-3B). The expressions of *Mkp-1*, *JunD*, *Smad3*, and *Lef1* were modestly but equally elevated with PTH in both genotypes (Table 2-3B). Conversely, the mRNA expression of the receptor for advanced glycation end products (*Rage*) was attenuated by hormone treatment in both WT and *Nmp4-KO* mice (Table 2-3B).

Next we characterized the expression of genes that support bone formation by analyzing femoral RNA obtained 24 hr after the last injection of intermittent PTH or vehicle after 2 wks of treatment. We observed a treatment effect, but no genotype effect or genotype x treatment interaction for *Runx2*, *Osterix*, *Col1a1*, *Alpl* and *Mmp13*, *Sost*, *Bmp2*, and *Pthrp* mRNA profiles (Table 2-3B). Intermittent hormone treatment did not impact the expression of PTH-related peptide (*Pthrp*) in either genotype (Table 2-3B).

Our preliminary evaluation of gene expression in the tibia showed that the RNA profiles at 3 wks of treatment were generally similar to those observed for the femur at the same time point with the exception of *Nfatc1*, which was still significantly elevated in the tibia of the null mice (Table 2-3C). Additionally, the decrease in the *Rankl/Opg* ratio did not reach significance in the tibia as demonstrated for the femur (Table 2-3C).

DISCUSSION:

The present data demonstrate that *Nmp4/CIZ* significantly blunts PTH-stimulated improvement in cancellous bone throughout the skeleton, that this repression of bone gain is apparent between 2 wks and 7 wks of hormone treatment, and that *Nmp4/CIZ* suppresses osteoclast as well as osteoblast number and activity likely by regulating key transcription factors critical to the development of both cells. The global impact of *Nmp4* on the trabecular skeleton is in stark contrast to recent studies showing the site-specific effects of *Rage* (Philip, Childress et al. 2010) and connexin 43 (Chung, Castro et al. 2006) on PTH-induced cancellous bone improvement.

Nmp4/CIZ repression of the PTH-mediated increase in trabecular bone was not observed during the initial 2 wk treatment period; WT and KO mice showed equivalent hormone-stimulated increases in BMD, BMC, trabecular improvement, and enhanced expression of numerous genes that support bone formation. At 7 wks of hormone challenge the striking expansion of the null trabecular compartment had been added and bone histomorphometry indicated that both the KO and WT mice exhibited a diminished response to PTH consistent with previous observations on C57BL/6 mice (Iida-Klein, Zhou et al. 2002). However, starting at 3 wks of hormone challenge the KO mice exhibited an enhanced and sustained PTH-induced increase in serum osteocalcin. The significance of the 2-3 wk lag period required for distinguishing the difference in PTH-stimulated bone formation between the *Nmp4*-KO and WT mice remains to be elucidated. Does this delay represent the time necessary to dramatically expand the null bone-forming osteoblast

population? Further histomorphometric analysis at various time points throughout the treatment regimen is required to address this question.

Of particular significance was our discovery of an osteoclast phenotype in the *Nmp4*-KO mouse. The null mice had significantly higher serum CTX; more osteoclasts were recovered from *Nmp4*-KO marrow cultures than from WT cultures, and the null osteoclasts were more active as determined by in vitro resorption of dentin. Interestingly, PTH had a more significant impact on decreasing the osteoclast-covered bone surface in null mice without significantly lowering serum CTX, perhaps in part a consequence of the enhanced activity of the null osteoclasts. Despite the multiple lines of evidence suggesting higher bone resorption in the untreated nulls these mice are not osteopenic and in fact have a modestly enhanced skeleton, although the rate of bone accrual from 8-12 wks is marginally slower in the null animals. Femoral bone marrow-derived osteoblasts from *Nmp4*/*CIZ*-deficient mice exhibited an enhanced alkaline phosphatase expression and formed more mineralized nodules than wild-type osteoblasts (Morinobu, Nakamoto et al. 2005), suggesting in vivo that the null osteoblast outpaces the null osteoclast. Further study is required to determine if there is an increased rate of remodeling (activation frequency) with a positive bone balance in the untreated mice and if so, how this is achieved.

Although the in vivo mRNA expression profiles represent a composite of multiple marrow and bone cell types, the transiently enhanced expression of *c-fos*, *Fra-2*, and *Nfatc1* in the null mice may be part of the molecular mechanism contributing to the apparent increased number of osteoblasts and osteoclasts. *Fra-2* plays a significant role in chondrocyte differentiation and matrix production in embryonic and newborn mice (Karreth, Hoebertz et al. 2004) and in regulating the size of osteoclasts (Bozec, Bakiri et al. 2008).

The contribution of c-Fos to the PTH anabolic response involves both osteoblasts and osteoclasts; in the former it is part of the immediate-early gene response (Liang, Hock et al. 1999) and as such is critical for subsequent induction of select target genes. As a key regulator of bone cell growth and differentiation, c-Fos often interacts with RUNX2 (Qin, Raggatt et al. 2004). PTH stimulation of *Mmp-13* transcription in osteoblast-like cells requires the cooperative interaction between the c-Fos•c-Jun AP-1 complex and RUNX2 (D'Alonzo, Selvamurugan et al. 2002), and *Nmp4*/*CIZ* dampens this induction (Shah, Alvarez et al. 2004). Consequently, the heightened PTH-stimulated increase in osteoblast c-Fos activity in the *Nmp4*-KO mice may boost hormone transcriptional induction of some

genes supporting the anabolic response. The impact of *Nmp4/CIZ* on *c-fos* and *Fra-2* was specific within the context of the PTH-induced immediate-early response because we did not observe differences in other aspects of this gene program including *Nurr1*, a transcription factor participating in PTH-mediated osteoblast gene induction (Nervina, Magyar et al. 2006), *Mkp-1*, a phosphatase implicated in PTH-mediated osteoblast cell cycle arrest (Qin, Li et al. 2005), *JunD*, involved in osteoblast differentiation (Wagner 2010), or *Smad3* and *Lef1*, trans-acting proteins involved in coupling the PTH and Wnt signaling pathways in osteoblasts (Tobimatsu, Kaji et al. 2006).

In addition to its role as a PTH-responsive osteoblast transcription factor c-Fos is critical to osteoclastogenesis and plays a role in supporting the precursor cell's capacity to undergo differentiation (Boyle, Simonet et al. 2003). It fulfills this role in part by mediating the induction of *Nfatc1*, another key transcription factor that supports osteoclastogenesis and osteoblast development (Takayanagi 2007); the elevation of *c-fos* mRNA expression in the nulls may ultimately contribute to the enhanced *Nfatc1* expression in these mice. Additionally, c-Fos has multiple and complex roles in regulating osteoblast-derived signals that regulate osteoclastogenesis and mature osteoclast activity including the RANKL/OPG signaling axis by governing the transcriptional activity of the *Opg* gene in the osteoblast and by activating RANKL target genes in osteoclasts; c-Fos also activates the IFN- γ -driven RANKL negative feedback pathway in the osteoclast (Fu, Jilka et al. 2002, Takayanagi, Kim et al. 2002). The *Rankl/Opg* ratio was attenuated in the null mice, which achieved significance in the femur by 3 wks of treatment; perhaps this ultimately contributed some protective effect from the enhanced osteoclast activity. *Nmp4/CIZ* had negligible impact on the mRNA expression of other osteoclastogenic cytokines including *Mcp-1*, a cytokine involved in osteoclast recruitment (Li, Qin et al. 2007), *M-csf* and its receptor *c-fms* that activate the proliferation and survival of osteoclast precursors (Negishi-Koga and Takayanagi 2009). The significantly attenuated expression of the pro-apoptotic gene, *Bax*, in the null mice may contribute to a longer-lived osteoblast, critical to the PTH-induced anabolic mechanism (Bellido, Ali et al. 2003), but further studies are required to confirm this possibility.

Recent studies with *c-fos*-null animals indicate that interaction between immature osteoclasts and pre-osteoblasts may be necessary for an optimal response to intermittent PTH; specifically the osteoclast precursors support the differentiation of pre-osteoblasts (Koh, Demiralp et al. 2005, Zhao, Irie et al. 2006, Luiz de Freitas, Li et al. 2009). In one potential scenario this coupling is mediated by the bidirectional interaction between an

EphrinB2 ligand on the pre-osteoclast and the EphB4 receptor on the pre-osteoblast (Zhao, Irie et al. 2006, Luiz de Freitas, Li et al. 2009). Forward signaling from the osteoclast precursor to the pre-osteoblast enhances differentiation of the latter whereas reverse signaling suppresses osteoclast differentiation (Zhao, Irie et al. 2006). Therefore, PTH appears to activate both forward and reverse EphrinB-EphB4 signaling resulting in the enhancement of bone formation and the restraining of resorption (Luiz de Freitas, Li et al. 2009). This is consistent with the observed increased expression of EphB4 in the *Nmp4*-KO mice and the marginally enhanced ephrinB2 expression in these animals. Future osteoblast-osteoclast co-culture studies will be needed to investigate the potential impact of *Nmp4*/CIZ on the reciprocal regulation of these cells.

We propose that *Nmp4*/CIZ governs both the osteoblast and osteoclast cellular arms of the PTH-induced anabolic response by controlling the size, activity, and/or PTH-responsiveness of these cell populations in part via the modest suppression of several key transcription factors and receptors critical to the developmental and/or response pathways of both cells. The complex sequence of molecular and cellular events underlying *Nmp4*/CIZ regulation of bone remodeling remains to be elucidated. *Nmp4*/CIZ has been previously identified as an attractive potential therapeutic target for treating osteoporosis (Krane 2005), and the present finding that this protein not only regulates the osteoblast but also the osteoclast underscores this assertion.

TABLE 2-1: Real-time PCR primers from Assays-on-Demand™ (Applied Biosystems™, Foster City CA).

GENE (mRNA)		ABI Assay ID
<i>Alpl</i>	(Alkaline phosphatase)	Mm01187117_m1
<i>Bcl2</i>	(B-cell lymphoma 2)	Mm00477631_m1
<i>Bmp2</i>	(Bone morphogenic protein 2)	Mm01340178_m1
<i>c-fms</i>	(Colony stimulating factor 1 receptor [CSF1R])	Mm01266652_m1
<i>c-fos</i>	(FBJ murine osteosarcoma oncogene)	Mm00487425_m1
<i>Col1a1</i>	(Type I; pro-alpha1(I) chain)	Mm00801666_g1
<i>EphB4</i>	(Ephrin type-B receptor 4)	Mm01201157_m1
<i>EphrinB2</i>	(EPH-related receptor tyrosine kinase ligand 5)	Mm00438670_m1
<i>Fra-2</i>	(fos-related antigen 2)	Mm00484442_m1
<i>Igf-1</i>	(Insulin-like growth factor 1)	Mm0043559_m1
<i>JunD</i>	(Jun proto-oncogene related gene d)	Mm00495088_s1
<i>Lef1</i>	(Lymphoid enhancer-binding factor-1)	Mm00550265_m1
<i>M-csf</i>	(Macrophage colony stimulating factor 1)	Mm00432686_m1
<i>Mcp-1</i>	(Monocyte chemotactic protein-1)	Mm00441242_m1
<i>Mkp-1</i>	(MAPK phosphatase 1)	Mm00457274_g1
<i>Mmp-13</i>	(Matrix metalloproteinase 13)	Mm00439491_m1
<i>Nfatc1</i>	(nuclear factor of activated T-cells, cytoplasmic 1)	Mm012479445_m1
<i>Nurr-1</i>	(Nuclear receptor-related factor 1)	Mm00443056_m1
<i>Opg</i>	(Osteoprotegerin)	Mm00435452_m1
<i>Osterix</i>	(Sp7 transcription factor)	Mm00504574_m1
<i>Pthr1</i>	(Parathyroid hormone receptor 1)	Mm00441046_m1
<i>Pthrp</i>	(Parathyroid hormone-related peptide)	Mm00436057_m1
<i>Rage</i>	(receptor for advanced glycation endproducts)	Mm00545815_m1
<i>Rankl</i>	(Receptor activator for nuclear factor κ B ligand)	Mm00441908_m1
<i>Runx2</i>	(Runt-related transcription factor 2)	Mm00501578_m1
<i>Smad3</i>	(Sma- and Mad-related protein)	Mm01170760_m1
<i>Sost</i>	(Sclerostin)	Mm00470479_m1

TABLE 2-2A: PTH-induced improvements in femoral trabecular architecture were equivalent in WT and *Nmp4*-KO mice, after the first 2 wks of treatment. The WT and *Nmp4*-KO mice were treated with intermittent PTH or vehicle (number of mice/experimental group=6-7) for 2 wks. A two-factor ANOVA was used to evaluate the individual parameters. Units: Conn. D in mm⁻³, Tb N in mm⁻¹, Tb Th and Tb Sp in mm. (Geno=Genotype, Treat=Treatment, G x T= Genotype x Treatment interaction)

	WT		KO		2-WAY ANOVA p-value		
	<u>VEH</u>	<u>PTH</u>	<u>VEH</u>	<u>PTH</u>	<u>Geno</u>	<u>Treat</u>	<u>G x T</u>
BV/TV	0.016±0.001	0.042±0.012	0.019±0.007	0.047±0.017	0.3349	<0.0001	0.8654
Conn D	0.86±0.81	22.11±7.10	1.66±1.09	14.14±11.74	0.1904	<0.0001	0.1131
SMI	3.39±0.21	2.72±0.39	3.51±0.25	3.24±0.37	0.0170	0.0009	0.1197
Tb N	1.61±0.19	1.78±0.19	1.98±0.35	2.44±0.39	0.0002	0.0131	0.2100
Tb Th	0.043±0.002	0.056±0.004	0.042±0.003	0.052±0.005	0.1232	<0.0001	0.4117
Tb Sp	0.629±0.066	0.575±0.058	0.523±0.103	0.422±0.080	0.3048	0.0004	0.4783

TABLE 2-2B: Cortical architecture at the midshaft femur from WT and *Nmp4*-KO mice treated with vehicle or intermittent PTH for 2 wks (number of mice/experimental group=7-10). The parameters include cortical area (CA, mm²), marrow area (MA, mm²), and total area (TA, mm²) and the maximum, minimum, and polar moments of inertia (*I*_{MAX}, *I*_{MIN}, and *J*, respectively [mm⁴]). A two-factor ANOVA was used to evaluate the individual parameters.

	WT		KO		2-WAY ANOVA p-values		
	<u>VEH</u>	<u>PTH</u>	<u>VEH</u>	<u>PTH</u>	<u>Genotype</u>	<u>Treatment</u>	<u>G x T</u>
MA	1.40±0.08	1.34±0.07	1.39±0.09	1.39±0.13	0.5363	0.4618	0.4141
CA	0.98±0.03	1.04±0.06	1.01±0.07	1.08±0.07	0.1073	0.0067	0.6478
TA	2.38±0.09	2.38±0.11	2.40±0.13	2.47±0.17	0.2392	0.4539	0.4223
<i>I</i> _{MAX}	0.41±0.02	0.41±0.05	0.40±0.04	0.43±0.06	0.9661	0.2440	0.2649
<i>I</i> _{MIN}	0.21±0.02	0.23±0.02	0.23±0.02	0.26±0.03	0.0084	0.0382	0.6726
<i>J</i>	0.63±0.04	0.64±0.07	0.63±0.07	0.69±0.09	0.3048	0.1254	0.3670

TABLE 2-2C: Values for percent change (%Δ) BMD and BMC between 8 wks and 12 wks of age. Mice were challenged with vehicle or intermittent PTH for 2 wks (10-12 wks of age; number of mice/experimental group=6-7). The listed p-values were determined with a two-factor ANOVA. Abbreviations: WB (whole body), FM (femur), Sp (spine).

	WT		KO		2-WAY ANOVA p-values		
	<u>VEH</u>	<u>PTH</u>	<u>VEH</u>	<u>PTH</u>	<u>Gene</u>	<u>Treat</u>	<u>G x T</u>
%ΔWB BMD	5.27±3.0	10.28±2.83	6.18±3.6	9.04±2.81	0.8895	0.0032	0.3791
%ΔWB BMC	15.94±7.4	22.73±8.79	6.73±6.14	16.34±8.56	0.015	0.0116	0.6410
%ΔFm BMD	12.86±4.84	18.49±1.69	8.93±5.0	13.84±3.74	0.0113	0.0026	0.8220
%ΔFm BMC	29.71±11.7	36.0±11.6	11.74±8.9	23.59±8.7	0.0009	0.0332	0.4950
%ΔTb BMD	7.25±3.5	14.43±4.90	5.98±4.73	8.64±4.86	0.0545	0.0096	0.2086
%ΔTb BMC	9.70±7.20	24.84±6.07	6.67±4.53	11.61±8.68	0.0045	0.0007	0.0608
%ΔSp BMD	6.22±7.26	12.93±6.41	9.57±11.24	10.99±9.44	0.8366	0.2421	0.4423
%ΔSP BMD	7.60±8.61	15.11±11.39	6.59±15.10	10.96±8.96	0.5635	0.1903	0.7246

TABLE 2-2D: Bone histomorphometry of the distal femur from WT and *Nmp4*-KO mice treated with intermittent PTH or vehicle for 7 wks (number of mice/experimental group=5-6). The parameters include mineral apposition rate (MAR), mineralizing surface/bone surface (MS/BS), bone formation rate (BFR), the TRAP-stained surface to bone surface (TRAP+ S/BS), and the number of TRAP-stained cells on the bone surface (TRAP+ N/BS). A two-factor ANOVA was used to evaluate the impact of genotype and treatment on the individual parameter. A Tukey's HSD post hoc test was used to determine differences between treatment groups if a significant genotype x treatment interaction was indicated (TRAP+ S/BS). Groups not connected by the same letter are significantly different.

	WT		KO		2-WAY ANOVA p-values		
	<u>VEH</u>	<u>PTH</u>	<u>VEH</u>	<u>PTH</u>	<u>Gene</u>	<u>Treat</u>	<u>G x T</u>
MAR ($\mu\text{m}/\text{day}$)	2.80 \pm 0.20	3.30 \pm 0.21	2.88 \pm 0.22	3.19 \pm 0.16	0.8288	<0.0001	0.2628
MS/BS (%)	0.53 \pm 0.08	0.49 \pm 0.05	0.52 \pm 0.03	0.50 \pm 0.04	0.9331	0.0507	0.3275
BFR ($\mu\text{m}^2/\mu\text{m}/\text{day}$)	1.49 \pm 0.08	1.61 \pm 0.	1.49 \pm 0.16	1.59 \pm 0.15	0.9135	0.0905	0.9175
Trap ⁺ S/BS (%)	0.37 \pm 0.03	0.36 \pm 0.09	0.48 \pm 0.07	0.33 \pm 0.12	0.2420	0.0383	0.0549
						<u>Tukey's HSD</u>	
						KO VEH	A
						WT VEH	A B
						WT PTH	A B
						KO PTH	B
Trap ⁺ N/BS (mm^{-1})	0.45 \pm 0.06	0.41 \pm 0.11	0.60 \pm 0.10	0.41 \pm 0.10	0.0863	0.0110	0.0918

TABLE 2-3A: Comparative femoral RNA expression of WT and Nmp4-KO mice treated with PTH or vehicle for 2 wks (number of mice/experimental group=6-9) or 3 wks (number of mice/experimental group=6) and harvested 1 hr after the last injection. The listed p-values were determined with a two-factor ANOVA. A Tukey's HSD post hoc test was used to determine differences between treatment groups if a significant genotype x treatment interaction was indicated. Groups not connected by the same letter are significantly different.

	WT		KO		2-WAY ANOVA p-values		
	<u>VEH</u>	<u>PTH</u>	<u>VEH</u>	<u>PTH</u>	<u>Gene</u>	<u>Treat</u>	<u>G x T</u>
c-fos (2wks)	0.73±0.25	7.94±1.00	1.87±0.71	12.04±2.31	<0.001	<0.0001	0.0121
						<u>Tukey's HSD</u>	
						KO VEH	A
						WT VEH	B
						WT PTH	C
						KO PTH	C
c-fos (3wks)	1.04±0.31	8.73±2.07	1.05±0.31	8.33±1.85	0.7380	<0.0001	0.7235
Fra-2 (2wks)	0.72±0.15	4.25±0.50	0.96±0.13	5.56±0.97	0.0028	<0.0001	0.0301
						<u>Tukey's HSD</u>	
						KO VEH	A
						WT VEH	B
						WT PTH	C
						KO PTH	C
Fra-2 (3wks)	1.01±0.12	5.32±1.23	1.03±0.18	4.72±0.98	0.3905	<0.0001	0.3441
Nfatc1 (2wks)	1.03±0.43	1.46±0.31	1.48±0.43	1.96±0.27	0.0051	0.0074	0.8659
Nfatc1 (3wks)	1.00±0.11	1.76±0.48	1.02±0.27	1.41±0.26	0.2008	0.0002	0.1699
EphB4 (2wks)	0.80±0.16	1.27±0.12	0.98±0.22	1.41±0.21	0.0466	<0.0001	0.7544
EphB4 (3wks)	1.01±0.16	1.78±0.39	0.95±0.33	1.74±0.40	0.7131	<0.0001	0.9257
EphrinB2 (2)	0.75±0.18	5.16±0.68	1.19±0.27	5.87±1.23	0.0658	<0.0001	0.6555
EphrinB2 (3)	1.02±0.24	6.85±2.82	1.01±0.32	6.24±1.05	0.6209	<0.0001	0.6355
Opg (2wks)	0.85±0.14	0.82±0.14	1.23±0.41	0.97±0.21	0.0150	0.1625	0.2862
Opg (3wks)	1.03±0.29	1.19±0.33	1.13±0.26	1.34±0.26	0.2943	0.1372	0.8389
Rankl (2wks)	0.96±0.11	21.34±6.20	1.19±0.59	16.75±3.43	0.1492	<0.0001	0.1124
Rankl (3wks)	1.04±0.34	13.72±4.58	0.82±0.26	11.04±1.79	0.1663	<0.0001	0.2367
Rankl/Opg (2)	1.14±0.18	27.39±12.45	0.94±0.23	17.84±5.60	0.0954	<0.0001	0.1092
Rankl/Opg (3)	1.04±0.18	11.53±2.04	0.73±0.22	8.60±2.38	0.0207	<0.0001	0.0558

TABLE 2-3B: Comparative femoral RNA expression of WT and Nmp4-KO mice treated with PTH or vehicle for 2 wks (number of mice/experimental group=6-9) and harvested 1 hr or 24 hr after the last injection. The listed p-values were determined with a two-factor ANOVA. A Tukey's HSD post hoc test was used to determine differences between treatment groups if a significant genotype x treatment interaction was indicated. Groups not connected by the same letter are significantly different.

	WT		KO		2-WAY ANOVA p-values		
	<u>VEH</u>	<u>PTH</u>	<u>VEH</u>	<u>PTH</u>	<u>Gene</u>	<u>Treat</u>	<u>G x T</u>
1hr post-injection							
M-csf	1.13±0.72	2.14±0.70	1.19±0.09	2.87±0.53	0.1056	<0.0001	0.1665
Mcp-1	0.79±0.20	2.60±0.90	0.99±0.24	2.61±0.70	0.6657	<0.0001	0.7156
Bcl2	0.96±0.12	1.02±0.14	1.06±0.20	1.03±0.08	0.2997	0.7913	0.4563
Bax	1.02±0.25	0.91±0.14	0.69±0.12	0.71±0.04	0.0005	0.4604	0.3321
Nurr1	0.69±0.22	56.37±6.56	2.06±1.49	58.62±14.05	0.5750	<0.0001	0.8914
Mkp-1	0.83±0.09	2.31±0.90	1.13±0.48	1.95±0.32	0.8708	<0.0001	0.1022
JunD	0.80±0.16	0.94±0.16	0.78±0.19	1.10±0.16	0.3366	0.0036	0.2206
Smad3	0.78±0.12	1.97±0.34	1.05±0.26	2.14±0.63	0.1736	<0.0001	0.7403
Lef1	0.99±0.19	1.52±0.30	1.08±0.21	1.36±0.27	0.7196	0.0006	0.2293
Rage	0.87±0.16	0.74±0.13	1.07±0.35	0.72±0.27	0.3655	0.0261	0.2829
24hr post-injection							
Runx2	0.86±0.21	1.45±0.34	0.59±0.23	1.35±0.84	0.2960	0.0007	0.6482
Osterix	0.63±0.20	1.61±0.48	0.49±0.37	1.67±0.96	0.8385	<0.0001	0.6460
Col1a1	0.92±0.14	2.35±0.65	0.75±0.49	2.70±2.45	0.8424	0.0017	0.5964
Alpl	0.96±0.18	2.95±0.69	0.81±0.47	2.42±1.63	0.3286	<0.0001	0.5814
Mmp13	0.73±0.21	1.05±0.28	0.51±0.22	1.23±0.61	0.3987	0.0007	0.3997
Sost	1.17±0.22	1.79±0.31	1.15±0.38	1.59±0.33	0.3328	<0.0001	0.4419
Bmp2	1.01±0.14	1.41±0.24	0.91±0.26	1.15±0.39	0.0898	0.0036	0.4394
Pthr1	0.86±0.23	1.59±0.40	0.68±0.28	1.38±0.68	0.2223	<0.0001	0.9071
Pthrp	0.75±0.18	1.10±0.44	0.89±0.44	1.00±0.44	0.9024	0.1154	0.4214

TABLE 2-3C: Comparative tibial RNA expression of WT and Nmp4-KO mice treated with PTH or vehicle for 3 wks (number of mice/experimental group=6) and harvested 1 hr after the last injection. The listed p-values were determined with a two-factor ANOVA.

	WT		KO		2-WAY ANOVA p-values		
	<u>VEH</u>	<u>PTH</u>	<u>VEH</u>	<u>PTH</u>	<u>Gene</u>	<u>Treat</u>	<u>G x T</u>
c-fos	1.05±0.39	9.05±3.57	1.66±1.19	10.65±3.05	0.2775	<0.0001	0.6243
Fra-2	1.02±0.23	4.62±1.63	1.28±0.31	7.21±3.08	0.0604	<0.0001	0.1178
Nfatc1	1.02±0.20	1.42±0.60	1.36±0.45	2.00±0.53	0.0262	0.0136	0.5470
EphB4	1.02±0.22	1.80±0.75	1.25±0.34	2.07±0.34	0.2372	0.0010	0.9216
EphrinB2	1.08±0.45	5.13±3.31	1.22±0.31	7.40±2.19	0.1551	<0.0001	0.2065
Opg	1.03±0.25	1.4±0.63	1.07±0.23	1.57±0.40	0.5314	0.0181	0.6969
Rankl	1.01±0.18	10.51±3.46	0.79±0.18	11.19±3.61	0.8226	<0.0001	0.6618
Rankl/Opg	1.07±0.49	7.98±1.64	0.76±0.16	7.07±0.75	0.1248	<0.0001	0.4467

FIGURE 2-1 (A-C)

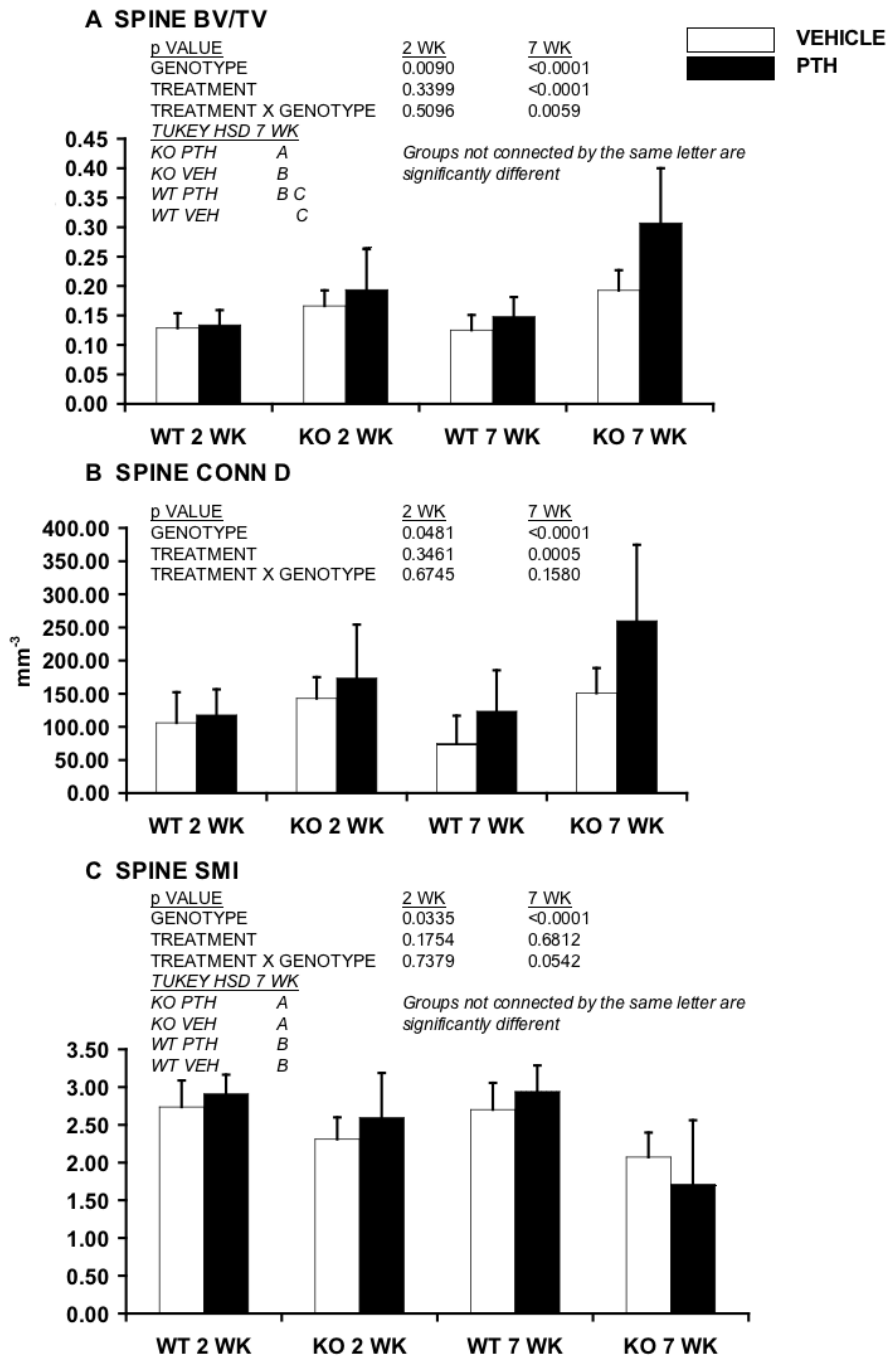


Figure 2-1 (D-F)

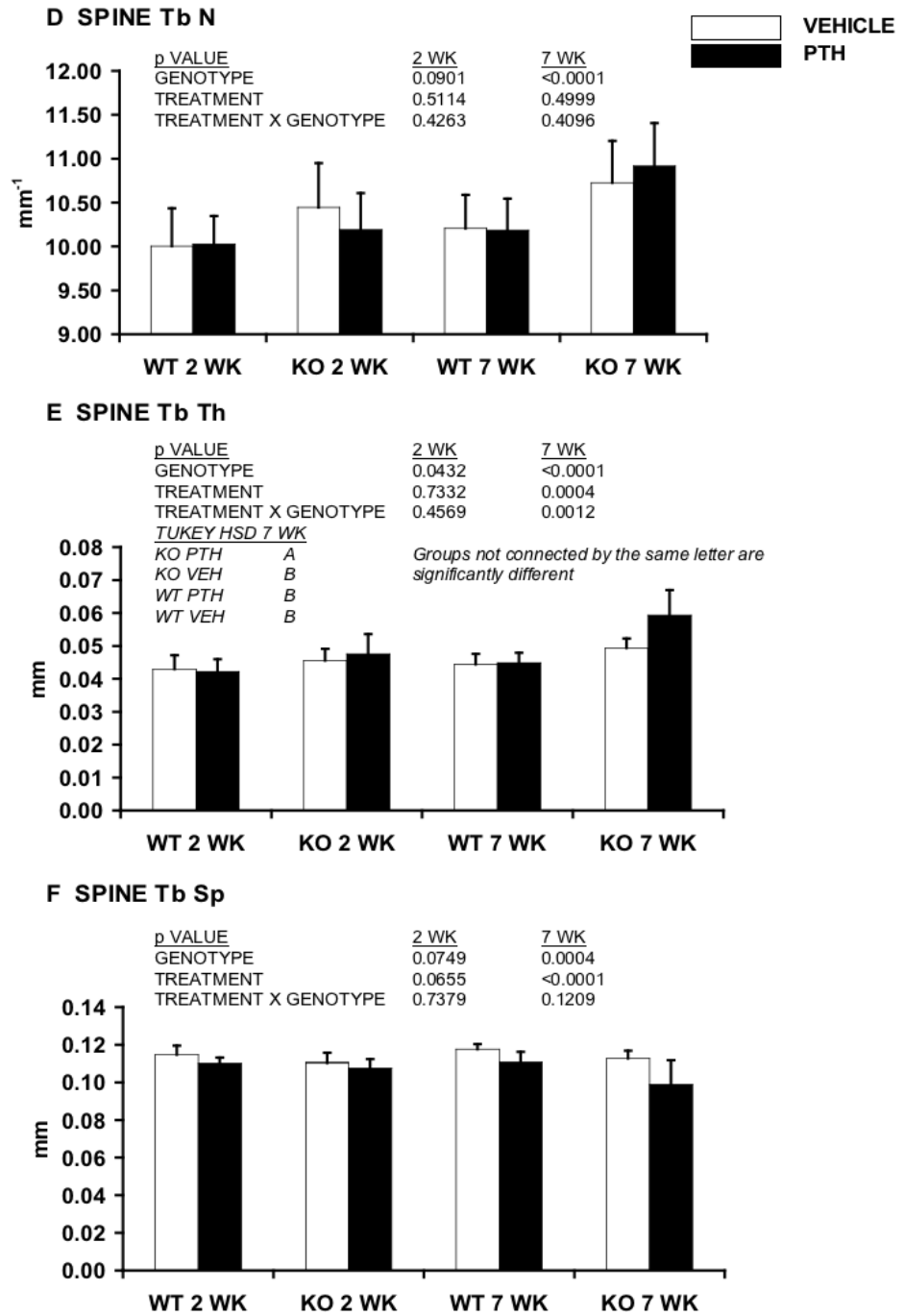


Figure 2-1 (G)

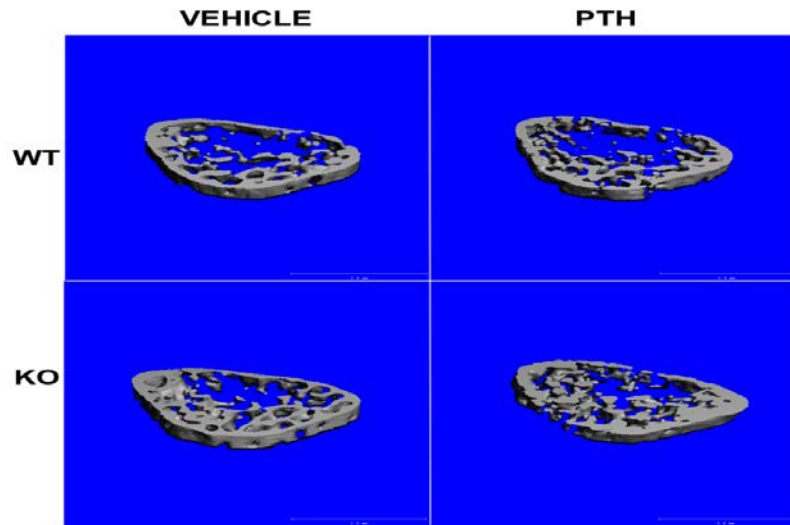


Figure 2-1: Disabling *Nmp4* enhanced PTH responsiveness of vertebral cancellous bone. Micro-CT-acquired vertebral (L5) trabecular architecture including (A) BV/TV, %; (B) Conn D, mm^{-3} ; (C) SMI, (D) Tb N mm^{-1} , (E) Tb Th mm, (F) Tb Sp mm was compared between WT and *Nmp4*-KO mice that had been treated with intermittent hPTH(1-34) 30 $\mu\text{g}/\text{kg}/\text{day}$ or vehicle for 7 wks (number of mice/experimental group=11-12). To evaluate the early hormone response we compared bones from WT and *Nmp4*-KO mice that had been treated with intermittent PTH or vehicle for 2 wks using the same experimental design (number of mice/experimental group=5-7). No improvement was observed after 2 wks of intermittent PTH treatment in either the WT or null animals (A-F). There was a genotype effect for BV/TV, Conn D, SMI, and Tb Th (A, B, C, and E, respectively) consistent with the enhanced trabecular architecture of the null mice, regardless of treatment. (G) μCT images of vertebral trabecular bone from WT and *Nmp4*-KO mice that had been treated with intermittent PTH or vehicle for 7 wks, Scale bar=1mm. Data is presented as average \pm SD. The listed p-values were determined with a two-factor ANOVA. A Tukey's HSD post hoc test was used to determine differences between the treatment groups if a significant genotype x treatment interaction was indicated.

Figure 2-2 A-C

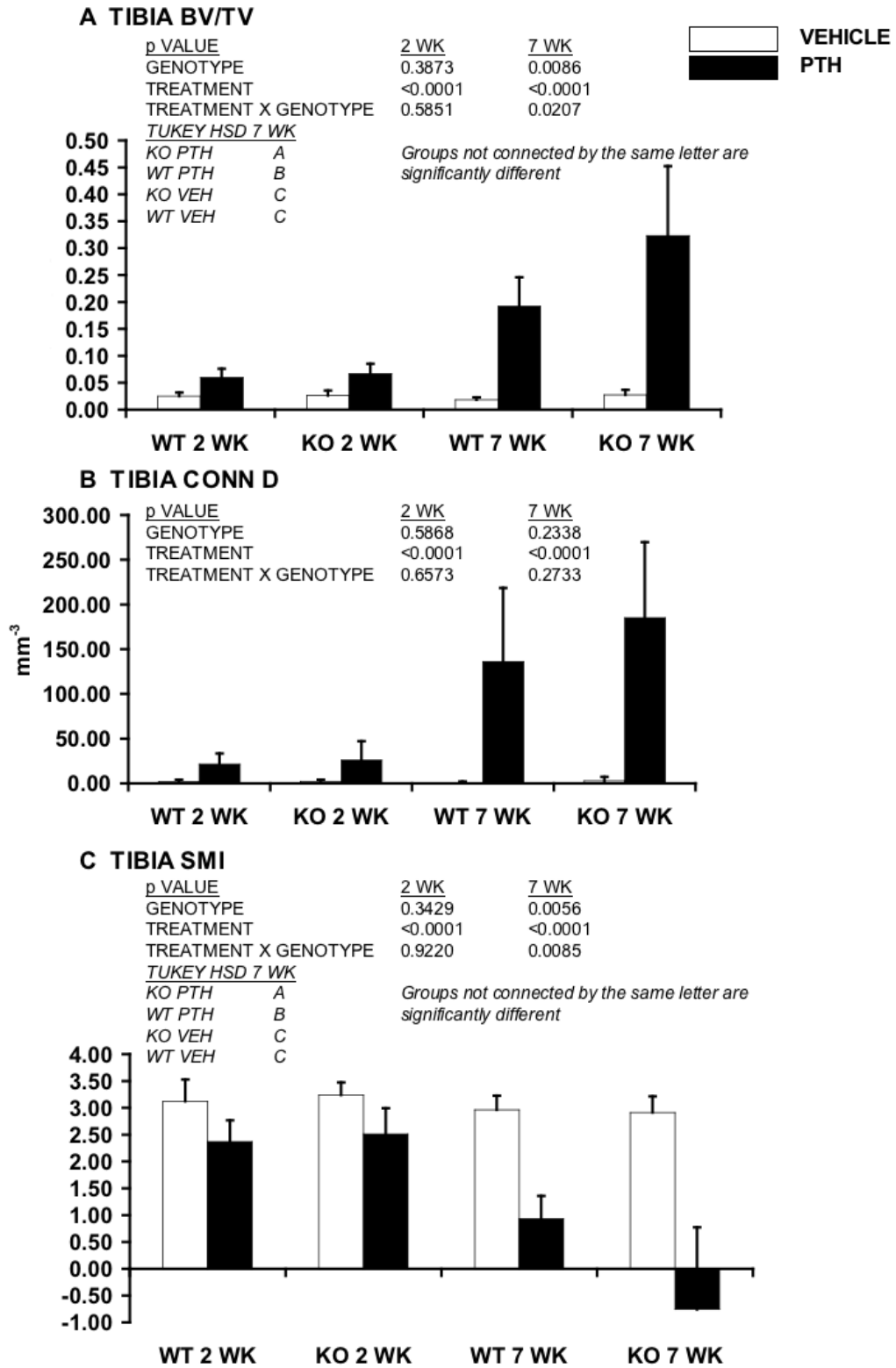


Figure 2-2 D-F

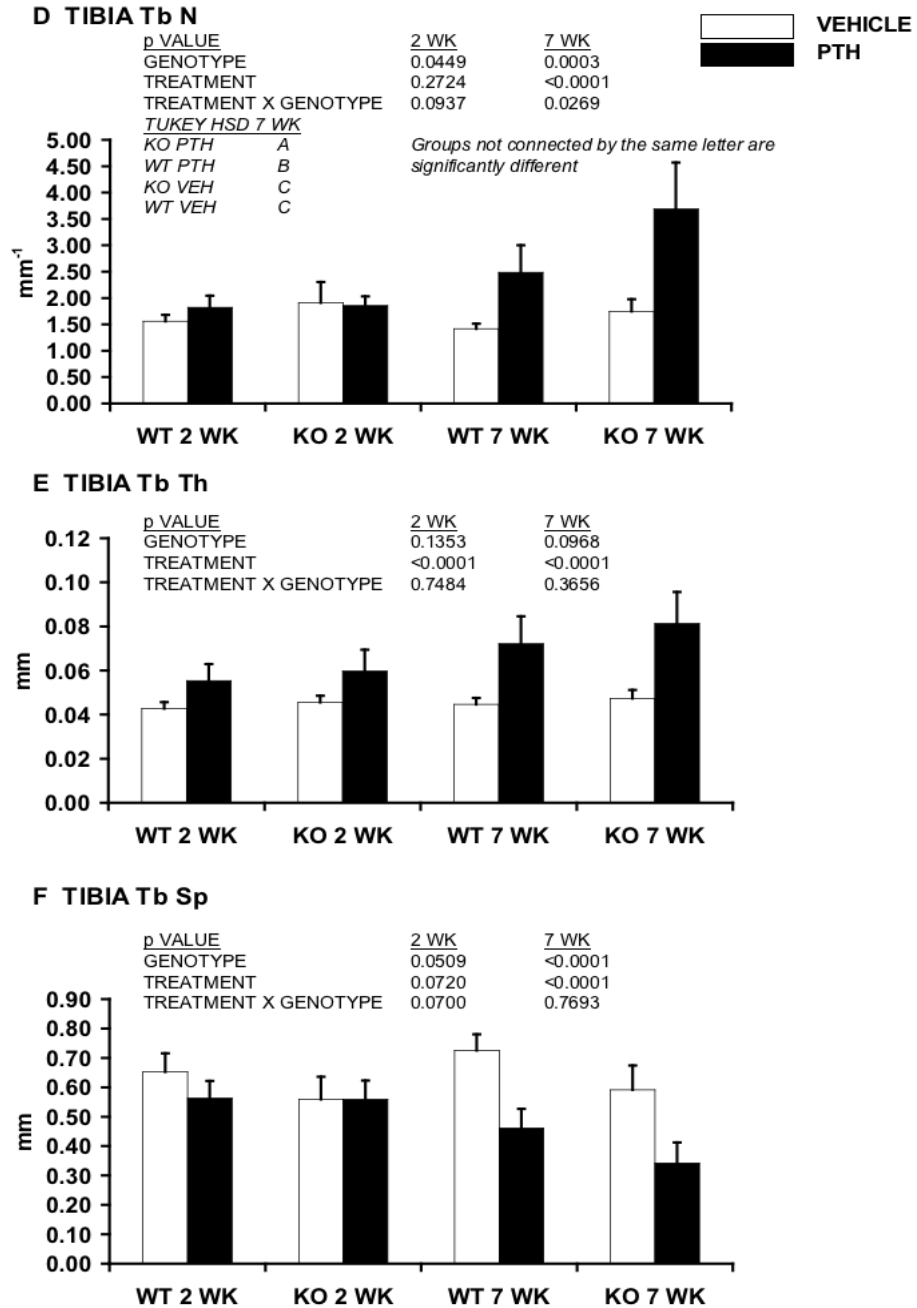


Figure 2-2G

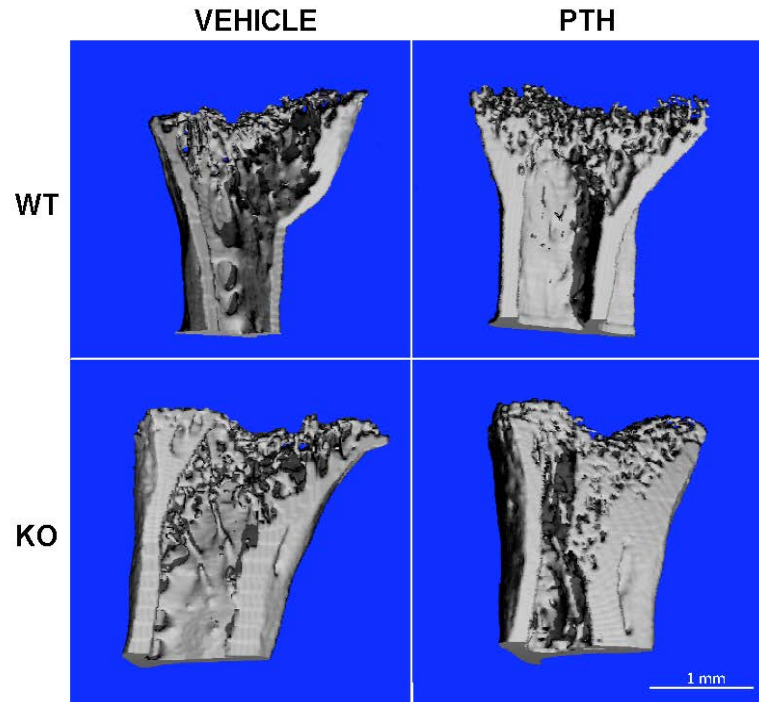


Figure 2-2: *Nmp4*-KO mice exhibited an enhanced PTH-induced increase in tibial trabecular bone. Micro-CT-acquired tibial trabecular architecture including (A) BV/TV, %; (B) Conn D, mm⁻³; (C) SMI, (D) Tb N mm⁻¹, (E) Tb Th mm, (F) Tb Sp mm was compared between WT and *Nmp4*-KO mice that had been treated with intermittent PTH or vehicle for 7 wks (number of mice/experimental group=8). To evaluate the early hormone response we compared bones from WT and *Nmp4*-KO mice that had been treated with intermittent PTH or vehicle for 2 wks (number of mice/experimental group=7-9). Both genotypes showed equal hormone-induced improvement of tibial (A) BV/TV, (B) Conn D, (C) SMI, and (E) Tb Th during the initial 2 wks of treatment. There was a genotype effect for (D) Tb N and (F) Tb Sp indicating enhanced aspects of tibial architecture in the null mice at 12 wks of age irrespective of treatment. (G) μ CT images of tibial trabecular bone from WT and *Nmp4*-KO mice that had been treated with intermittent PTH or vehicle for 7 wks, Scale bar=1mm. The listed p-values were determined with a two-factor ANOVA. A Tukey's HSD post hoc test was used to determine differences between the treatment groups if a significant genotype x treatment interaction was indicated.

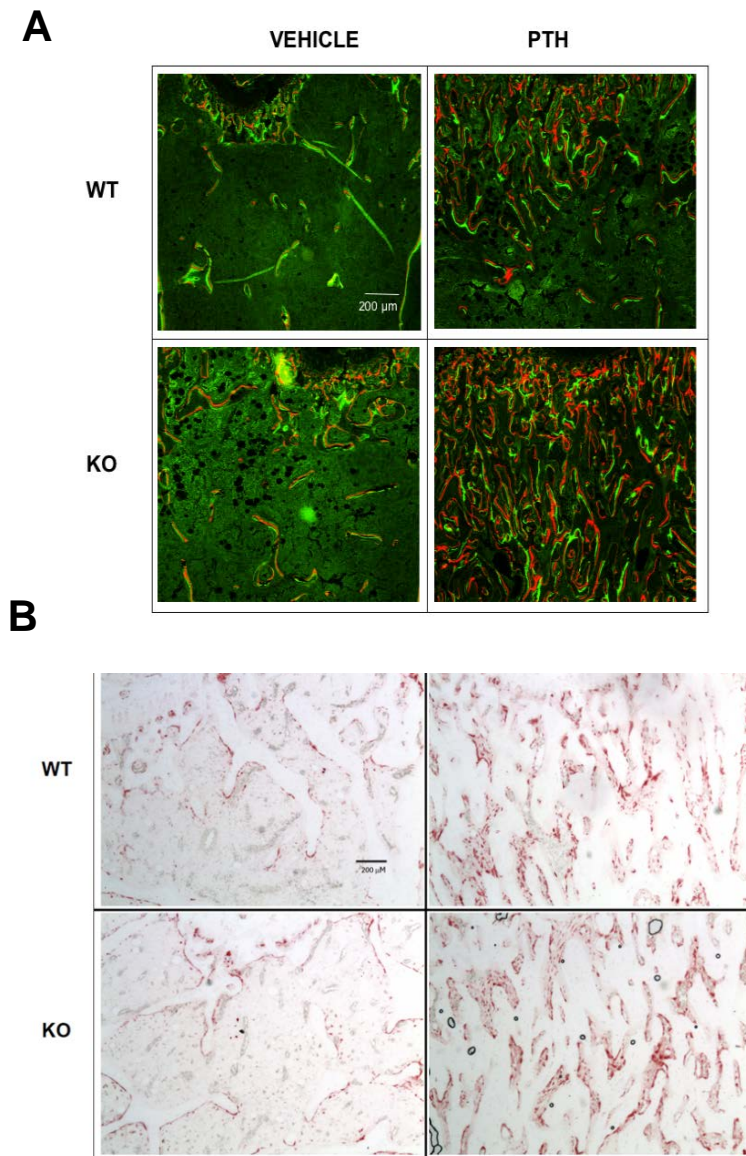


Figure 2-3: [A] PTH-induced improvements in femoral trabecular architecture were enhanced in *Nmp4*-KO mice, after 7 wks of treatment. The femoral tissue sections were obtained from WT and *Nmp4*-KO mice treated with intermittent PTH or vehicle for 7 wks (number of mice/experimental group=5-6). Additionally, animals were administered by intraperitoneal injection calcein green (20mg/kg) and alizarin red (25mg/kg) 6 days and 3 days before euthanasia, respectively. [B] Sections were stained for tartarate resistant acid-phosphatase (TRAP) to evaluate osteoclast number and surface. Histological sections were prepared as described in the Materials and Methods. Scale bar=200 μm

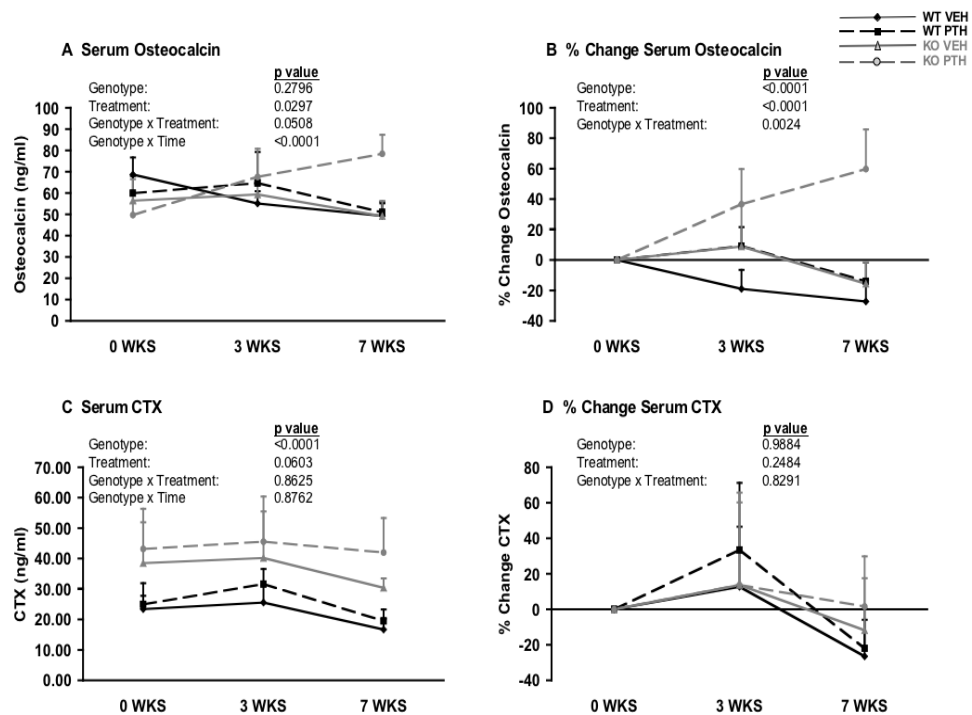


Figure 2-4: PTH-treated *Nmp4*-KO mice exhibited strikingly distinct serum chemistries from the WT animals. Whole blood was collected and serum separated from WT and *Nmp4*-KO mice treated with intermittent PTH or vehicle (number of mice/experimental group=6-7) at baseline just prior initiation of treatment, at 3 wks of treatment, and at 7 wks of treatment. (A) The raw longitudinal serum osteocalcin concentrations showed no genotype effect, but revealed a significant treatment effect, a genotype x treatment interaction and a genotype x time interaction indicating that the WT and null mice had equivalent baseline values but that the *Nmp4*-KO had an enhanced response to hormone and a higher rate of increase over the experimental time period. (B) The % change data confirmed the raw longitudinal data revealing a significant genotype effect (higher rate of osteocalcin increase in the nulls), a treatment effect, and a genotype x treatment interaction over the experimental period. (C) The raw longitudinal serum CTX concentrations showed a genotype effect, but no significant treatment effect, no genotype x treatment interaction and no genotype x time interaction. (D) The % change CTX data showed no significant responsiveness to hormone treatment in WT and null mice. The listed p-values were determined with a repeated-measures MANOVA (longitudinal data) or a two-factor ANOVA (% change data).

CHAPTER 3

DISABLING NMP4 INCREASES MESENCHYMAL STEM CELL AND OSTEOPROGENITOR FREQUENCY IN MICE RENDERING ANIMALS HYPER- RESPONSIVE TO ANABOLIC BONE AGENTS

*He Y¹, *Childress P², Hood M Jr²., Alvarez, M², Kacena MA³, Hanlon M², McKee B²,
Bidwell JP², Yang FC¹

1. Department of Pediatrics, Indiana University School of Medicine (IUSM), Indianapolis, IN 46202.
2. Department of Anatomy and Cell Biology, (IUSM).
3. Department of Orthopaedic Surgery, IUSM.

*These authors contributed equally to this work.

**Material in this Chapter was published in:
Stem Cells and Development February 1, 2013 vol.22, issue 3, pages 492-500.**

ABSTRACT:

Parathyroid hormone (PTH) anabolic osteoporosis therapy is intrinsically limited by unknown mechanisms. We previously showed that disabling the transcription factor *Nmp4/CIZ* in mice expanded this anabolic window while modestly elevating bone resorption. This enhanced bone formation requires a lag period to materialize. Wild type (WT) and *Nmp4*-knockout (KO) mice exhibited equivalent PTH-induced increases in bone at 2wks of treatment but by 7wks the null mice showed more new bone. At 3wks treatment serum osteocalcin, a bone formation marker, peaked in WT mice but continued to increase in null mice. To determine if 3wks when the addition of new bone diverges is and to investigate its cellular basis, we treated 10-wk-old *null* and WT animals with human PTH (1-34) [30 µg/kg/day] or vehicle before analyzing femoral trabecular architecture and bone marrow (BM) and peripheral blood (PBL) phenotypic cell profiles. PTH-treated *Nmp4*-KO mice gained over 2-fold more femoral trabecular bone than WT by 3wks. There was no difference between genotypes in BM cellularity or profiles of several blood elements. However, the KO mice exhibited a significant elevation in CFU-F cells, CFU-F^{ALK PHOS+} cells (osteoprogenitors), and a higher percentage of CFU-F^{ALK PHOS+} cells/CFU-F cells consistent with an increase in CD45-/CD146+/CD105+/nestin+ mesenchymal stem cell frequency. Null BM exhibited a 2-fold enhancement in CD8+ T cells known to support osteoprogenitor differentiation and a 1.6-fold increase in CFU-GM colonies (osteoclast progenitors). We propose that *Nmp4/CIZ* limits the PTH anabolic window by restricting the number of BM stem, progenitor, and blood cells that support anabolic bone remodeling.

INTRODUCTION:

Anabolic therapy is the preferred pharmacological intervention for osteoporosis (Trivedi, Goswami et al. 2010) and PTH is the only FDA-approved drug that adds bone to the osteoporotic skeleton; however, its bone-forming activity, or “anabolic window” is intrinsically limited to about two years, thereafter falling to baseline (Cusano and Bilezikian, Bilezikian 2008, Cusano and Bilezikian 2010). Therefore, PTH is not approved as a long-term osteoporosis therapy and its use is indicated only for those patients who are at a high risk of fractures or who are unresponsive to other available therapies (Silverman and Christiansen 2012).

While the mechanisms regulating the extent of the PTH anabolic window are unknown, we demonstrated that disabling the transcription factor nuclear matrix protein 4/cas interacting zinc finger protein (*Nmp4/CIZ*) in mice significantly extends and augments PTH bone-forming capacity; treatment of WT and *Nmp4*-KO mice with intermittent PTH for 7wks resulted in significant increases in serum osteocalcin, a marker for bone formation, but these serum profiles as a function of time were strikingly different (Robling, Childress et al. 2009, Childress, Philip et al. 2011). In the WT mice, serum osteocalcin peaked at 3wks of treatment and returned to baseline by 7wks of hormone administration (Childress, Philip et al. 2011). However, in the null mice, this PTH-induced surge in serum osteocalcin exceeded that observed in the WT mice and was still climbing at the end of the 7wk treatment regimen (Childress, Philip et al. 2011). Consistent with this sustained serum osteocalcin surge, at the end of the 7wk treatment period the null mice had gained significantly more femoral, vertebral, and tibial trabecular bone than WT mice while maintaining robust increases in cortical bone (Robling, Childress et al. 2009, Childress, Philip et al. 2011). These enhanced increases in cancellous bone in the *Nmp4*-KO skeleton all showed significant treatment x genotype interactions, thus demonstrating that *Nmp4/CIZ* suppresses PTH-stimulated anabolism (Robling, Childress et al. 2009, Childress, Philip et al. 2011).

When in the PTH treatment regimen does bone formation in the *Nmp4*-KO mice eclipse WT growth and what sustains this extended and enhanced anabolic activity? The WT and *Nmp4*-KO mice exhibited equivalent PTH-induced increases in trabecular bone during the first 2wks of treatment, however, at this treatment point femoral mRNA profiles revealed a transient enhanced increase in PTH-stimulated *c-fos* and *Fra-2* expression in the null mice as well as an elevated expression of *Nfatc1* in these animals (Childress, Philip et al. 2011). Although these transcription factors mediate numerous functions within

the context of bone, this is consistent with an enhanced PTH-induced increase in mesenchymal stem cell self-renewal and/or recruitment of null osteoblasts and osteoclasts into the anabolic window (Qin, Tamasi et al. 2005, Satija, Gurudutta et al. 2007, Bozec, Bakiri et al. 2008). Interestingly, the untreated *Nmp4*-KO mice had a modest but significantly elevated bone mineral density and bone mineral content compared to WT animals (Robling, Childress et al. 2009) despite modestly elevated levels of serum C-terminal telopeptides of type I collagen (CTX), a marker for bone resorption. The *Nmp4*-KO bone marrow (BM) yielded approximately 1.8-fold more osteoclasts in vitro compared to WT marrow and the null osteoclasts were significantly more active than their WT counterparts (Childress, Philip et al. 2011). Therefore, bone formation was exceeding resorption but how this occurred was not clear (e.g., osteoblast-osteoclast coupling (Kular, Tickner et al. 2012) and/or intrinsic differences in stem and progenitor pools that support bone formation or resorption).

To address whether the enhanced PTH-stimulated addition of trabecular bone in the *Nmp4*-KO mice is coincident with the initial surge in the serum osteocalcin and to determine the cellular basis of this sustained enhanced anabolic activity, we treated WT and *Nmp4*-KO female mice with intermittent PTH for 3 wks before harvesting femurs, femoral BM, and peripheral blood (PBL). Our data reveal that the *Nmp4*-KO mice show significantly enhanced PTH-stimulated addition of trabecular bone at 3wks of hormone treatment and that *Nmp4* has a profound regulatory role in BM population dynamics. Disabling this transcription factor results in alterations in stem, progenitor, and blood cell populations that accommodate the prolongation of the PTH anabolic window while maintaining bone remodeling. These data reveal novel aspects of how the PTH anabolic window is regulated and have implications for a novel adjuvant osteoporosis therapy.

MATERIALS AND METHODS:

Mice: *Nmp4*-KO mice, backcrossed onto a C57BL/6J background for 6-7 generations (Robling, Childress et al. 2009, Childress, Philip et al. 2011), and their WT littermates were used for these studies. Our local Institutional Animal Care and Use Committee approved all experiments and procedures involving the production and use of the mice described in this investigation.

PTH treatment: Before initiating hormone treatment 8 wk-old female WT and *Nmp4*-KO mice were given 100 μ l sterile saline by subcutaneous (sc) injection once daily to habituate them to handling. At 10 wks of age, animals were sorted into four treatment groups based on equivalent mean-group-body weight. These four groups included 1) vehicle-treated WT; 2) PTH-treated WT; 3) vehicle-treated *Nmp4*-KO and 4) PTH-treated *Nmp4*-KO mice. Experimental animals were injected sc with human PTH 1-34 (hPTH(1-34), Bachem Bioscience Inc, PA) at 30 μ g/kg/day, daily or vehicle control (0.2% BSA/0.1% 1.0 mM HCl in saline, Abbott Laboratory, North Chicago, IL) for 3 weeks. In a separate experiment, the BM of untreated female WT and *Nmp4*-KO mice (13wks of age) was harvested to compare multipotent mesenchymal stem cell (CD45-/CD146+/CD105+/Nestin+) frequency.

CFU-F^{ALK^{PHOS}+} assay (Nishida, Yamaguchi et al. 1994): BM was flushed from femurs, single cell suspensions prepared, and cells were seeded into 6-well plates at an initial density of 1×10^6 cells/well. Each culture well contained 2 ml of complete α -MEM medium supplemented with 100 IU/ml penicillin, 100 μ g/ml streptomycin, 25 μ g/ml amphotericin, 2 mM L-glutamine (Gibco BRL, Grand Island, NY), ascorbic acid (50 μ g/ml, Sigma), and 10% fetal bovine serum (FBS; Sigma). Medium was changed every two days for 14 days. Subsequently, cells were fixed and stained for alkaline phosphatase using a Sigma-Aldrich Alkaline Phosphatase Staining Kit and then counted for colony forming units-fibroblastic/alkaline phosphatase+ (CFU-F^{ALK^{PHOS}+}). Colonies were defined as positive staining with 25 or more cells per colony. After counting CFU-F^{ALK^{PHOS}+} colonies, the cells were stained with crystal violet and all colonies were counted for total CFU-F.

Flow cytometry: Whole BM was isolated by flushing the femurs of experimental mice with α -MEM supplemented with 10% FBS. PBL was collected from the mice by cardiac puncture. The red blood cells (RBCs) were lysed with RBC lysis buffer (Qiagen, Valencia,

CA) before the PBL and BM was processed for flow cytometric analysis. All antibodies for flow cytometry were purchased from BD Biosciences (San Jose, CA). Stained samples were analyzed on an FACS Calibur (BD Biosciences) and results were quantified using FlowJo Version 8.8.6 software (TreeStar Inc, Ashland OR).

Clonogenic assays: Colony-forming units (CFU-Cs) were assayed as previously described (Yang, Watanabe et al. 1998). Briefly, 2.5×10^4 BM mononucleated cells (BMMNCs) or 25 μ l PBL were seeded onto a 35-mm gridded dish containing methylcellulose and murine stem cell factor (SCF, 100ng/mL), murine granulocyte-macrophage colony stimulating factor (GM-CSF, 10ng/mL), murine interleukin 3 (IL3, 5ng/mL), murine recombinant macrophage-colony stimulating factor (M-CSF, 10 ng/mL) and human erythropoietin (Epo, 4 U/mL) for 7 days at 37°C in a 5% CO₂ incubator. Colonies were scored using an inverted light microscope. All cytokines were purchased from PeproTech (Rocky Hills, NC).

Hemavet analysis: PBL was collected from the WT and *Nmp4-KO* mice and processed for blood cell enumeration using the Hemavet 950 FS according to the manufacturer's instructions (Drew Scientific, Dallas, TX).

Micro computed tomography (μ CT): After euthanasia, a 2.6-mm span ($\sim 5 \text{ mm}^3$ of medullary space) of the distal femoral metaphysis was scanned in 70% ethanol on a desktop μ CT (μ CT 35; Scanco Medical AG, Bassersdorf, Switzerland) at 10 μ m resolution using 55-kVp tube potential and 400-msec integration time, to measure trabecular three-dimensional morphometric properties as previously described (Niziolek, Murthy et al. 2009). From the 3D constructs, trabecular bone volume per total volume (BV/TV, %), connectivity density (Conn.D, mm^{-3}), structure model index (SMI), trabecular number (Tb.N, mm^{-1}), trabecular thickness (Tb.Th, mm), and spacing (Tb.Sp, mm) were calculated using the Scanco software.

Statistical analysis: The program JMP version 7.0.1 (SAS Institute, Cary, NC) was used to process all statistical evaluations. We employed a two-way ANOVA for the PTH studies using genotype and treatment as the independent variables. If a genotype x treatment interaction was indicated, the data were analyzed by a Tukey HSD post hoc test to determine significant differences between the experimental groups. Statistical significance was set at $p \leq 0.01$ to guard against type I errors. A separate experiment was conducted

using a distinct group of our experimental mice for the purpose of comparing the frequency of multipotent mesenchymal stem cells (CD45-/CD146+/CD105+/Nestin+) in untreated female WT and *Nmp4*-KO mice. These data were analyzed with a two-sample *t*-test, assuming unequal variances and statistical significance was set at $p \leq 0.05$. The numbers of mice per treatment group are indicated in the appropriate figures and tables.

RESULTS:

Nmp4-KO mice exhibited an enhanced increase in femoral trabecular bone after 3wks of treatment

To determine if the divergence between the WT and *Nmp4*-KO mice in serum osteocalcin levels at 3wks is coincident with the beginning of the enhanced addition of trabecular bone in the null animals observed at 7wks (Childress, Philip et al. 2011) we sorted WT and *Nmp4*-KO mice into four treatment groups and harvested the femurs for μ CT analysis as described in the Materials and Methods. Although the WT and null mice had previously shown equivalent PTH-induced increases in trabecular bone at 2wks of treatment (Childress, Philip et al. 2011), in the present study the null mice exhibited significantly augmented PTH-stimulated increase in femoral trabecular bone compared to their WT littermates at 3wks (Figure 3-1). The *Nmp4*-null mice showed a more robust PTH-stimulated increase in BV/TV compared to the WT animals during the first 3wks of treatment (Figure 3-1A). The KO mice added approximately 2.3-fold more bone than their WT littermates in response to PTH (Figure 3-1A). The 2-way ANOVA indicated a strong genotype x treatment interaction and the Tukey HSD post hoc determined that there was no difference in BV/TV between the vehicle-treated WT and KO animals (Figure 3-1A). While PTH treatment increased connectivity parameters (Conn.D, mm^{-3}) for both genotypes, a significantly greater enhancement was observed in *Nmp4*-KO mice compared to WT mice (Figure 3-1B). Again there was no trabecular number (Tb.N, mm^{-1} , Figure 3-1E) and decreased spacing (Tb.Sp, mm, Figure 3-1F) in both genotypes.

BM cellularity, spleen weight, and the profiles of most blood elements did not differ between the WT and Nmp4-KO mice

To address whether there are differences between the *Nmp4*-null and WT mice in the BM or PBL cellular profiles supportive of the observed enhanced PTH-induced addition of trabecular bone, we obtained immunophenotypic, clonogenic, and hematological

profiles at 3wks of treatment (Tables 3-1 through 3-3). The spleen weight measured, as % of total body weight did not differ with genotype but did modestly increase with PTH treatment in both WT and null mice (Table 3-1). The profiles of blood elements between the *Nmp4*-KO and WT mice were unremarkable. We observed no differences between any of the treatment groups in the BM and PBL profiles of the RBCs, WBCs, platelets, neutrophils, lymphocytes, eosinophils, monocytes, B-cell lineages, CD4+ T cells, or the Lin(-)Sca-1(+)c-Kit(+) (LSK) cells (Tables 3-1 and 3-2). Finally, there were no differences between WT and *Nmp4*-KO mice in CFU-C, CFU-G, CFU-GEMM, and CFU-M cells (Table 3). PTH treatment had no impact on any of these parameters (Tables 3-1 through 3-3).

Nmp4-KO BM yielded more multipotent MSCs (CD146+/nestin+), CFU-F^{Alk^{Phos+}}, CFU-GM, and CD8+ T cells than WT BM.

To determine if the source of this augmented bone formation in *Nmp4*-null mice is derived, in part, from an expanded pool of osteoprogenitors we obtained BM from our experimental groups for analysis of CFU-F^{Alk^{Phos+}} colonies as described in the Materials and Methods. We recovered approximately 4-fold more CFU-F^{Alk^{Phos+}} colonies from the null mice than the WT animals (Figure 3-2A). The total number of CFU-F colonies was significantly elevated in the *Nmp4*-KO cultures (Figure 3-2B) and the percentage of CFU-F^{Alk^{Phos+}}/total CFU-F colonies was significantly increased in the cultures from the *Nmp4*-null BM as compared to the WT BM (Figure 3-2C). There was a trend toward increased yield of CFU-F and CFU-F^{Alk^{Phos+}} cells with PTH treatment in both genotypes but this was not significant. Therefore, we next addressed whether the frequency of the self-renewing multipotent mesenchymal stem cell (CD45-/CD146+/CD105+/nestin+), the precursor of CFU-F-derived lineages including osteoprogenitors, is elevated in untreated *Nmp4*-KO mice. Indeed, we observed a nearly 4-fold increase in this cell phenotype in the null BM (Figure 3-2D).

Nmp4 has no significant influence on the percentage of CD4+ T cells in the BM or PBL (Table 2) but recent studies have demonstrated that CD8+ T cells play an obligatory role in the PTH anabolic response via their release of the glycoprotein Wnt10b a potent agonist for osteoprogenitors (Terauchi, Li et al. 2009, Bedi, Li et al. 2012). Indeed the present data show that the percentage of CD8+ T cells in the null BM was 2-fold greater than observed in the WT BM (Figure 3-3A), but there was no difference in the percent CD8+ T cells in the PBL between the genotypes (Figure 3-3B). Additionally, PTH treatment had no effect on the size of this population of cells in either the BM or PBL.

Next, to address whether the observed modest elevation in bone resorption in the null mice and the enhanced number of osteoclasts derived from their BM [7] is due, in part, to an increase in osteoclast progenitors, we evaluated the number of CFU-GM cells from our treatment groups. Indeed the *Nmp4*-null mice exhibited a modest (~1.6-fold) but significant increase in CFU-GM cells as compared to their WT littermates (Figure 3-4). PTH had no effect on the number of these cells (Figure 3-4).

DISCUSSION:

A significant drawback to the use of PTH as an osteoporosis drug is that its anabolic potency declines within a relatively short period of time, which is particularly problematic in treating a chronic degenerative disease (Baron and Hesse 2012). The cellular and molecular mechanisms underlying this closing of the PTH anabolic window are unknown. We have recently determined that deleting the transcription factor *Nmp4/CIZ* from mice significantly extends the PTH anabolic window and results in enhanced trabecular bone formation without compromising hormone-stimulated gains in cortical bone (Robling, Childress et al. 2009, Childress, Philip et al. 2011).

An intriguing aspect of the *Nmp4*-KO mouse response to anabolic doses of PTH is that the enhanced addition of trabecular bone requires a lag period to materialize (Childress, Philip et al. 2011). Previously, we reported that both WT and null mice exhibited equivalent PTH-stimulated increases in trabecular bone during the first 2wks of a 7wk treatment. In this study we compared hormone-induced increases in femoral cancellous bone after 3wks of treatment and indeed observed that the *Nmp4*-KO mice exhibited a greater than 2-fold increase in PTH-induced accrual of femoral trabecular bone formation compared to their WT littermates. This enhanced response to PTH was manifested in an augmented increase in BV/TV, trabecular connectivity (Conn D), and trabecular thickness (Tb Th). Additionally, PTH had a greater impact on the structural model index (SMI) in the null mice. A decrease in SMI indicates a change in cancellous architecture from a rod-like to a plate-like morphology and is a result of alterations in modeling and remodeling (Ding and Hvid 2000, Riggs and Parfitt 2005, Allen and Burr 2006). This suggests that PTH-stimulated increases in bone strength are enhanced in the *Nmp4*-KO mice although this must be confirmed by biomechanical testing.

Our data indicate that deleting *Nmp4/CIZ* establishes a BM microenvironment that is primed for anabolic signals. We observed no differences in femur cellularity, % spleen

weight, or in the profiles of the vast majority of blood elements, however, there was a striking difference in the number of osteoprogenitor cells as evaluated by the clonogenic CFU-F^{Alk^{phos+}} assay. The *Nmp4*-null BM yielded 4-fold more of these colonies than did the WT BM. In an earlier study Noda and colleagues observed that BM cultures from null mice yielded about 3-fold more mineralized nodules than WT mice (Morinobu, Nakamoto et al. 2005), which is equivalent to measuring CFU-osteoblasts (OB) colonies (Owen and Friedenstein 1988). In the present study, we also determined that the total number of CFU-F colonies obtained from the null mice was significantly elevated as was the % CFU-F^{Alk^{phos+}}/total CFU-F. These data together suggest that *Nmp4* suppresses the frequency of CFU-F cells and impedes commitment to the osteogenic lineage. This is consistent with the elevated number of CD45-/CD146+/CD105+/nestin+ cells obtained in the *Nmp4*-KO mice. These cells are self-renewing multipotent mesenchymal stem cells and contain all the bone-marrow colony-forming-unit fibroblastic colony activity (Sacchetti, Funari et al. 2007, Méndez-Ferrer, Michurina et al. 2010). PTH did not significantly impact the number of CFU-F^{Alk^{phos+}} colonies recovered from the BM of either genotypes although there was a trend toward modestly elevating the frequency of these cells. A variety of studies have shown conflicting stimulatory and inhibitory effects of PTH on osteoprogenitor proliferation (Isogai, Akatsu et al. 1996, Onyia, Miller et al. 1997, Wang, Liu et al. 2007); however, the prevailing view is that intermittent PTH recruits osteoprogenitors into the osteoblast differentiation pathway and enhances their survival instead of increasing the size of this progenitor pool (Jilka 2007). It is the accumulation of repeated new waves of osteoprogenitors with enhanced osteogenic potential that mediates the PTH-stimulated increase in bone mass (Wang, Liu et al. 2005, Wang, Liu et al. 2007). This may also explain the observed lag period before the enhanced PTH-induced bone formation phase is initiated in the *Nmp4*-null mice. If indeed the anabolic effect of intermittent PTH is the result of consecutive waves of committed osteoblast differentiation accumulated from each PTH exposure, in which hormone only acts on the BM early osteoprogenitor cells (Wang, Liu et al. 2007), then the rate of PTH osteoprogenitor recruitment would be equivalent in both the WT and KO mice, but the WT osteoprogenitor pool would be depleted before the KO population. This is consistent with the observed equivalent addition of bone during the first 2wks of treatment but the divergence in both serum osteocalcin and bone formation in the null mice at 3wks (Childress, Philip et al. 2011). Finally, the *Nmp4*/*CIZ*-KO osteoblast exhibits a modest but significant enhanced response to numerous anabolic stimuli, including PTH, BMP2, and mechanical loading (Shen,

Nakamoto et al. 2002, Morinobu, Nakamoto et al. 2005, Yang, Bidwell et al. 2010, Alvarez, Childress et al. 2012); therefore, an expanded population of such cells is certainly consistent with the augmented skeletal bone mineral density and bone mineral content of the null animals.

The expanded *Nmp4*-KO osteoprogenitor pool may be supported by the 2-fold increase in BM CD8⁺ T cells as compared to the WT mice. CD8⁺ T cells express the PTH receptor PTHR1 and support intermittent hormone anabolic activity via their secretion of the glycoprotein Wnt10b a potent agonist of osteoblast activity (Terauchi, Li et al. 2009, Bedi, Li et al. 2012). PTH-induced bone formation was significantly reduced in T cell-deficient mice and in these mice reconstituted with *Wnt10b*^{-/-} T cells (Terauchi, Li et al. 2009). Interestingly, we observed no difference in the level of CD8⁺ T cells in the PBL suggesting that the recruitment and/or the retention of these cells is enhanced in the null BM microenvironment. BM CD8⁺ T cells consist chiefly (~50%) of CCR7⁺ L-selectin⁺ central memory cells (Mazo, Honczarenko et al. 2005) and the mechanisms underlying this concentration in the marrow involves PSGL-1-mediated rolling and VCAM-1-VLA-4-mediated arrest in BM venules (Mazo, Honczarenko et al. 2005). The retention of these cells may be enhanced by CXCL12 (a ligand for CXCR4 on central memory T cells) (Mazo, Honczarenko et al. 2005). Finally, IL15-dependent homeostatic proliferation of memory T cells contributes to their disproportionate presence in the BM (Becker, Coley et al. 2005, Herndler-Brandstetter, Landgraf et al. 2011). Whether the null BM microenvironment is enriched in these various cytokines and/or selectin ligands and adhesion molecules remains to be determined.

A second provocative aspect of the *Nmp4*-KO skeletal phenotype is that the baseline bone mineral density and bone mineral content are slightly increased despite a modest elevation of bone resorption (Childress, Philip et al. 2011). While the increase in osteoclast number may be attributed to coupling (e.g., increased osteoblast support of an increase in osteoclastogenesis (Kular, Tickner et al. 2012), the present data suggests this reflects intrinsic differences in osteoclast progenitor populations. We observed a modest (1.6-fold) but statistically significant increase in CFU-GM cells in the null mice as compared to their WT counterparts. Although CFU-C cells were elevated in the *Nmp4*-KO mice this only approached significance and there was no difference in the levels of CFU-M cells between the genotypes. The precise lineage of the osteoclast and its relationship to other hematopoietic cells is controversial; however, there are a number of studies supporting the hypothesis that the osteoclast lineage branches to terminal differentiation

via the CFU-GM cells before further passage toward the monocyte/macrophage lineage (Menaar, Kurihara et al. 2000, Hodge, Kirkland et al. 2004).

The present data suggest that the heightened bone anabolism and modestly elevated bone resorption in the global *Nmp4*-KO mouse is derived, in part, from a unique confluence of BM stem, progenitor and blood cells. The null BM harbors an expanded pool of MSCs (CD146+/nestin+), osteoprogenitors and CD8+ T cells, which together supply the osteoblasts necessary for the observed augmented bone-forming activity, even in the presence of elevated bone resorption driven by the modestly enlarged CFU-GM pool (1.6-fold) that contributes the osteoclasts. This may support an environment of enhanced anabolic remodeling. The use of *Nmp4*/CIZ conditional KO mice will be necessary to disentangle the contribution of each of these cell types to this phenomenon. It is certainly tenable that multiple stem/progenitor types are necessary for maintaining an open PTH anabolic window; that one transcription factor has significant direct and/or indirect control over these populations was unexpected despite the fact that *Nmp4*/CIZ is expressed in multiple cell and tissue types (Thunyakitpisal, Alvarez et al. 2001). *Nmp4*/CIZ has been proposed as a potential target for osteoporosis therapy (Krane 2005) and the present data further develop this idea suggesting that disabling *Nmp4*/CIZ may provide an adjuvant therapy for extending PTH clinical efficacy by expanding the stem/progenitor populations sustaining its anabolic action.

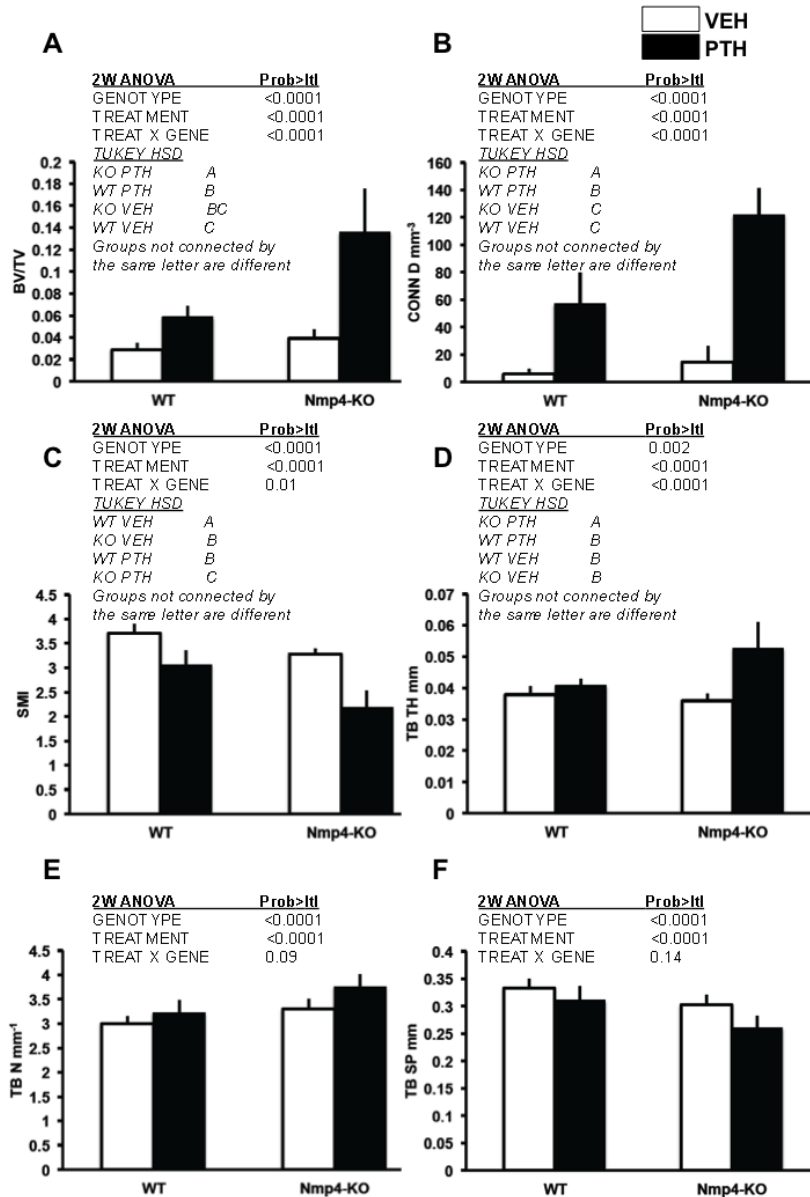


Figure 3-1: Disabling *Nmp4* enhanced PTH-induced increases in femoral cancellous bone after 3wks of treatment. Micro-CT-acquired femoral trabecular architecture including (A) BV/TV %; (B) Conn D mm⁻³; (C) SMI; (D) Tb Th mm; (E) Tb N mm⁻¹; (F) Tb Sp mm was compared between WT and *Nmp4*-KO mice that had been treated with intermittent hPTH(1-34) 30µg/kg/day or vehicle for 3 wks (average ± SD, number of mice/experimental group=10). Statistical differences were determined using a two-way ANOVA. A Tukey's HSD post hoc test was used to determine differences between the treatment groups if a significant genotype x treatment interaction was indicated and there was such an interaction for BV/TV, Conn D, SMI, and Tb Th .

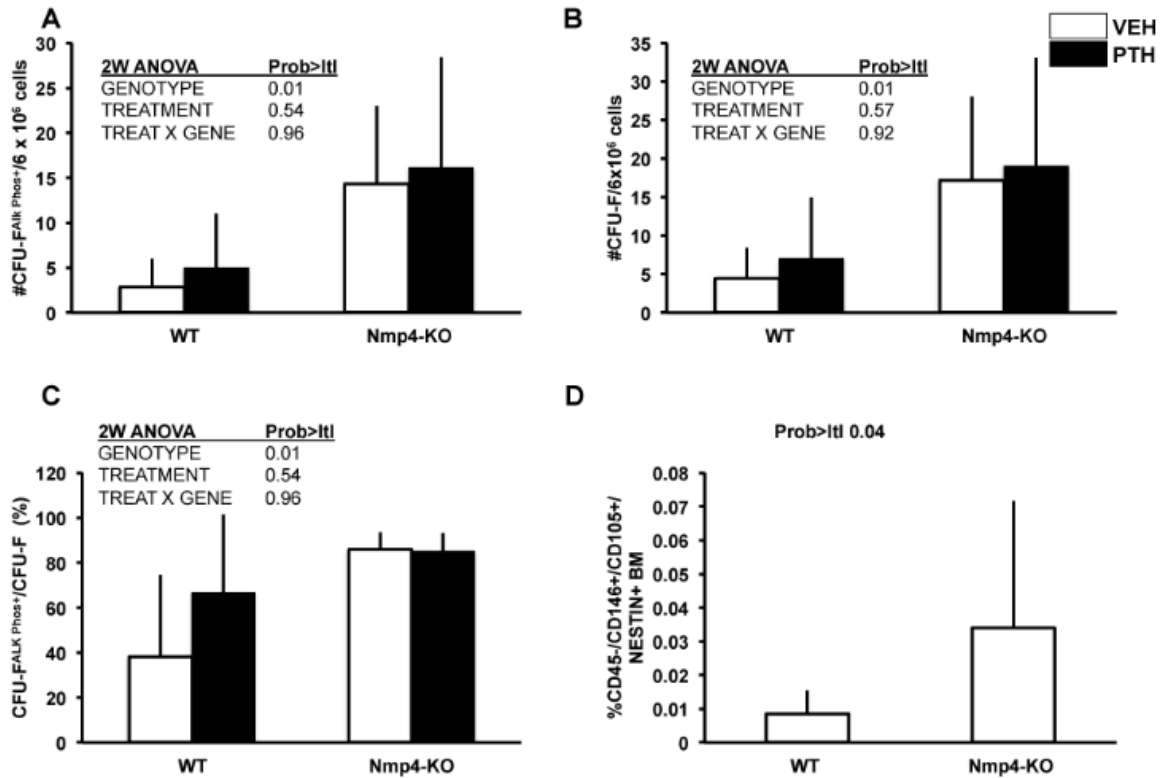


Figure 3-2: *Nmp4*-KO BM yielded more osteogenic stem and progenitor cells irrespective of treatment. [A] Total number of CFU-F^{Alk Phos+} colonies in BM cultures derived from WT and *Nmp4*-KO mice treated with intermittent hPTH(1-34) 30µg/kg/day or vehicle for 3 wks [B] Total number of CFU-F colonies [C] The percent CFU-F^{Alk Phos+} colonies/total CFU-F colonies (average ± SD, number of mice/experimental group=6-8; statistical differences determined by a two-way ANOVA) [D] The frequency of femoral CD45-/CD146+/CD105+/Nestin+ multipotent mesenchymal stem cells in untreated WT and *Nmp4*-KO mice; FACS was used to evaluate the BM from each mouse as described in the Materials and Methods (average ± SD, number of mice/experimental group =12-20; statistical difference was determined using a two sample t-test assuming unequal variances).

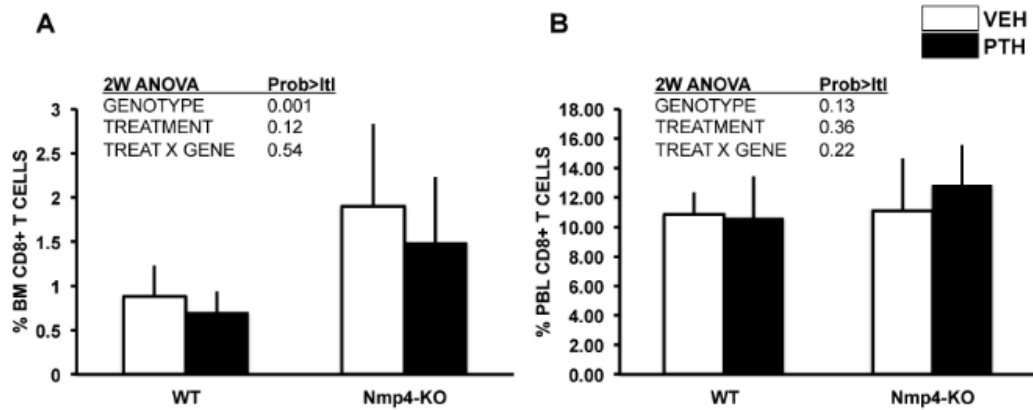


Figure 3-3: *Nmp4*-KO BM harbored more CD8+ T cells than WT BM irrespective of treatment. [A] FACS analysis showed that there were significantly more CD8+ T cells in the BM of *Nmp4*-KO mice as compared to that observed in WT mice. [B] No differences between WT and *Nmp4*-KO mice in CD8+ T cells were detected in the PBL (average \pm SD, number of mice/experimental group 11-14; statistical differences were determined using a two-way ANOVA)

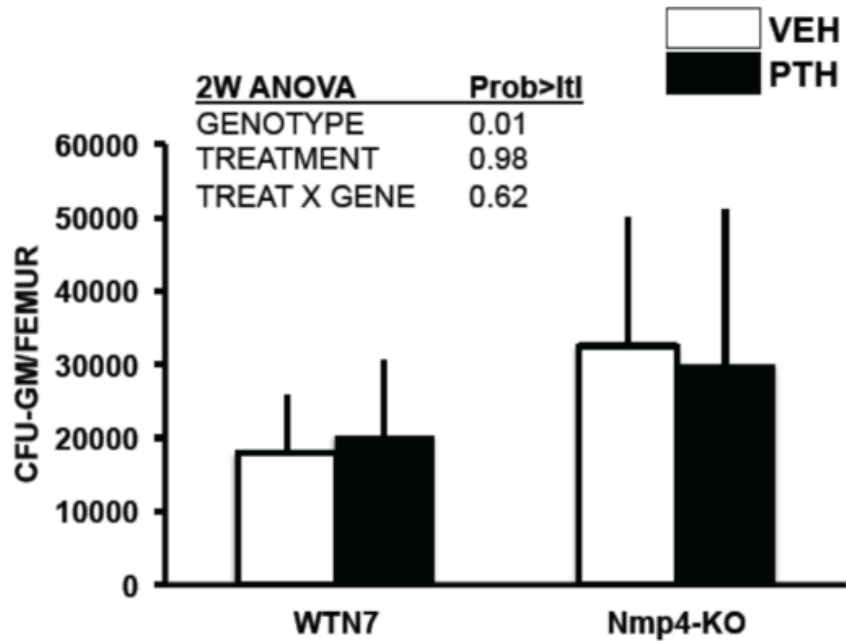


Figure 3-4: More CFU-GM cells were obtained from *Nmp4*-KO mice than WT mice, irrespective of treatment. Intermittent hPTH (1-34) 30µg/kg/day or vehicle was administered for 3wks as described in the Materials and Methods (average ± SD, number of mice/experimental group=10-14; statistical differences were determined using a two-way ANOVA).

TABLE 3-1: Peripheral blood of the WT and *Nmp4*-KO mice was analyzed using the Hemavet 950 as described in the Materials and Methods. WT and null mice were treated with intermittent PHT or vehicle for 3 weeks (number of mice/experimental group=9-14). A two-factor ANOVA was used to evaluate the impact of genotype and treatment on the individual parameters. Statistical significance was set at $p < 0.01$ to guard against type I errors. % spleen weight is the weight of the organ divided by the total body weight. Abbreviations: EO eosinophils; LY Lymphocytes; MO monocytes; NE neutrophils; PLT platelets; RBC red blood cells; WBC white blood cells.

	WT		<i>Nmp4</i> ^{-/-}		2-WAY ANOVA p-values		
	VEH	PTH	VEH	PTH	Geno	Treat	G x T
Cellularity	9.1±6.2	8.1±5.6	14.3±7.1	11.5±6.6	0.04	0.33	0.64
% Spleen Wt.	0.40±0.3	0.47±0.06	0.42±0.08	0.46±0.07	0.84	0.01	0.49
WBC (K/μl)	4.8±1.1	4.9±1.4	4.5±1.6	5.6±1.6	0.07	0.16	0.24
NE (K/μl)	0.70±0.28	0.62±0.4	0.56±0.32	0.73±0.33	0.86	0.67	0.22
NE %	14.2±3.3	12.6±6.1	12.7±12.8	12.8±4.7	0.88	0.33	0.82
LY (K/μl)	4.0±0.78	4.1±1.1	3.7±1.4	4.8±1.3	0.62	0.11	0.26
LY %	82.4±4.3	83.8±5.9	82.2±8.1	84.4±4.8	0.88	0.33	0.82
MO (K/μl)	0.13±0.05	0.14±0.06	0.16±0.09	0.12±0.03	0.89	0.53	0.21
MO %	2.7±0.87	2.9±1.0	3.6±2.1	2.2±0.53	0.69	0.15	0.66
EO (K/μl)	0.03±0.05	0.3±0.04	0.04±0.05	0.02±0.03	0.92	0.49	0.51
EO %	0.54±0.88	0.56±0.53	1.17±1.57	0.43±0.52	0.42	0.24	0.23
RBC (M/μl)	9.6±0.46	9.1±1.5	8.96±1.2	8.8±1.4	0.09	0.67	0.38
PLT (K/μl)	494±125	487±167	379±208	488±143	0.27	0.32	0.26

TABLE 3-2: Immunophenotypic evaluation of BM and PBL cell types in WT and *Nmp4*-KO mice using FACS analysis as described in the Materials and Methods. Mice were treated with PTH or vehicle for 3 weeks (number of mice/experimental group=11-14). Statistical significance was set at p<0.01. Abbreviations: LSK, lin-/Sca1+/c-Kit+.

	WT		<i>Nmp4</i> ^{-/-}		2-WAY ANOVA p-values		
	<u>VEH</u>	<u>PTH</u>	<u>VEH</u>	<u>PTH</u>	<u>Geno</u>	<u>Treat</u>	<u>G x T</u>
Pre-B (BM)	11.6±7.2	12.1±7.0	7.6±4.7	9.7±5.7	0.08	0.45	0.65
Pre-B (PBL)	17.5±6.5	20.0±7.8	11.7±6.5	16.9±7.6	0.04	0.06	0.52
Immature B (BM)	5.9±1.3	6.3±2.7	6.8±3.5	6.3±4.4	0.64	0.95	0.65
Immature B (PBL)	20.7±10.9	22.3±8.5	25.1±11.3	22.8±0.11.6	0.43	0.90	0.54
Mature B (BM)	13.5±3.5	3.5±3.7	3.0±3.0	3.5±3.4	0.81	0.75	0.79
Mature B (PBL)	5.7±3.8	5.5±4.8	7.2±6.7	8.3±6.7	0.20	0.79	0.68
CD4+ T (BM)	1.6±0.39	1.4±0.40	1.9±0.74	2.0±1.0	0.03	0.73	0.36
CD4+ T (PBL)	15.8±0.05	15.6±4.3	16.3±5.5	17.1±3.7	0.41	0.79	0.68
Myeloid (BM)	34.5±5.7	36.4±4.8	32.0±7.6	34.1±11.2	0.30	0.38	0.97
Myeloid (PBL)	6.0±2.5	5.3±1.3	5.9±2.9	7.4±4.4	0.24	0.65	.22
LSK (BM)	0.11±0.06	0.11±0.06	0.12±0.14	0.26±0.05	0.05	0.07	0.09
LSK (PBL)	0.03±0.03	0.03±0.03	0.03±0.04	0.02±0.03	0.60	0.95	0.92

TABLE 3-3: Clonogenic assays of WT and *Nmp4*-KO mice as described in the Materials and Methods. WT and null mice were treated with intermittent PTH or vehicle for 3 weeks (number of mice/experimental group=10-14). A two-factor ANOVA was used to evaluate the impact of genotype and treatment on the individual parameters. Statistical significance was set at $p < 0.01$ to guard against type I errors.

	WT		<i>Nmp4</i> ^{-/-}		2-WAY ANOVA p-values		
	<u>VEH</u>	<u>PTH</u>	<u>VEH</u>	<u>PTH</u>	<u>Geno</u>	<u>Treat</u>	<u>G x T</u>
CFU-C	27307±13080	31311±17107	44898±22460	40573±27265	0.04	0.98	0.52
CFU-G	1145±2204	963±1402	560±998	284±460	0.12	0.54	0.93
CFU-GEMM	941±1219	762±830	1065±1817	847±987	0.78	0.61	0.96
CFU-M	7409±4319	9405±7227	11229±6172	9629±6478	0.27	0.91	0.33

CHAPTER 4

A GENOME-WIDE MAP OF NMP4 OCCUPANCY SUGGESTS PATHWAYS RESPONSIBLE THE ROLE OF NMP4 IN ATTENUATING PTH-INDUCED BONE FORMATION FOLLOWING OVARECTOMY

Paul Childress¹, Keith Stayrook², Marta B Alvarez³, Zhiping Wang^{4,5}, Yu Shao⁴, Selene Hernandez-Buquer¹, Youngzheng He^{6,7}, Daniel Horan¹, Fredrick M Pavalko⁸ Stuart J Warden^{9,10}, Alexander G Robling¹, Feng-chun Yang^{6,7} Matthew R Allen¹, Venkatesh Krishnan², Yunlong Liu^{4,5}, Joseph Bidwell^{1,4}

1. Department of Anatomy & Cell Biology, Indiana University School of Medicine (IUSM), Indianapolis, IN, 46202
2. Lilly Research Laboratories, Eli Lilly and Company, Indianapolis, Indiana, USA.
3. Orthopaedic Surgery IUSM
4. Department of Medical and Molecular Genetics, IUSM
5. Center for Computational Biology and Bioinformatics, IUSM
6. Department of Pediatrics, IUSM
7. Herman B Wells Center for Pediatric Research
8. Cellular & Integrative Physiology
9. Center for Translational Musculoskeletal Research, School of Health and Rehabilitation Sciences, IN University
10. Department of Physical Therapy, School of Health and Rehabilitation Sciences, IN University

Material in this chapter is being prepared for publication.

ABSTRACT:

Parathyroid hormone (PTH) is an osteoanabolic for treating osteoporosis but its potency wanes. Disabling the transcription factor Nmp4 in healthy, ovary-intact mice enhances bone response to PTH and BMP2 and protects from unloading-induced osteopenia. These Nmp4^{-/-} mice exhibit expanded bone marrow (BM) populations of osteoprogenitors and supporting CD8⁺ T cells. To determine whether the Nmp4^{-/-} phenotype persists in an osteoporosis model we compared PTH response in ovariectomized (ovx) wild type (WT) and Nmp4^{-/-} mice. To identify potential Nmp4 target genes we performed bioinformatic/pathway profiling on Nmp4 ChIP-seq data from various cell lines. Mice (12wks) were ovx or sham-operated 4wks before the initiation of PTH therapy. Skeletal phenotype analysis included μ CT, histomorphometry, serum profiles, FACS sorting and the growth/mineralization of cultured WT and Nmp4^{-/-} BM mesenchymal stem/progenitor cells (MSPCs). ChIP-seq data were derived using MC3T3-E1 pre-osteoblasts, murine embryonic stem cells, and two blood cell lines. Ovx Nmp4^{-/-} mice exhibited an improved response to PTH therapy coupled with elevated numbers of osteoprogenitors and CD8⁺ T cells, but were not protected from ovx-induced bone loss. Cultured Nmp4^{-/-} MSPCs displayed accelerated proliferation and enhanced mineralization. ChIP-seq/gene ontology analyses identified target genes likely under Nmp4 control as enriched for negative regulators of biosynthetic processes. PTH regulation of Nmp4 occupancy was gene-specific. Moreover, bioinformatic profiling predicted the mTOR/IGF1/insulin pathway as an Nmp4 target. We confirmed that disabling Nmp4 enhanced IGF1-induced Akt phosphorylation in osteoprogenitors. This pathway is critical for mediating PTH anabolism. Therefore, changes in Nmp4 status may lead to improvements in osteoprogenitor response to therapeutic cues.

INTRODUCTION:

Patients with severe osteoporosis are often treated with parathyroid hormone (PTH), a potent osteoanabolic agent (Kraenzlin and Meier 2011), however, the bone-building ability of this drug or its 'anabolic window' wanes, likely due to latent increases in bone resorption. (Yu, Neer et al. 2011, Baron and Hesse 2012, Cipriani, Capriani et al. 2012). This limits its effectiveness to treat a chronic degenerative disease. Recent advances in bone-forming agents have shown that one can increase the extent of bone mass accrual with anti-SOST treatment compared to PTH (McClung, Grauer et al. 2014). However, there may be unique pathways triggered by PTH, which allows for sustained targeting of early osteogenesis as evidenced by serum markers of bone formation such as N-terminal propeptide of type 1 procollagen (P1NP) and osteocalcin (OCN, (Saag, Zanchetta et al. 2009, Padhi, Jang et al. 2011)). In contrast to PTH, anti-SOST antibodies may have a limited capacity for targeting osteoprogenitors as evidenced by a relatively transient up-regulation of collagen-based markers such as P1NP (McClung, Grauer et al. 2014). Therefore given PTH's unique mode of action, therapies that could enhance PTH-mediated recruitment of osteoprogenitors may add value to some patients. How to achieve this enhancement is not clear. For example, attempts to extend and enhance PTH efficacy by combining treatment with anti-resorptive medications have met with mixed success and have generally been underwhelming (Black, Greenspan et al. 2003, Finkelstein, Wyland et al. 2010, Cosman, Eriksen et al. 2011).

Blocking the activity of *Nmp4/CIZ* (nuclear matrix protein 4/cas interacting zinc finger protein, 'Nmp4') in mice dramatically enhanced their response to anabolic doses of PTH (Robling, Childress et al. 2009, Childress, Philip et al. 2011, He, Childress et al. 2013), suggesting a potential strategy for an adjuvant therapy (Krane 2005). Intermittent exogenous doses of hormone stimulated equivalent new bone formation in wild type (WT) and *Nmp4*^{-/-} mice during the first 2wks of challenge, but at 3wks of treatment the null mice exhibited greater than a 2-fold increase in new trabecular bone compared to their WT littermates (Childress, Philip et al. 2011). This augmented skeletogenesis in the *Nmp4*^{-/-} mice was extended to 7wks of treatment and was observed in the femur, tibia, and vertebra. Serum osteocalcin continued to rise at this time point in the *Nmp4*^{-/-} mice but had decreased in the WT animals (Childress, Philip et al. 2011). However, the PTH response of the cortical compartment was equivalent throughout treatment in the WT and null mice (Robling, Childress et al. 2009).

Nmp4^{-/-} bone may have a generalized heightened response to systemic or local anabolic cues. For example, these mice also exhibited augmented BMP2-induced ectopic bone formation compared to their WT littermates (Morinobu, Nakamoto et al. 2005). The *Nmp4*-null mice showed an accelerated osseous regeneration after marrow ablation (Morinobu, Nakamoto et al. 2005) and did not lose bone during hind limb unloading, which appeared to derive from an enhanced osteoblast activity (Hino, Nakamoto et al. 2007).

Prerequisite for an adjuvant therapy target, disabling *Nmp4* has little impact on the health, longevity, or global baseline phenotype of the mouse, with a few exceptions. The *Nmp4*^{-/-} baseline skeletal phenotype (i.e., bone mineral density and/or content and trabecular architecture) is generally equivalent compared to WT animals], although we have occasionally observed an unprovoked increase in bone properties in *Nmp4*^{-/-} mice (Morinobu, Nakamoto et al. 2005, Robling, Childress et al. 2009, Childress, Philip et al. 2011, He, Childress et al. 2013). Similarly, male *Nmp4*^{-/-} mice exhibit variable degrees of spermatogenic cell degeneration resembling germinal-cell aplasia with focal spermatogenesis resulting in *sporadic* infertility (Nakamoto, Shiratsuchi et al. 2004).

Our recent work suggests that the cellular basis of the osteoanabolic repressor function of *Nmp4* is due to its effect on the bone marrow derived stromal stem/progenitor cells aka mesenchymal stem progenitor cells (MSPCs). *Nmp4*^{-/-} mice have significantly more osteoprogenitor cells in their marrow, which lie in wait to be quickly mobilized to differentiate into active osteoblasts upon stimulation with various osteoanabolic stimuli (He, Childress et al. 2013). There was no difference between WT and *Nmp4*^{-/-} BM cellularity or profiles of several blood elements however, the null mouse exhibited a 4-fold increase in CD45⁻/CD105⁺/nestin⁺/CD146⁺ BM osteoprogenitor cells. These markers are a common hallmark to CFU-F cells with osteogenic potential (Isern, Martín-Antonio et al. , Méndez-Ferrer, Michurina et al. 2010) and indeed 4-fold more CFU-F^{Alk^{phos}+} and CFU-F^{Ob} cells have been recovered from these mice compared to the WT animals (Morinobu, Nakamoto et al. 2005, He, Childress et al. 2013). A second, related phenomenon we have observed in *Nmp4*^{-/-} mice is a 2-fold increase in the prevalence of CD8⁺ T-cells in the femoral marrow—the lymphocyte population that provides potent input to induce MSPCs down the osteoblast differentiation pathway (Terauchi, Li et al. 2009, Li and Durbin 2010, Bedi, Li et al. 2012, He, Childress et al. 2013). These blood cells express the PTHR1 receptor and support the PTH anabolic response via the release of Wnt10b upon hormone challenge, which drives osteoprogenitor differentiation to pre-osteoblasts and mature

matrix-producing bone cells (Terauchi, Li et al. 2009, Li and Durbin 2010, Bedi, Li et al. 2012).

There is little information on the molecular mechanisms and cellular pathways that mediate the anti-anabolic action of Nmp4. This transcription factor is a Cys₂His₂ zinc finger protein that primarily localizes to the nucleus although there is evidence for cytoplasmic activity (Nakamoto, Yamagata et al. 2000, Bidwell, Childress et al. 2012). The zinc fingers recognize the DNA minor groove of an AT-rich consensus sequence and two transactivation domains can suppress or activate transcription depending on the cellular context (Alvarez, Thunyakitpisal et al. 1998, Nakamoto, Yamagata et al. 2000, Thunyakitpisal, Alvarez et al. 2001, Torrungruang, Alvarez et al. 2002, Shah, Alvarez et al. 2004). The amino terminus of the rodent protein contains an SH3-binding domain that associates with the adaptor signaling protein p130Cas, but the functional significance of this interaction remains unknown.

The *Nmp4*^{-/-} progenitor cells and their progeny have an exaggerated stimulus response at the levels of transcription and cell signaling (Shen, Nakamoto et al. 2002, Yang, Bidwell et al. 2010, Alvarez, Childress et al. 2012). *Nmp4*-null bone marrow stromal cells (BMSCs) show an enhanced transcriptional response to PTH and BMP2 (Shen, Nakamoto et al. 2002, Shah, Alvarez et al. 2004, Yang, Bidwell et al. 2010, Alvarez, Childress et al. 2012). The *Nmp4*^{-/-} derived calvarial cells exhibit an increased load-induced phosphorylation of Pi3k and Akt and beta-catenin nuclear translocation (Yang, Bidwell et al. 2010). Analogous to heightened response to anabolic signals in *Nmp4*^{-/-} osteolineage cells, osteoclast preparations from the null mice exhibited a heightened response to the remodeling signals of RANKL and M-CSF (Childress, Philip et al. 2011).

In the present study we addressed whether *Nmp4*-null mice are resistant to ovariectomy (ovx)-induced bone loss and if disabling Nmp4 improves PTH-based bone therapy in an OVX model. We used expanded cultures of WT and *Nmp4*^{-/-} mesenchymal stem/progenitor cells (MSPCs) to probe the cell autonomous proliferative and mineralization activities of this cell population. To delineate the framework of the Nmp4 anti-anabolic network we performed genome-wide chromatin immunoprecipitation sequencing (ChIP-seq) on MC3T3-E1 cells and combined these data with the data available for Nmp4 (a.k.a. Znf384) from the Mouse Encyclopedia of DNA Elements (ENCODE) Consortium for transcription factors (Consortium, Stamatoyannopoulos et al. 2012). Bioinformatic profiling, gene ontology (GO), and pathway analysis were performed

on these data sets to infer a map of the negative regulation of bone anabolism under *Nmp4* control.

MATERIALS AND METHODS:

Mice: Male and female *Nmp4*^{-/-} mice, backcrossed onto a C57BL/6J background for 7 generations (Robling, Childress et al. 2009, Childress, Philip et al. 2011, He, Childress et al. 2013), and their WT littermates were produced and maintained in our colony at Indiana University Bioresearch Facility, Indiana University School of Dentistry. Our local Institutional Animal Care and Use Committee approved all husbandry practices and experimental procedures and regimens described in this investigation.

Bilateral ovariectomy surgery: 12wk-old virgin mice were anesthetized using isoflurane inhalation followed by a mixture of xylazine and ketamine administered intraperitoneally. A 1-2cm dorsal incision was made in the midline below the level of the last rib and the skin bluntly dissected from the muscle on either side of the incision. Through the skin incision, the muscle wall was incised 1cm lateral to the midline 1-2cm below the last rib to enter the abdominal cavity. The periovarian fat pad was located and gently grasped and exteriorized. Care was taken not to directly handle the ovary to avoid abdominal implantation of ovarian tissue. While holding the periovarian fat pad with forceps, the fallopian tube between the fat pad and uterus was clamped and crushed using mosquito hemostats. The crushed area was cut with scissors and the fat pad with ovary removed. The procedure was repeated on the contralateral side. The skin incision was closed with one or two surgical wound clips. The sham surgeries involved all the outlined steps except the crushing the fallopian tubes and the actual removal of the ovaries. To confirm the efficacy of OVX, uteri were weighed following euthanasia.

PTH treatment: At 16 wks of age, ovx animals were sorted into four treatment groups based on equivalent mean-group-body weight. These four groups included 1) vehicle-treated WT; 2) PTH-treated WT; 3) vehicle-treated *Nmp4*^{-/-} and 4) PTH-treated *Nmp4*^{-/-} mice. Mice were injected subcutaneously (sc) with human PTH 1-34 (Bachem Bioscience Inc, PA) at 30µg/kg/day, daily or vehicle control (0.2% BSA/1.0µN HCl in saline, Abbott Laboratory, North Chicago, IL) for the length of time indicated.

Cell culture: Cells from ATCC (MC3T3-E1 subclone 4) were maintained in α -MEM medium supplemented with 100 IU/ml penicillin, 100 μ g/ml streptomycin, 25 μ g/ml amphotericin, 2 mM L-glutamine (Gibco BRL, Grand Island, NY), ascorbic acid (50 μ g/ml, Sigma-Aldrich, St Louis, MO), and 10% fetal bovine serum (FBS; Sigma-Aldrich, St Louis, MO). Expanded mesenchymal stem/progenitor cell (MSPC) cultures were established as previously described [Wu et al., 2006]. Briefly, long bone BM was isolated from euthanized mice 6-8wks of age and the mononuclear cells (BMMNCs) were isolated using a Ficoll gradient. These cells were plated in Mesencult™ Media + Mesencult™ Stimulatory Supplement (StemCell™ Technologies, Vancouver BC, Canada) and maintained in culture for 3-4wks without passage and fed every 5-7 days by removing 50% of the old media and adding 50% fresh media, very gently so as not to disturb the cells. At approximately 80% confluence, the cells were passaged at 1:3 dilution for two more passages before use or were frozen for storage. Cells were used for experiments between passages 5-10. For comparing cell proliferation rates between WT and *Nmp4*^{-/-} MSPCs, the cells were transferred to α -MEM medium without the ascorbic acid in 12-well plates at 5,000 cells/well (Day 0). Cells were counted on Day 2, 4, and 6 post-seeding prior to refreshing the medium for the remaining cells. To evaluate mineralizing capacity cells were transferred to α -MEM medium and after 48hrs (Day 0) the medium was supplemented with ascorbic acid (5-50 μ g/ml, Sigma Aldrich), dexamethasone (0-10nM, Sigma-Aldrich), and 10mM glycerol 2-phosphate disodium salt hydrate (BGP, Sigma-Aldrich). For controls, cells were passaged into fresh Mesencult™ medium without the osteogenic/mineralization supplements. Cells were stained for alkaline phosphatase activity using naphthol AS-MX phosphate and fast red violet B salt following the manufacturer's instructions (Sigma cat# 85L3R-1KT) or for mineralization using alizarin red.

To assess the impact of *Nmp4* on IGF1 responsiveness, immortalized WT and *Nmp4*^{-/-} BM stromal cells (BMSCs) (Alvarez, Childress et al. 2012) were seeded in complete α -MEM with ascorbic acid and grown to confluency (one day) and starved of serum (0.1% FBS) overnight. The cells were then treated with IGF1 (Sigma-Aldrich) at 10ng/mL for 30 minutes. Cell lysates were collected in 2X Laemmli sample buffer and prepared for Western analysis.

Western analysis: The cell lysates harvested in 2X Laemmli sample buffer were quantified by the amido black method and equal mass loaded onto a sodium dodecylsulfate–polyacrylamide gel (SDS–PAGE, 10%) and transferred to a PVDF membrane (Bio-Rad

Laboratories, Hercules, CA). The immunoblots were probed with Phospho-Akt (Ser473) antibody (Cat# 9271, Cell Signaling Technology, Danvers, MA, 01923) and developed with SuperSignal® West Femto Maximum Sensitivity Substrate Antibodies (Pierce). The antibody signals were detected using a LAS-1000 plus luminescent image analyzer (Fujifilm, Sunnyvale, CA). Subsequently the blots were stripped and re-probed with total Akt antibody (CAT 9272) and developed as described above. Results were expressed as ratio of phospho-AKT/total AKT.

Flow cytometry: Cellular surface marker profiles from BM and peripheral blood (PBL) were assessed as previously described (He, Childress et al. 2013)[He et al., 2013]. The antibodies employed for flow cytometry were obtained from BD Biosciences (San Jose, CA). Stained cells were analyzed on an FACS Calibur (BD Biosciences) and results were quantified using FlowJo Version 8.8.6 software (TreeStar Inc, Ashland OR).

Micro computed tomography (μ CT): Trabecular bone architecture was analyzed as we have previously described (Childress, Philip et al. 2011, He, Childress et al. 2013). Briefly, femurs and L5 vertebra were excised from the WT and *Nmp4^{-/-}* mice after euthanasia, the muscle and connective tissue removed, and the bones transferred to 10% buffered formalin, 4°C for 48 hr, after which the bones were placed in 70% ethanol (4°C) until analyzed. For femur analysis a 2.6-mm span (<5 mm³ of medullary space) of the excised distal femoral metaphysis was scanned in 70% ethanol on a desktop μ CT (μ CT 35; Scanco Medical AG, Bassersdorf, Switzerland) at 10 μ m resolution using 55-kVp tube potential and 400-msec integration time, to measure three-dimensional morphometric properties. The entire vertebra (L5) were scanned using standard methods (Skyscan 1172). Bones were reconstructed and analyzed using the manufacturer's software. The trabecular bone between the two growth plates was isolated from the cortical shell via manual tracing and assessed for trabecular architecture. From the three dimensional reconstructions the following parameters were obtained using the Scanco and Skyscan software analyses: trabecular bone volume per total volume (BV/TV, %), connectivity density (Conn.D, mm⁻³), structure model index (SMI), trabecular number (Tb.N, mm⁻¹), trabecular thickness (Tb.Th, mm), and spacing (Tb.Sp, mm) [Bouxsein et al., 2010].

Bone histomorphometry: All histomorphometric parameters were obtained as previously described (Childress, Philip et al. 2011) following the ASBMR guidelines (Dempster,

Compston et al. 2013). Briefly, mice were administered intraperitoneal injections of calcein green (20 mg/kg; Sigma-Aldrich) and alizarin red (25 mg/kg, Sigma-Aldrich) 6 and 3 days before euthanasia, respectively. The femur marrow cavity was exposed via cutting the anterior face of the epiphyseal plate. Bones were embedded in methyl-methacrylate subsequent to dehydration with graded alcohols, sectioned (4 μ m) with a Leica RM2255 microtome (Leica Microsystems, Wetzlar, Germany), and mounted unstained on microscope slides and imaged under fluorescent light with a microscope system (Childress, Philip et al. 2011). Bone formation rate (BFR), mineral apposition rate (MAR), and mineralizing surface (MS/BS) were obtained from a 0.03mm² metaphyseal region of interest from 250 μ m to 1750 μ m below the growth plate using ImagePro 3.1 software (Media Cybernetics, Bethesda, MD, USA).

Serum biochemistry: We analyzed serum N-terminal propeptide of type 1 procollagen (P1NP) to evaluate global bone formation in our experimental mice using the Rat/Mouse P1NP EIA from IDS Immunodiagnostic Systems (Scottsdale, AZ) following the manufacturer's instructions. To follow bone resorption we analyzed serum C-terminal telopeptides (CTX) with the RatLaps™ ELISA (Immunodiagnostic Systems Inc) (Childress, Philip et al. 2011).

Quantitative real-time PCR (qRT-PCR) analysis: ChIP-qPCR was used to authenticate select ChIP-seq profiles employing SYBR Green assays and SYBR Green Supermix (Bio-rad, Hercules, CA). qRT-PCR reactions were carried out in triplicate on specific genomic regions. The resulting signals were normalized for primer efficiency by carrying out qRT-PCR reactions for each primer pair using Input DNA.

Chromatin immunoprecipitation sequencing (ChIP-seq) and ChIP analysis: Cells from ATCC (MC3T3-E1 subclone 4) were seeded into twenty-one 150mm plates at an initial density of 50,000 cells/plate (320 cells/cm²) and maintained in α MEM complete medium + ascorbic acid. On Day 14 post-seeding, cells were treated with 25nM hPTH(1-34) or vehicle control for 1hr before harvest. Subsequent to treatment cells were fixed with 1% formaldehyde for 15min and quenched with 0.125M glycine. Cell pellets were frozen in an ethanol dry ice bath and shipped to Active Motif for FactorPath™ analysis. The chromatin was isolated from the pellets by adding lysis buffer followed by disruption with a Dounce homogenizer. Lysates were sonicated and the DNA sheared to an average length of 300-

500 bp. Genomic DNA (Input) was prepared by treating aliquots of chromatin with RNase, proteinase K and heat for de-crosslinking, followed by ethanol precipitation. Pellets were resuspended and the resulting DNA was quantified on a NanoDrop spectrophotometer. Extrapolation to the original chromatin volume allowed quantitation of the total chromatin yield. An aliquot of chromatin (30µg) was precleared with protein A agarose beads (Invitrogen, ThermoFisher Scientific, Waltham, MA). Genomic DNA regions of interest were isolated using 4µg antibody against ZNF384 (Sigma HPA004051, Lot A57874). Complexes were washed, eluted from the beads with SDS buffer, and subjected to RNase and proteinase K treatment. Crosslinks were reversed by incubation overnight at 65°C, and ChIP DNA was purified by phenol-chloroform extraction and ethanol precipitation.

ChIP Sequencing (Illumina): ChIP and Input DNAs were prepared for amplification by converting overhangs into phosphorylated blunt ends and adding an adenine to the 3'-ends. Illumina genomic adapters were ligated and the sample was size-fractionated (200-300 bp) on an agarose gel. After a final PCR amplification step (18 cycles), the resulting DNA libraries were quantified and sequenced on HiSeq 2000. Sequences (50nt reads, single end) were aligned to the mouse genome (mm10) using the BWA algorithm. Alignments were extended in silico at their 3'-ends to a length of 150 bp, which is the average genomic fragment length in the size-selected library, and assigned to 32-nt bins along the genome. The resulting histograms (genomic "signal maps") were stored in BAR and bigWig files. ZNF384 peak locations were determined using the MACS algorithm (v1.4.2) with a cutoff of pvalue = $1e-7$ (Li and Durbin 2009).

Bioinformatic profiling: In addition to generating our own Nmp4 ChIP-seq data from the MC3T3-E1 cells we used Nmp4 (Znf384) ChIP-seq data from murine embryonic stem cell line (ES-E14) and the B-cell lymphoma cell lines Ch12 and MEL from the ENCODE Consortium for transcription factors 2011 Freeze data sets in NarrowPeak format (Rosenbloom et al., 2013). To assign an Nmp4 peak to a promoter region it had to be within -5kb to +2kb from a transcription start site (TSS). To assign a peak to an intragenic region it had to be located within the range defined by the TSS and the transcription end site (TES), and not within the promoter range of the same gene. To assign a peak to an intergenic region it had to be -10,000kb from the TSS and +10,000kb from the TES, and not within the promoter range of the same gene. A peak could be assigned to multiple functional regions in an area of the genome harboring multiple genes. A common example

of this is an area with genes on both strands. A peak may not fit any of these definitions and was assigned to the classification “other”. This methodology yielded 34,317 functional assignments for the peaks in the MC3T3-E1 cells.

GEM analysis: Genome wide Event finding and Motif discovery (GEM) (Guo, Mahony et al. 2012) was used to derive the Nmp4 consensus sequence. The latest mouse genome build (mm10) was employed together with the GEM default ChIP-seq read distribution file and a minimal k-mer width of 6 and maximum of 20.

Gene Ontology: Gene ontology analysis was conducted using DAVID (Huang, Sherman et al. 2009), and terms summarized using REVIGO (Supek, Bošnjak et al. 2011, Auerbach, Chen et al. 2013). The ENCODE ChIP-Seq Significance Tool was employed to identify enriched transcription factors in our Nmp4 gene target list (Auerbach, Chen et al. 2013). Additionally some functional analysis was also generated through the use of QIAGEN’s Ingenuity Pathway Analysis (IPA®, QIAGEN Redwood City, www.qiagen.com/ingenuity).

Bone phenotype statistical analysis: Statistical evaluations were processed using the program JMP version 7.0.1 (SAS Institute, Cary, NC). The animal studies employed a two-way ANOVA using genotype and treatment as the independent variables followed by either a Tukey HSD or LS Means post hoc test if a genotype x treatment interaction was indicated. Statistical significance was set at $p \leq 0.05$. To compare growth rates of the WT and *Nmp4*^{-/-} MSPCs derived from various experimental mice, we evaluated the slopes of log-transformed cell counts regressed onto experimental day using a t-test. The numbers of mice per treatment group and replicates/treatment for the cell studies are indicated in the appropriate figures and tables.

RESULTS:

Nmp4^{-/-} mice are not protected from ovx-induced bone loss

To determine whether genetically disabling Nmp4 activity protects mice from ovx-induced bone loss as it does from unloading-associated osteopenia (Hino, Nakamoto et al. 2007), we removed the ovaries or performed sham operations on both WT and *Nmp4*^{-/-} mice (Figure 4-1). Both the ovx WT and ovx *Nmp4*^{-/-} mice experienced significant weight gain at 4wks post-op (Table 4-1) consistent with previous mouse studies (Vieira Potter 2012). Additionally, ovx resulted in a significant decrease in uterine weight in both

genotypes (Table 4-1). There was no genotype x treatment interaction in either of these parameters.

Both WT and *Nmp4*^{-/-} mice exhibited significant bone loss 4wks after ovx surgery as measured in the trabecular bone compartment of the distal femur and the L5 vertebra (Table 4-1). The *Nmp4*^{-/-} mice exhibited a trend towards enhanced loss of bone that neared significance in the distal femur (BV/TV, genotype x treatment interaction = 0.06, Table 4-1) and reached significance in the L5 vertebra (BV/TV, genotype x treatment interaction <0.05, Table 4-1). Despite this enhanced (or nearly enhanced) rate of bone loss the *Nmp4*^{-/-} animals maintained more trabecular bone compared to WT mice during the first 4wks after ovariectomy. Finally, we observed no differences in the level of serum bone formation marker P1NP or the resorption marker CTX at 4wks post-op between the genotypes (Table 4-1).

Ovx Nmp4^{-/-} mice show an enhanced bone gain response to PTH therapy

With a separate group of ovx mice we initiated treatment of both WT and *Nmp4* null animals with PTH (30µg/kg/day) and vehicle control 4wks after surgery. The duration of hormone therapy lasted 4wks (8wks post-op) and 8wks (12wks post-op). The ovx *Nmp4*^{-/-} mice showed an enhanced PTH-induced gain in femoral BV/TV and Conn D at 4wks and 8wks of therapy compared to their ovx WT littermates as well as an augmented gain in trabecular thickness at 8wks (Figure 4-2, Table 4-2). The null mice also showed an enhanced PTH response at the L5 vertebra at 8wks of treatment (Figure 4-3, Table 4-2). Specifically the 2-way ANOVA indicated strong genotype x treatment effects for the distal femur for both 4wks and 8wks therapy and for the L5 vertebra for 8wks therapy (see Figures 4-2A and 4-3A); the post-hoc tests concluded that the difference between the genotypes was within the hormone-treated groups. The vehicle-treated ovx WT and ovx *Nmp4*^{-/-} groups showed no difference in BV/TV (Figures 4-2 and 4-3) at the end of the treatment regimens indicating that the modest enhanced loss in bone in the *Nmp4*^{-/-} was stabilized by 4wks therapy. PTH significantly elevated MAR, MS/BS, and BFR at the end of 4wks treatment as shown by strong treatment effects (Table 4-3). However, there was no genotype effect or genotype x treatment interaction for any of these parameters (Table 4-3). Hormone significantly elevated serum levels of the bone formation marker P1NP and the resorption marker CTX at 8wks of therapy, but there was no treatment x genotype interaction for either of these parameters (Table 4-3).

FACS analysis of the BM CD45-/CD105+/CD146+/nestin+ osteoprogenitors revealed a significant elevation in the number of these cells in the BM obtained from the *Nmp4*^{-/-} mice at the end of 4wk therapy, irrespective of treatment (Figure 4-4A). This is consistent with our previous observation in the ovary-intact null mice [He et al., 2013]. By the end of 8wks treatment (12wks post-op) the observed increase in the number of these *Nmp4*^{-/-} cells in the BM failed to reach statistical significance, but there was a significant elevation in the number of the PBL *Nmp4*^{-/-} osteoprogenitors in the vehicle-treated mice (Figure 4-4D). The *Nmp4*^{-/-} mice showed a significant elevation in CD8+ T cells in both the BM and the PBL throughout the entire therapy regimen (Figure 4-4B & E). PTH significantly decreased the numbers of these cells in the BM at 8wks therapy in both genotypes (Figure 4-4B) but had no impact on the number of these cells in the PBL (Figure 4-4E). Disabling *Nmp4* had little to no effect on CD4+ T cells, nor did treatment with PTH (Figure 4C and 4F). The modest increase in BM CD4+ T cells approached significance ($p < 0.06$) but this was not reflected in the PBL, just as we previously observed in the ovary-intact mice [He et al., 2013].

To determine if the enhanced osteogenic potential of the BM could be reliably and reproducibly maintained in vitro in MSPC cultures over several passages and in the absence of supporting cells (e.g. T-cells) we established expanded WT and *Nmp4*^{-/-} MSPCs from ovary-intact mice. The expanded *Nmp4*^{-/-} MSPCs from ovary-intact mice exhibited modest but significantly enhanced proliferation compared to the WT cells (Figure 4-5A). Both the null and WT expanded MSPCs showed strong alkaline phosphatase expression (Figure 4-5B). However, the expanded *Nmp4*^{-/-} MSPCs were typically more mineralization competent than WT cells under various concentrations of dexamethasone and ascorbic acid (Figure 4-5B). Finally, the expanded *Nmp4*^{-/-} and WT MSPCs exhibited varying degrees of alkaline phosphatase staining while maintained in Mesencult™ medium, depending on the confluence of the cells and time in culture (3-9 days), however no mineralization was observed in these control cultures (data not shown).

Genome-wide ChIP-seq/gene ontology analysis reveals Nmp4 target genes and potential pathways of the anti-anabolic axis.

Nmp4 is expressed in nearly all cells, yet the most singular consequence of globally disabling this protein is the enhanced mobilization of bone cells upon osteoanabolic induction (Morinobu, Nakamoto et al. 2005, Robling, Childress et al. 2009, Childress, Philip et al. 2011, He, Childress et al. 2013). As a first step in understanding

the origins of this phenotype, which may have clinical significance, we needed the following information: (1) the identity of the Nmp4 target genes including 'core' target genes common to multiple cell types; (2) identify common functions of these core genes to distinguish pathways that make osteoprogenitors particularly vulnerable to the effects of Nmp4 and (3) experimental confirmation of some of these pathways. To begin to understand how Nmp4 works we set out to understand (4) whether Nmp4 targets functional regions of the genome, (5) if it binds directly to DNA or via other proteins, and (6) whether osteoanabolic agents, e.g. PTH, alter Nmp4 DNA-binding along target genes.

The potential Nmp4 target genes identified by ChIP-seq in the MC3T3-E1 (vehicle-treated) cells and those established in the three ENCODE cell lines were compared using those genes that had one or more peaks associated with the TSS. A Venn diagram of these genes showed that 2114 Nmp4 'core' target genes were common to the four cell lines (Figure 4-6A, and Appendix 1). These core target genes were classified into functionally related categories using gene ontology (GO) analysis with the Database for Annotation, Visualization, and Integrated Discovery (DAVID) tool (Huang, Sherman et al. 2009). The functional annotation-clustering algorithm was applied to the target list, which is able to give a more insightful view of the relationships between annotation categories and terms compared to other analytic modules (Huang, Sherman et al. 2009). The significance of group classification was defined by enrichment scores based on Fisher exact statistics (false discovery rate, FDR $p < 0.05$). The DAVID-derived biological profile was further summarized using REVIGO (Supek, Bošnjak et al. 2011). GO analysis of the core target genes designated Nmp4 as a negative regulator of cellular biosynthetic processes showing significant enrichment for genes involved in the regulation of transcription, chromatin modification, protein catabolic processes, regulation of the cell cycle, and mRNA processing/splicing (Figure 6B). Interestingly, the genes *specific* to any one particular cell line or specific to vehicle-treated or PTH-treated MC3T3-E1 cells did not yield a distinct biological process profile that reached statistical significance as obtained with the core target genes (data not shown). However, peak-associated genes common to the vehicle- and PTH-treated MC3T3-E1 cells yielded a profile nearly identical to that obtained with the core target genes.

DAVID also uses the KEGG (Kyoto Encyclopedia of Genes and Genomes) database to map large gene lists to signaling pathways (Huang, Sherman et al. 2009). The DAVID/KEGG profile of the Nmp4 core target genes included the TOR and insulin signaling pathways (Table 4-4) and indeed the insulin/IGF1->IRS1->PI3K->Akt signaling

response limb is common to many of the pathways listed (see Figure 4-7A). This is also consistent with our IPA analysis (Appendix 2). Since PTH anabolic action is mediated, in part, by local production of IGF1 [Elis et al., 2010], we addressed whether *Nmp4*^{-/-} BM stromal cells (BMSCs) exhibit an enhanced response to this growth factor. A 30min challenge with IGF1 induced a significantly enhanced Akt phosphorylation in the *Nmp4*-null cells as compared to WT-derived cells (Figure 4-7B). The IPA analysis also identifies the glucocorticoid signaling pathway and the glucocorticoid receptor gene (*Nr3c1*) as *Nmp4* targets (Supplemental Tables 1 and 2), a particularly potent differentiation signal to osteoprogenitors (Eijken, Koedam et al. 2006, Hamidouche, Haÿ et al. 2008, 2012).

Next we probed existing datasets for enriched transcription factors within our *Nmp4* core target gene list using the ENCODE ChIP-seq Significance Tool (Auerbach, Chen et al. 2013) (Table 4-5). This profile shows that *Nmp4* binding in the promoter regions of its target genes predominantly co-occurs with proteins that regulate chromatin organization and with proteins that contribute to maintaining stem/progenitor pluripotency/multipotency and the poised gene state, e.g. CHD2, SIN3a, and GCN5 (Lin, Srajer et al. 2007, Nascimento, Cox et al. 2011, Harada A 2012).

In an effort to gain further understanding of how *Nmp4* regulates gene expression we prepared a genome-wide functional region map of the *Nmp4* binding sites for all four cell types as described in Materials and Methods. The majority of the occupancy peaks were located in or near the TSS or in intragenic regions, areas typically associated with regulatory functions (Figure 4-8A). To determine if *Nmp4* binds directly to DNA or can associate with the genome via other proteins we used the discovery algorithm GEM to derive the *Nmp4* consensus-binding site from the MC3T3-E1 data. In support of previous studies by our lab and others the derived binding site matched the unusual homopolymeric (dA-dT) consensus sequence previously derived by cyclic amplification and electrophoretic mobility shift assay (Alvarez, Thunyakitpisal et al. 1998, Nakamoto, Yamagata et al. 2000) (Figure 4-8B). No other consensus sequences were identified suggesting a single and direct mode of genome association, mediated by the Cys2His2 DNA-binding domain (Torrunguang, Alvarez et al. 2002). To determine whether PTH challenge altered *Nmp4* DNA-binding along target genes we generated genome-wide *Nmp4* ChIP-seq profiles using the pre-osteoblast cell line MC3T3-E1 treated with hPTH(1-34) or vehicle control for 1hr. We used the 1hr time point because we observed the most significant differences in femoral mRNA expression profiles between WT and *Nmp4*^{-/-} mice 1hr after injection (Childress, Philip et al. 2011). Hormone reduced *Nmp4* genome-wide

occupancy from a total of 15,446 to 13,109 binding sites. However, at the level of the single gene there was a diversity of changes in *Nmp4* occupancy, i.e. PTH was observed to remove (e.g. *Nid2*), induce (e.g. *Ccdc53*) or have no effect on *Nmp4*-DNA association (e.g. *Akt2*, *Arb2*) (Figure 4-9; also see ChIP-qPCR confirmation of *Nmp4* binding, Figure 4-11).

DISCUSSION:

Bone restoration by PTH therapy is improved in ovx mice by disabling *Nmp4*. The ovx *Nmp4*^{-/-} mice displayed an enhanced hormone-induced recovery of femoral and L5 trabecular BV/TV despite delaying treatment until 4wks post-op to allow for significant bone loss. Both the ovx WT and ovx *Nmp4*^{-/-} mice showed strong responses to PTH therapy. After 4wks and 8wks of treatment the WT mice displayed a 3.2-fold and 4.6-fold increase in femoral BV/TV over vehicle-treated mice, respectively. However the *Nmp4*^{-/-} mice showed a 3.6-fold and 8.8-fold increase over the same time period resulting in a very strong genotype x treatment interaction. Differences in PTH-mediated BV/TV restoration efficacy between the WT and *Nmp4*^{-/-} mice took longer to manifest in the L5 vertebra and was less striking although statistically significant (1.3-fold vs 1.6-fold at 8wks in the WT and *Nmp4*^{-/-} mice, respectively). We observed similar PTH-responsive femoral and L5 profiles between younger, ovary-intact WT and *Nmp4*-null mice (Robling, Childress et al. 2009, Childress, Philip et al. 2011, He, Childress et al. 2013). The histomorphometry and serum data reported here tracked the PTH-induced increases in bone mass in the ovx animals showing strong treatment effects for bone formation parameters MAR, BFR, and MS/BS (at 4wks treatment) as well as strong increases in bone remodeling serum P1NP and CTX (at 8wks treatment). However, these parameters did not distinguish the genotypes in regards to the amount of bone formed over this time period as was achieved with the μ CT data. Interestingly, the histomorphometry data did not distinguish the differences in PTH-induced bone formation in ovary-intact WT and *Nmp4*^{-/-} mice (Childress, Philip et al. 2011). Therefore, this may indicate that *Nmp4* regulates PTH-induced bone formation predominantly in the early treatment period, consistent with an expanded pool of osteoprogenitors poised for mobilization. A more extensive time course for harvesting histomorphometry samples may be required to capture this aspect of the phenomenon.

The most robust phenotypic characteristic of *Nmp4* ablation is the exaggerated bone formation response to PTH or BMP2, which suggests that the adult mice harbor an

increased number of BM MSPCs with heightened sensitivity to osteoanabolic signals. Disabling *Nmp4* has no observable impact on embryonic or perinatal skeletal development. Adult MSPCs are a heterogeneous population of multipotent stem, progenitor, and stromal cells that contribute to BM homeostasis (Mizoguchi, Pinho et al. 2014). In mouse bone marrow much of the CFU-F activity is in the nestin+ cell population and in the human marrow the CD146+ population (Sacchetti, Funari et al. 2007, Mizoguchi, Pinho et al. 2014). In ovary-intact, *Nmp4*^{-/-} mice we observed a 4-fold increase in the frequency of CD45-/CD105+/CD146+/nestin+ cells irrespective of treatment (PTH vs vehicle control), which paralleled the magnitude increase in CFU-F and CFU-F^{alk phos+} cell number in culture (He, Childress et al. 2013). Similarly, the ovx *Nmp4*^{-/-} mice exhibited an approximate 3-fold increase in the CD45-/CD105+/CD146+/nestin+ cells at 8wks post-op compared to the ovx WT animals. Nevertheless, it is not clear whether this potential source of osteoprogenitors is inexhaustible since at 12wks ovx post-op there was no statistical difference in the number of BM CD45-/CD105+/CD146+/nestin+ cells between the *Nmp4*^{-/-} and WT mice but there was a significant increase in the number of these cells in the vehicle-treated null PBL. The origins and functional significance of circulating osteoprogenitors are not fully understood (Pirro, Leli et al. 2010, Pignolo and Kassem 2011), but these cells may contribute to the enhanced osteogenic reserve of the *Nmp4*^{-/-} mice.

The enhanced osteogenic potential of the *Nmp4*^{-/-} BM as measured by the frequency of cells capable of becoming osteoprogenitors persists in expanded *Nmp4*^{-/-} MSPC cultures over 5-10 passages and removed from the supporting CD8+ T cells. In culture these cells displayed a modest increase in proliferative activity and perhaps this aspect of the phenotype contributes to the observed expanded pool of osteoprogenitors in vivo. In an earlier study, Noda and colleagues demonstrated that *Nmp4*^{-/-} BM yielded significantly more CFU-F^{Ob} mineralizing colonies at passage P₀ than WT BM [Morinobu et al., 2005]. Our present data extend these observations and show that the serially passaged *Nmp4*^{-/-} MSPCs maintain a strikingly enhanced capacity for mineralization compared to the capacity of the WT cultures. The mechanisms underlying this phenotype remain to be elucidated, however the IGF1/Akt pathway plays a significant role in MSC proliferation and mineralization [Kumar and Ponnazhagan, 2012; Xian et al., 2012] and the glucocorticoid pathway governs MSC mineralization (Langenbach and Handschel 2013), both targets of *Nmp4*. Taken together these observations suggest that there is a cell autonomous role of *Nmp4* for regulating MSPC osteogenesis.

Further parsing of the enhanced *Nmp4*^{-/-} BM osteogenic potential implicates the elevated frequency of CD8+ T cells in both ovary-intact and ovx *Nmp4*^{-/-} mice, although this requires functional confirmation in these models. The ovx null animals exhibited elevated numbers of CD8+ T cells in both BM and PBL compartments throughout the entire treatment regimen, similar to what we previously observed in the younger ovary-intact *Nmp4*^{-/-} mice, although this increase was limited to the BM (He, Childress et al. 2013). The elevated number of CD8+ T cells is intriguing since these cells are documented to amplify the PTH anabolic response (Terauchi, Li et al. 2009, Bedi, Li et al. 2012). MSCs regulate T cell proliferation and survival (Wang, Zhao et al. 2012) and perhaps disabling *Nmp4* de-represses this aspect of the cell-cell interaction, although this apparent alteration in proliferation/survival may be a cell autonomous feature of the *Nmp4*^{-/-} T cell phenotype. It remains to be determined whether the *Nmp4*^{-/-} phenotype requires CD8+ T cells for enhanced PTH anabolism or whether this phenomena is dependent on increased MSC number/function or both.

Disabling *Nmp4* did not protect the mice from ovx-induced bone loss, indeed the initial rate of loss during the first 4wks after ovariectomy was higher (L5) or nearly higher (distal femur) in the *Nmp4*^{-/-} mice. These animals harbor a modestly elevated number of osteoclast progenitors (CFU-GM) (He, Childress et al. 2013) that upon differentiation exhibit an enhanced bone-resorbing activity in vitro (Childress, Philip et al. 2011). Therefore a decrease in estrogen might accentuate this aspect of the phenotype. Moreover, differences in sex steroid levels may underlie why intact male *Nmp4*^{-/-} mice did not lose bone under hind limb suspension (Hino, Nakamoto et al. 2007). As mentioned, the *Nmp4*^{-/-} baseline phenotype includes an occasional unprovoked enhancement in trabecular architecture, which we observed in the present study. That is to say, despite the elevated initial bone loss, the cohort of sham and ovx *Nmp4*^{-/-} mice had more femoral and L5 trabecular bone compared to WT at the time of harvest (Table 4-3). However, there was no statistical difference between vehicle-treated animals in either the 4wk or 8wk hormone therapy cohorts (Figures 4-2 and 4-3). Longitudinal studies for serum turnover markers coupled with pQCT in live mice could be used to track the real-time dynamics of ovx-induced bone loss and subsequent therapy-induced bone gain between the WT and *Nmp4*^{-/-} mice. In lieu of this, we employed a 2-way ANOVA, which incorporates differences in control groups, to evaluate whether there is an interaction between genotype and treatment.

Bioinformatic profiling of ChIP-seq data derived from bone, blood, and embryonic stem cells identifies *Nmp4* as a negative regulator of cellular biosynthetic processes and distinguishes several pathways by which this transcription factor potentially regulates the number and stimuli responsiveness of MSC-derived osteoprogenitors. Although *Nmp4* is constitutively expressed in several tissues (Thunyakitpibal, Alvarez et al. 2001) and targets many of the same genes in multiple cell types, several of these core target genes are particularly consequential to osteogenesis and bone metabolism/physiology. It may be the unique expression profile of adult MSCs that make them particularly vulnerable to the action of *Nmp4* ablation in the global knockout. The enhanced frequency of *Nmp4*^{-/-} MSCs and their heightened sensitivity to osteoanabolic differentiation signals may occur by de-repressing pathways supporting these phenotypic characteristics while conversely diminishing the activities of pathways repressive to them. This hypothesis is consistent with previous studies identifying *Nmp4* as a context dependent transcription factor that can accommodate or suppress gene activity (Thunyakitpibal, Alvarez et al. 2001, Shen, Nakamoto et al. 2002, Torrungruang, Alvarez et al. 2002, Shah, Alvarez et al. 2004).

Our ChIP-seq/GO map predicts that *Nmp4* suppresses IGF1 and BMP2 stimulus response, both key local mediators of PTH anabolic action (Elis, Courtland et al. 2010, Yu, Zhao et al. 2012). We experimentally confirmed that the *Nmp4*^{-/-} bone marrow stromal cells exhibited an exaggerated IGF1-induced Akt phosphorylation compared to their WT counterparts. The IGF1-Akt pathway plays a well-described significant role in bone metabolism (Elis, Courtland et al. 2010, Bikle and Wang 2012, Sun, Kim et al. 2013, Tahimic, Wang et al. 2013). How the transcription factor *Nmp4* governs Akt signaling remains to be determined. *Nmp4* specifically targets *Akt2* of the three Akts expressed in mammals. *Akt2* is required for BMP2-mediated MSC osteogenic differentiation, while *Akt1* is dispensable [Mukherjee et al., 2010]. Loss of *Akt2* prevents induction of *Runx2* gene expression in MSCs (Mukherjee, Wilson et al. 2010). Other *Nmp4* Akt pathway target genes include phosphatidylinositol 3-kinase (*Pi3k*), pyruvate dehydrogenase kinase (*Pdk1*), β -arrestin 2 (*Arrb2*), and protein tyrosine phosphatase 4a1 (*Ptp4a1*). *Arrb2* plays multiple regulatory roles in bone response to anabolic PTH including the induction of MSC differentiation (Bouxsein, Pierroz et al. 2005, Yu, Zhao et al. 2012). Previous studies have demonstrated that *Nmp4* also suppresses BMP2 stimulus response in osteogenic cells (Shen, Nakamoto et al. 2002, Morinobu, Nakamoto et al. 2005, Alvarez, Childress et al. 2012) and our ChIP-seq/GO map identifies *Smad7* and *Tob2* as potential

Nmp4 target genes, both of which inhibit BMP signaling [Yano et al., 2012; Gámez et al., 2013; Ajima et al., 2008; Yoshida et al., 2000; Takahashi et al., 2012].

The ChIP-seq/GO analysis identified other potential Nmp4 targets worth exploring as primary or collateral pathways in suppressing MSC frequency and osteoanabolic response (Figure 4-10). Briefly, Nmp4 binds to the glucocorticoid receptor (*GR*) gene and IPA analysis identifies the GR signaling pathway as a significant Nmp4 target (Appendices 1 and 2). Endogenous glucocorticoids drive osteogenic differentiation [Hamidouche et al., 2008; Eijken et al., 2006] and the exaggerated mineralization of the *Nmp4*^{-/-} MSCs may in part, be the response of the cells to the low concentration of added dexamethasone. Nmp4 targets numerous genes that comprise or regulate heterochromatin including the polycomb repressive complexes 1 and 2 (PRC1, PRC2), which are epigenetic modifiers governing the equilibrium between stemness and differentiation in pluri- and multipotent cell populations (Aloia et al., 2013; Surface et al., 2010). Nmp4 itself may engage with chromatin complexes. The Nmp4 homopolymeric (dA•dT) consensus sequence can act as a nucleosome positioning signal (Hughes et al., 2012; Raveh-Sadka et al., 2012) and the ENCODE ChIP-seq Significance profile shows that Nmp4 co-occupies the core target genes with numerous chromatin remodeling proteins. The ubiquitin-proteasome and the unfolded protein response (UPR) pathways are identified as potential Nmp4 targets, and these may contribute to the observed enhanced IGF1/Akt and BMP2/SMAD signaling in the *Nmp4*^{-/-} osteogenic cells (Figure 4-10). Proteasomes regulate osteoblast differentiation [Zhao et al., 2003; Qiang et al., 2012] and proteasome inhibitors induce MSC osteogenic differentiation and enhance bone formation [Giuliani et al., 2007; Mukherjee et al., 2008; Lund et al., 2010]. Treatment of mouse embryonic fibroblasts with the proteasome inhibitor MG132 significantly increased Igf1-induced Akt phosphorylation, since this growth factor not only mediates Akt phosphorylation but also ubiquitination and degradation of the activated Akt [Wu et al., 2011]. BMP2-induced osteoblast differentiation activates the PERK–eIF2α–ATF4 UPR pathway [Tanaka et al., 2014; Saito et al., 2011]. Gadd34, an identified target gene of Nmp4, inhibits this BMP2-UPR mechanism [Schewe and Aguirre-Ghiso, 2009]. Thus disabling Nmp4 may decrease Gadd34 expression and contribute to the enhanced BMP2 response observed in the *Nmp4*-KO mice [Morinobu et al., 2005; Shen et al., 2002]. Finally, Nmp4 targets numerous transcription factors involved in regulating MSC self-renewal, proliferation, and osteogenic differentiation.

The present data also contribute to our knowledge as to how Nmp4 works at the molecular level. Nmp4 binds throughout the genome but is primarily localized to regions

near the TSS and within the gene, consistent with mediating a regulatory role. GEM analysis confirmed the AT-rich homopolymeric binding-site and did not identify other consensus sequences expected only if Nmp4 also interacted with the genome indirectly via other DNA-binding proteins. Nmp4 association with the genome is responsive to PTH since hormone decreased genome-wide occupancy in the MC3T3-E1 cells after 1hr of exposure. However, the impact of PTH on Nmp4 occupancy was gene and site-specific and hormone stimulation was observed to induce, remove, or have no effect on Nmp4 genomic occupancy. This may further augment the fine control that this transcription factor has over the regulation of osteoprogenitor and/or bone-forming capacity.

There is a critical need for more safe and improved osteoanabolic agents beyond teraparotide/PTH [Lewiecki, 2011]. We have taken a two-pronged approach in our research to serve this clinically unmet need: (1) identify molecular and cellular mechanisms that could be used, for example in an adjuvant setting to promote enhanced efficacy or less frequent dosing with current osteoanabolic agents; and (2) identify innovative approaches to identify new drug targets/pathways or mechanisms of action that would provide needed substrate for the future drug discovery initiatives in bone disease, including osteoporosis. Our discovery-driven approaches have mapped a global network of Nmp4-regulated pathways potentially comprising a bone anti-anabolic axis. Further functional studies charting the hierarchy and interactions of these network pathways will provide a novel integrated mechanism underlying the natural constraints on bone formation. We postulate that the Nmp4 anti-anabolic network may constitute a novel strategy to identify and reveal pharmacologically accessible pathways for adding new bone to the old skeleton.

Acknowledgements:

This work was supported in part by the Department of Defense (PR120563, JPB); Eli Lilly (062079-00002B, JPB); NIH (CTSI pre-doctoral fellowship TL1 000162, PC)

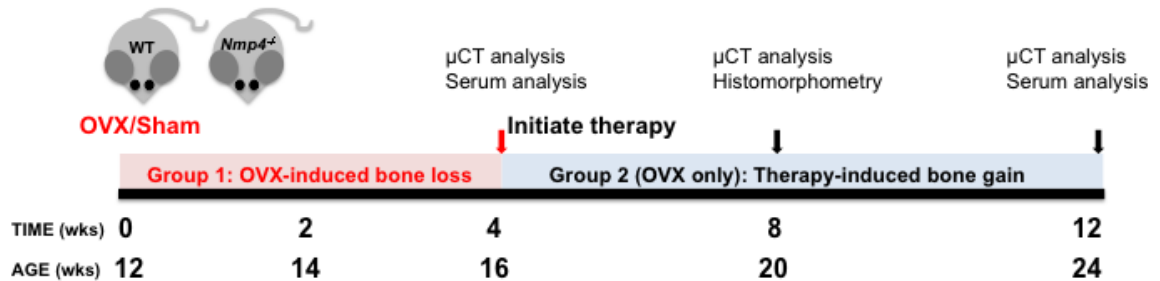


Figure 4-1: Schematic of treatment regimen for WT and *Nmp4^{-/-}* mice; Group 1 mice were subjected to ovariectomy (ovx) or sham operation at 12wks of age and evaluated for bone loss 4wks post-op (16wks of age). Group 2 mice were ovx at 12wks of age and began PTH or vehicle therapy at 16wks of age for a duration of 4wks and 8wks. Endpoint analyses included micro-computed tomography μ CT, serum analysis for N-terminal propeptide of type 1 procollagen (P1NP) and C-terminal telopeptides (CTX), and dynamic histomorphometry.

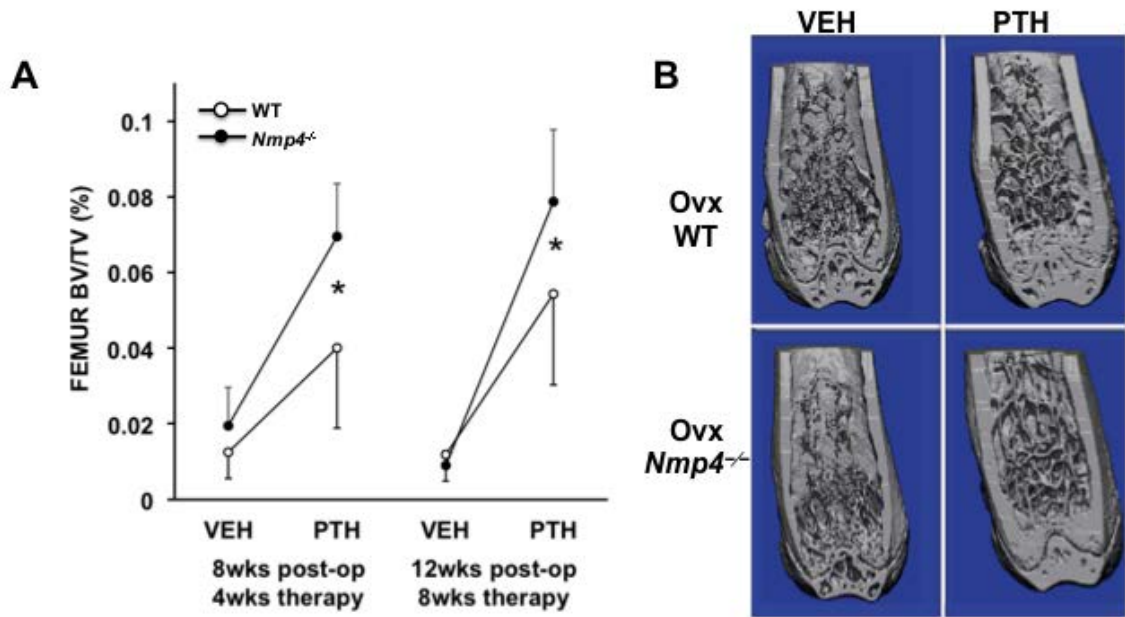


Figure 4-2: Disabling *Nmp4* enhances PTH restorative therapy in the distal femur of ovx *Nmp4^{-/-}* mice [A] Interaction plots of femoral trabecular bone volume/total volume (BV/TV) of ovx WT and ovx *Nmp4^{-/-}* mice as determined by μ CT at 4wks of treatment and 8wks of treatment. Data are average \pm SD, number of mice/experimental group = 8-9). Statistical differences were determined using a 2-way ANOVA and significance was set at $p \leq 0.05$. The Tukey's HSD post hoc test was used to determine differences between the treatment groups. There were genotype, treatment and genotype x treatment interaction at both time points. There was no difference between the vehicle-treated WT and *Nmp4^{-/-}* mice. [B] μ CT images showing PTH-induced improvements in distal femur trabecular architecture in ovx WT and *Nmp4^{-/-}* mice after 8 weeks of treatment (12wks post-op, 24wks of age).

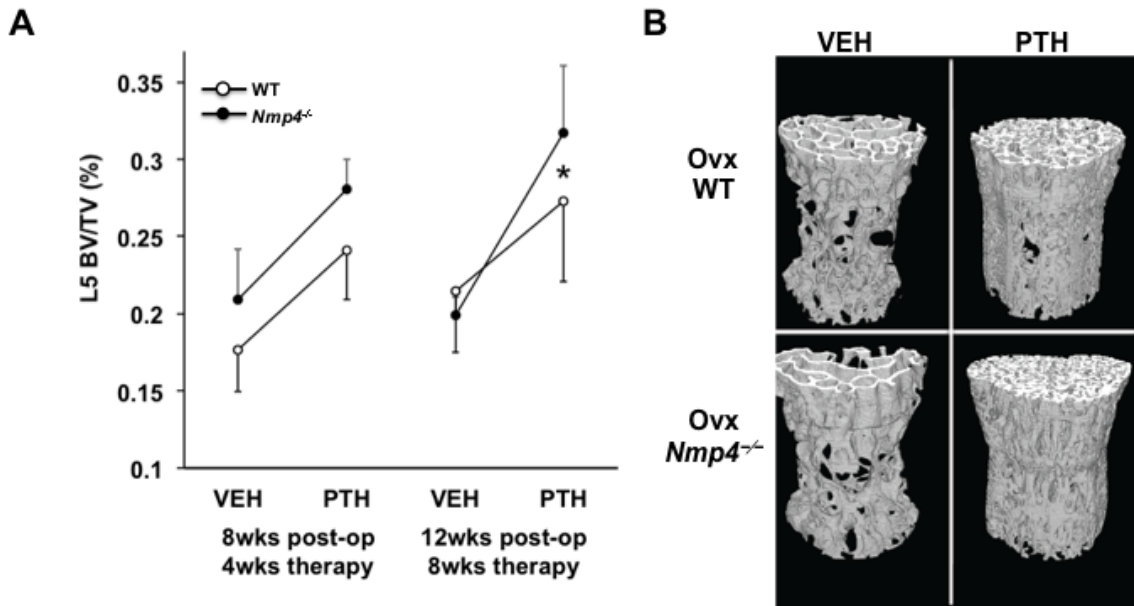


Figure 4-3: The exaggerated response to anabolic PTH persists in the L5 vertebra of ovx *Nmp4*^{-/-} mice. [A] Interaction plots of L5 vertebra bone volume/total volume (BV/TV) of ovx WT and ovx *Nmp4*^{-/-} mice as determined by μ CT at 4wks of treatment and 8wks of treatment. Data are average \pm SD, number of mice/experimental group = 8-9). Statistical differences were determined using a 2-way ANOVA and significance was set at $p \leq 0.05$. The LS Means Student t post hoc test was used to determine differences between the treatment groups. There were genotype, treatment effects at both time points and a genotype x treatment interaction at 8wks therapy. There was no difference between the vehicle-treated WT and *Nmp4*^{-/-} mice. [B] μ CT images showing PTH-induced improvements in L5 trabecular architecture in ovx WT and *Nmp4*^{-/-} mice after 8 weeks of treatment (12wks post-op, 24wks of age).

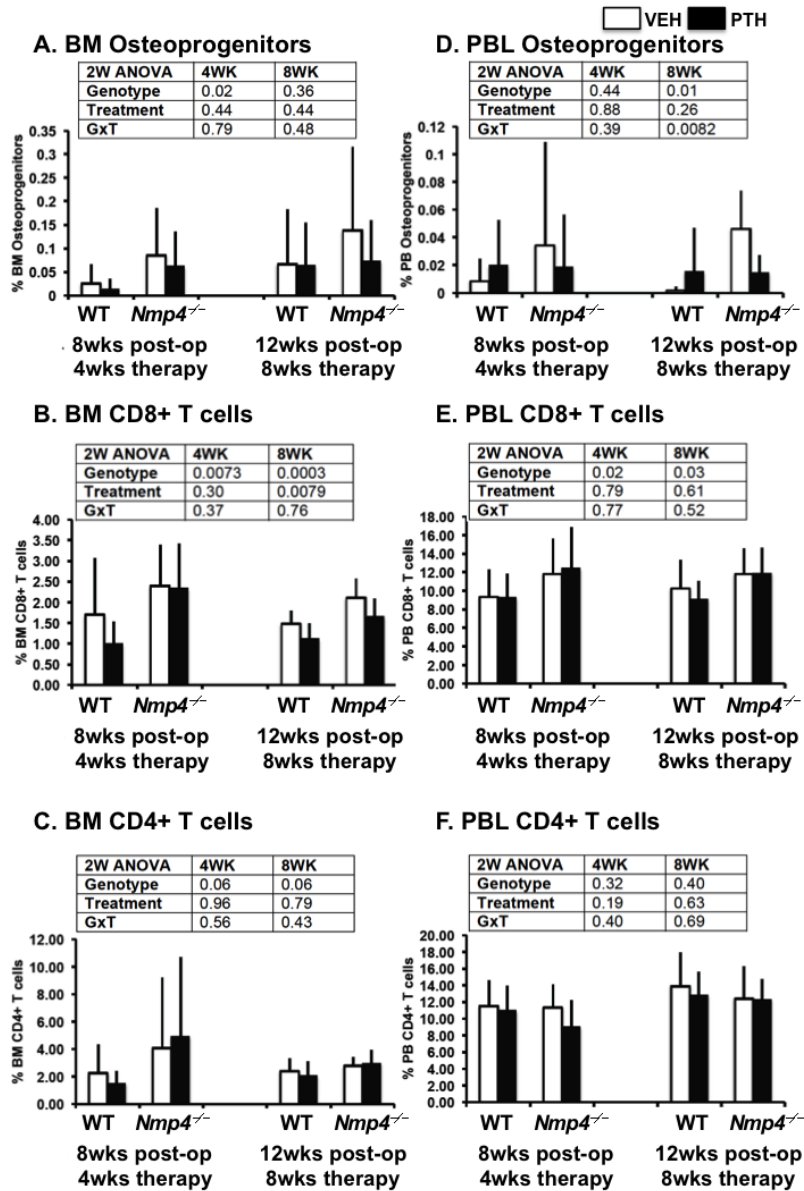


Figure 4-4: Ovx does not abrogate the expanded population of osteoprogenitors and CD8+ T cells in *Nmp4*^{-/-} mice. FACS analysis of BM and PBL osteoprogenitors, CD8+ T cells, and CD4+ T cells. [A, D] The frequency of femoral BM and PBL CD45-/CD105+/CD146+/CD105+/nestin+ osteoprogenitor cells in WT and *Nmp4*^{-/-} mice at the end of 4wks and 8wks treatment with intermittent PTH or vehicle control; [B, E] the frequency of BM and PBL CD8+ T cells from the WT and *Nmp4*^{-/-} mice; [C, F] the frequency of BM and PBL CD4+ T cells from the WT and null mice. Data are average ± SD, number of mice/experimental group = 8–9; Statistical differences were determined using a 2-way ANOVA and significance was set at p≤0.05.

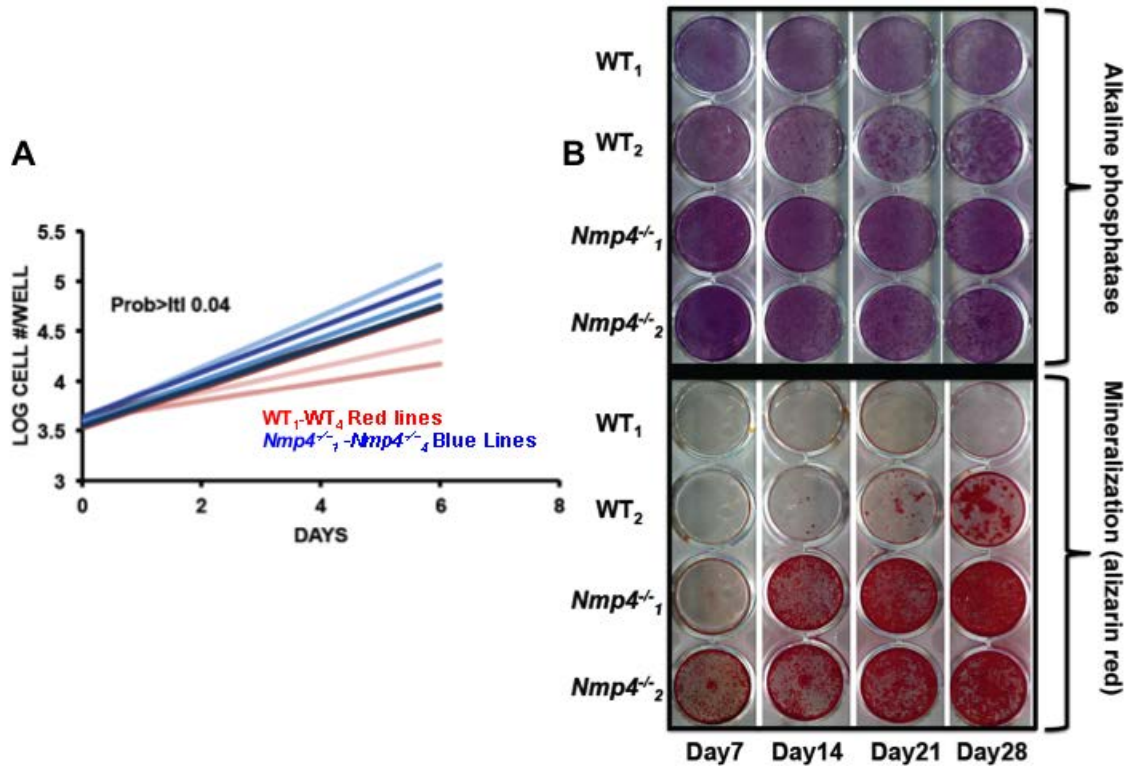


Figure 4-5: Expanded *Nmp4*^{-/-} MSCs exhibit enhanced proliferation and mineralization in culture. [A] Comparative growth rates of expanded WT and *Nmp4*^{-/-} MSCs. Cell counts/day (n=4 lines per genotype log₁₀ cells/well, 3 wells/sample, average ± SD, t test, t<0.05). Note: each 'line' is derived from a single mouse [B] Alkaline phosphatase (alk phos) and alizarin red staining of a WT and *Nmp4*^{-/-} MSC cultures from Day7-Day28. See text for details

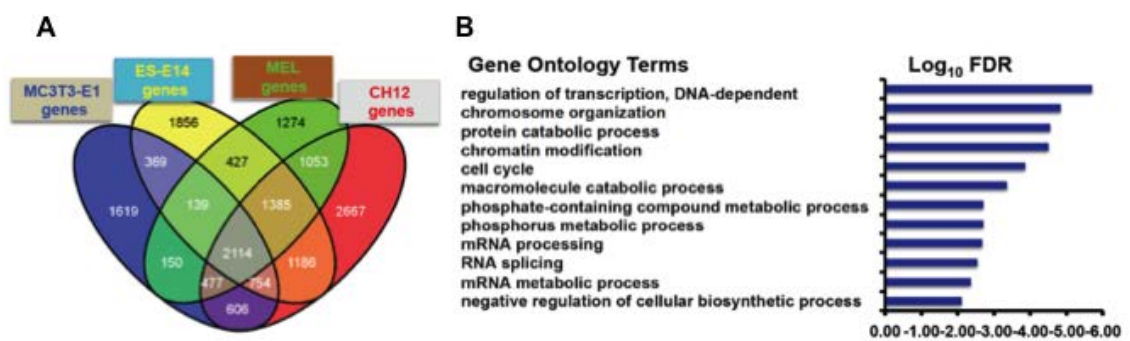


Figure 4-6: Nmp4 associates with core target genes common to multiple cell types and acts as a negative regulation of cellular biosynthetic processes [A] Venn diagram illustrating the shared Nmp4 target genes in the MC3T3-E1 osteoblast-like cells (vehicle-treated), and the three ENCODE cells lines, ES-E14 (embryonic stem cells), MEL, and CH12 cells (B-cell lymphomas). [B] DAVID/REVIGO gene ontology (GO) profile of Nmp4 core target genes.

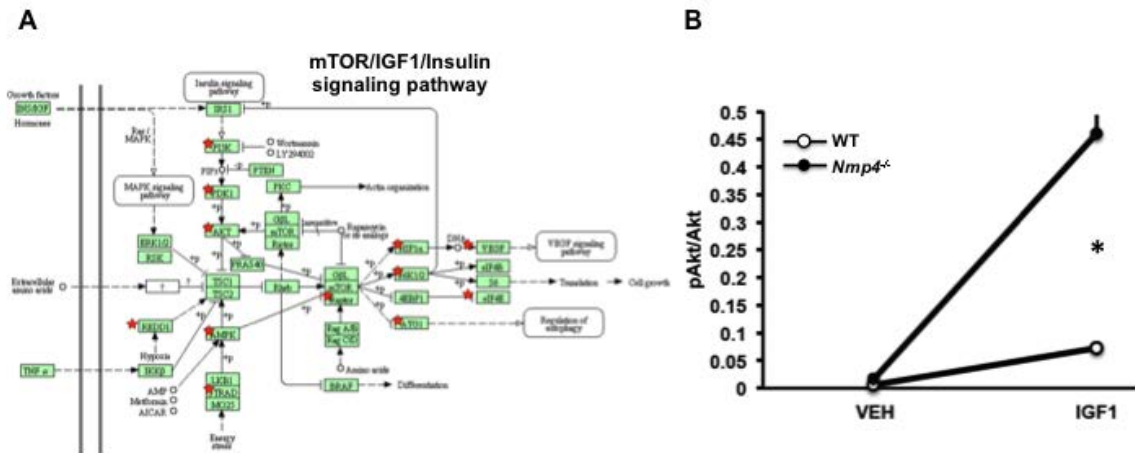


Figure 4-7: KEGG pathway analysis of the *Nmp4* ‘core’ genes predicts that the mTOR/IGF1/Insulin response limb is regulated by the proposed anti-anabolic axis. [A] KEGG readout from DAVID analysis showing the identity of *Nmp4* target genes (red stars) in the mTOR/IGF1/Insulin signaling pathway. [B] Interaction plot of IGF1-induced Akt phosphorylation in immortalized WT and *Nmp4*^{-/-} bone marrow stromal cells (BMSC). Data are average \pm SD, n=3 wells/treatment. Statistical differences were determined using a 2-way ANOVA and significance was set at $p \leq 0.05$. The Tukey’s HSD post hoc test was used to determine differences between the treatment groups. There was a genotype, treatment and genotype x treatment interaction. There was no difference between the vehicle-treated WT and *Nmp4*^{-/-} cells. This experiment was performed three separate times, all yielding the same result).

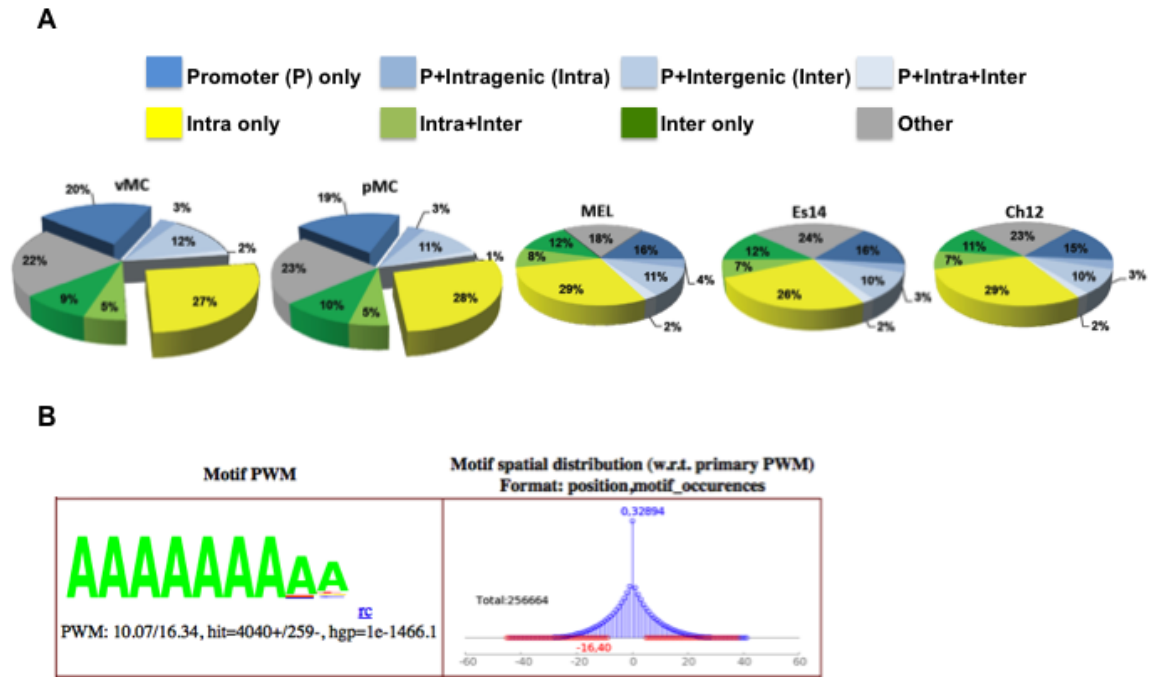


Figure 4-8: Nmp4 binds to AT-rich DNA typically proximal to TSS sites or within intragenic regions. [A] Genome-wide mapping of the Nmp4 binding sites show that most sites are distributed in the TSS and intragenic regions of the genome. ChIP-seq analysis included vehicle-treated and PTH-treated MC3T3-E1 osteoblast-like cells (vMC and pMC, respectively) and three murine cell lines from the ENCODE Consortium including ES-E14 (Es14), which are E14 undifferentiated mouse embryonic stem cells, and two mouse erythroleukemia cell lines (Ch12 and MEL) derived from B-cell lymphomas. [B] GEM analysis for the Nmp4 consensus sequence derived from MC3T3-E1 cells. A minimal k-mer width of 6 and maximum of 20 were used. The optimal position weight matrix (PWM) score for the MC3T3-E1 data was 10.07. The hypergeometric P-value (hgp) was $1e-1466.1$.

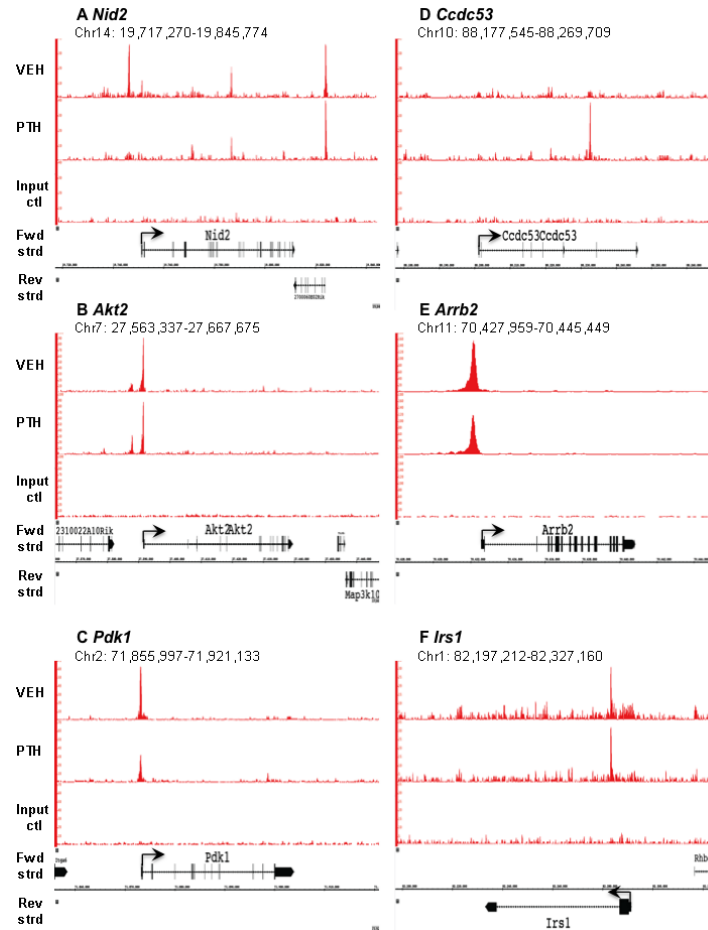


Figure 4-9: ChIP-seq reveals Nmp4 binding profiles at specific gene loci. Mouse MC3T3-E1 cells were seeded into twenty-one 150mm plates at an initial density of 50,000 cells/plate (320 cells/cm²) and maintained in α MEM complete medium + ascorbic acid for 14 days. Prior to harvest cells were treated with 25nM hPTH(1-34) or vehicle control for 1hr. Processing for ChIP-seq analysis was performed as described in the Materials and Methods. Sequences (50nt reads, single end) were aligned to the mouse genome (mm10) using the BWA algorithm. Alignments were extended in silico at their 3'-ends to a length of 150bp, which is the average genomic fragment length in the size-selected library, and assigned to 32-nt bins along the genome. Nmp4 (Znf384) peak locations were determined using the MACS algorithm (v1.4.2) with a cutoff of pvalue = 1e-7. The genomic loci including the chromosome number and nucleotide interval are indicated. Read scales are indicated on the Y-axis. An arrow indicates the transcriptional start sites and direction of transcription for each of the genes; vertical boxes within the gene indicate exons. The Nmp4 ChIP-seq gene profiles include (A) Nid2 (B) Akt2, (C) Pdk1 (D) ccdc53, (E) Arrb2 and (F) Irs1. The input DNA profiles were devoid of peaks.

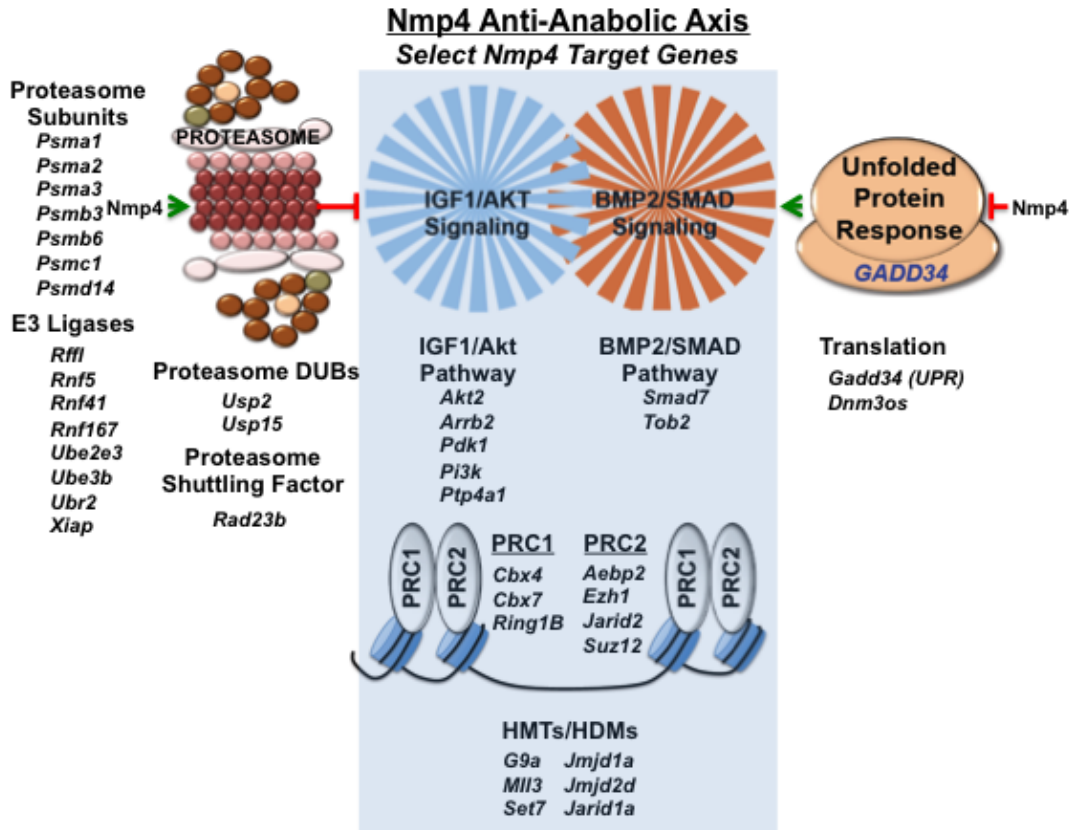


Figure 4-10: Schematic of hypothetical Nmp4 anti-anabolic axis based on ChIP-seq/GO analyses and experimental data. We propose that Nmp4 is a negative regulator of cellular biosynthetic processes; it suppresses target genes that are positive regulators of growth/development and conversely supports genes that repress these pathways. Disabling Nmp4 enhances the expansion of self-renewing osteoprogenitors while sensitizing them to osteoanabolic differentiation signals. This involves the alteration of polycomb repressor complex activity and chromatin accessibility. Nmp4 target genes that code for proteins comprising these complexes including histone methyltransferases (HMT) and histone demethylases (HDM) are listed. Furthermore we propose that Nmp4 regulates the expression of genes that govern the response to the local mediators of PTH action including the IGF1 and BMP2 signaling pathways. These include genes directly involved in these pathways and the collateral pathways of ubiquitin-proteasome activity and the unfolded protein response (UPR). This select list of Nmp4 target genes is from either the core target gene list or from the MC3T3-E1 list. Abbreviations: DUBs deubiquitinating enzymes, HMT histone methyltransferase; HDM histone demethylases; PRC1 polycomb repressor complex 1; PRC2 polycomb repressor complex 2

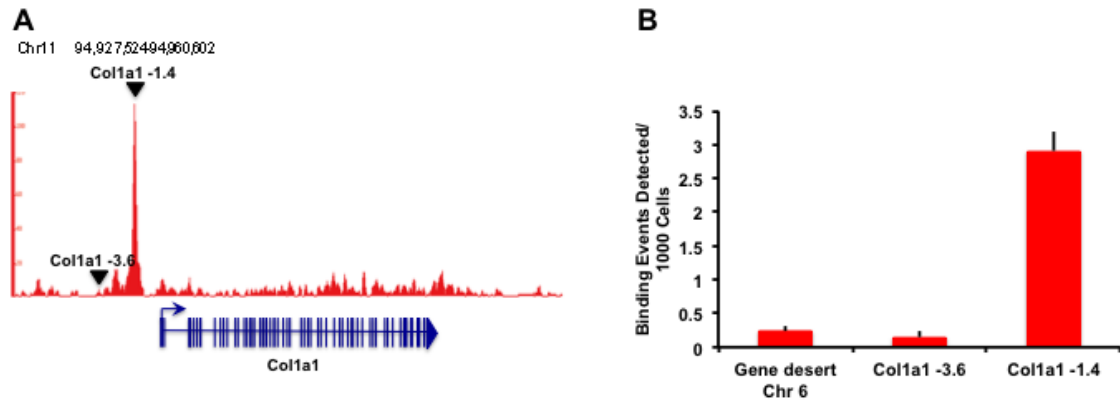


Figure 4-11: qRT-PCR validates the CHIP-seq profiles. [A] The Nmp4 CHIP-seq profile for the gene Col1a1. The genomic loci including the chromosome number and nucleotide interval are indicated. Read scale is indicated on the Y-axis. An arrow marks the transcriptional start site and direction of transcription; vertical boxes within the gene identify exons. [B] qRT-PCR was used to authenticate the CHIP-seq peaks as described in the Materials and Methods.

Table 4-1: Bone loss data.

The % change body weight, uterine weight, microCT (distal femur and L5 vertebra) and serum formation/resorption markers from WT and *Nmp4*^{-/-} mice after ovx or sham operation 4wks post-op. Data are average ± SD, number of mice/experimental group=8-14 [4 mice in WT SHAM uterine weight]). Statistical significance was set at p≤0.05 and differences were determined using a 2-way ANOVA. (G x T= Genotype x Treatment interaction)

	WT		<i>Nmp4</i> ^{-/-}		2-WAY ANOVA p-values		
	SHAM	OVX	SHAM	OVX	Genotype	Treatment	G x T
%Δ Body weight	2.48±7.73	8.65±5.48	4.14±4.70	5.66±2.94	0.69	0.03	0.17
Uterine weight (g)	0.10±0.05	0.04±0.02	0.10±0.02	0.05±0.02	0.30	<0.0001	0.34

Distal Femur

BV/TV	0.019±0.004	0.012±0.004	0.038±0.011	0.021±0.010	<0.0001	<0.0001	0.06
SMI	3.818±0.250	4.055±0.357	3.387±0.263	3.810±0.294	0.0008	0.0011	0.32
Tb.N (mm ⁻¹)	2.554±0.239	2.165±0.385	3.128±0.218	2.797±0.276	<0.0001	0.0004	0.76
Tb.Th (mm)	0.040±0.005	0.041±0.005	0.039±0.003	0.037±0.004	0.08	0.87	0.23
Tb.Sp (mm)	0.393±0.036	0.477±0.097	0.317±0.026	0.359±0.037	<0.0001	0.0012	0.25

L5 Vertebra

BV/TV	0.189±0.028	0.177±0.013	0.253±0.019	0.212±0.019	<0.0001	0.0004	0.05
Tb.N (mm ⁻¹)	3.797±0.513	3.580±0.285	4.491±0.345	4.022±0.254	<0.0001	0.0091	0.32
Tb.Th (mm)	0.050±0.003	49±0.002	0.056±0.002	0.053±0.002	<0.0001	0.0032	0.02
Tb.Sp (mm)	0.227±0.023	0.229±0.013	0.202±0.020	0.214±0.012	0.0013	0.25	0.44

Serum

	WT		<i>Nmp4</i> ^{-/-}		2-WAY ANOVA p-values		
	Pre-op	Post-op ^{4wks}	Pre-op	Post-op ^{4wk}	Gene	Treat	G x T
P1NP (ng/ml)	6.018±1.794	5.830±1.349	6.017±1.412	4.769±1.223	0.19	0.08	0.19
CTX (ng/ml)	13.498±2.423	12.932±2.910	13.372±1.878	12.898±2.717	0.92	0.46	0.96

Table 4-2: PTH-induced bone gain data.

MicroCT (distal femur and L5 vertebra) from ovx WT and ovx *Nmp4*^{-/-} mice after 4 wks and 8wks PTH/VEH therapy. Data are average ± SD, number of mice/experimental group = 8-9. Statistical significance was set at p≤0.05 and differences were determined using a 2-way ANOVA. (Geno=Genotype, Treat=Treatment, G x T= Genotype x Treatment interaction).

Distal Femur

4wks	WT				<i>Nmp4</i> ^{-/-}				2-WAY ANOVA p-values		
	VEH	PTH	VEH	PTH	Geno	Treat	G x T				
Conn D (mm ⁻³)	3.180±3.87	33.230±26.73	9.681±15.979	67.533±14.111	0.0018	<0.0001	0.03				
SMI	3.752±0.437	3.013±0.384	3.472±0.327	2.514±0.113	0.0025	<0.0001	0.36				
Tb.N (mm ⁻¹)	2.1±0.519	2.441±0.281	2.712±0.241	2.833±0.224	0.0002	0.06	0.36				
Tb.Th (mm)	0.039±0.010	0.042±0.007	0.033±0.003	0.044±0.003	0.54	0.004	0.09				
Tb.Sp (mm)	0.510±0.157	0.409±0.051	0.370±0.036	0.342±0.032	0.0019	0.04	0.24				
8wks											
Conn D (mm ⁻³)	3.123±5.307	38.658±14.91	0.982±1.103	58.128±13.570	0.03	<0.0001	0.0064				
SMI	3.808±0.479	2.470±0.284	3.589±0.218	2.262±0.141	0.05	<0.0001	0.96				
Tb.N (mm ⁻¹)	2.132±0.297	2.164±0.431	2.286±0.145	2.552±0.277	0.02	0.17	0.28				
Tb.Th (mm)	0.037±0.006	0.048±0.005	0.030±0.004	0.049±0.003	0.12	<0.0001	0.02				
Tb.Sp (mm)	0.476±0.072	0.471±0.109	0.438±0.033	0.378±0.045	0.01	0.20	0.27				

L5 Vertebra

4wks	WT				<i>Nmp4</i> ^{-/-}				2-WAY ANOVA p-values		
	VEH	PTH	VEH	PTH	Geno	Treat	G x T				
Tb.N (mm ⁻¹)	3.453±0.451	4.875±0.587	3.891±0.504	5.518±0.381	0.0049	<0.0001	0.56				
Tb.Th (mm)	0.051±0.002	0.049±0.002	0.054±0.004	0.051±0.001	0.04	0.03	0.60				
Tb.Sp (mm)	0.246±0.021	0.224±0.030	0.229±0.021	0.197±0.021	0.02	0.0036	0.52				
8wks											
Tb.N (mm ⁻¹)	4.046±0.917	5.648±1.191	3.627±0.235	5.906±0.754	0.79	<0.0001	0.26				
Tb.Th (mm)	0.053±0.003	0.049±0.004	0.055±0.001	0.054±0.001	0.0018	0.0044	0.09				
Tb.Sp (mm)	0.239±0.021	0.206±0.037	0.256±0.020	0.186±0.023	0.86	<0.0001	0.05				

Table 4-3: Histomorphometry and serum analyses.

Dynamic bone histomorphometry data of the distal femur from WT and *Nmp4^{-/-}* mice treated with intermittent PTH or vehicle for 4wks (8wks post-op). Sera data were collected at the end of 8wks treatment (12wks post-op). The parameters include mineral apposition rate (MAR), mineralizing surface/bone surface (MS/BS), and bone formation rate (BFR). Data are average \pm SD, number of mice/experimental group = 4-7. A 2-way ANOVA was used to determine statistical differences and significance was set at $p \leq 0.05$. (Geno=Genotype, Treat=Treatment, G x T= Genotype x Treatment interaction).

	WT		<i>Nmp4^{-/-}</i>		2-WAY ANOVA p-values		
	VEH	PTH	VEH	PTH	Geno	Treat	G x T
<u>Dynamic histo</u>							
MAR ($\mu\text{m}/\text{day}$)	2.28 \pm 0.37	3.80 \pm 0.73	2.29 \pm 0.37	3.61 \pm 0.40	0.70	<0.0001	0.66
MS/BS (%)	0.41 \pm 0.09	0.55 \pm 0.05	0.44 \pm 0.10	0.52 \pm 0.06	0.98	0.01	0.45
BFR ($\mu\text{m}^2/\mu\text{m}/\text{day}$)	0.95 \pm 0.28	2.09 \pm 0.52	1.01 \pm 0.25	1.86 \pm 0.22	0.60	<0.0001	0.37

Serum

	WT		<i>Nmp4^{-/-}</i>		2-WAY ANOVA p-values		
	VEH ^{8wks}	PTH ^{8wk}	VEH ^{8wk}	PTH ^{8wk}	Geno	Treat	G x T
P1NP (ng/ml)	3.147 \pm 0.653	10.066 \pm 2.66	2.806 \pm 0.760	8.042 \pm 3.304	0.19	<0.0001	0.34
CTX (ng/ml)	11.466 \pm 2.239	15.147 \pm 3.518	9.361 \pm 1.222	14.157 \pm 1.532	0.12	0.0002	0.56

Table 4-4: DAVID profile of KEGG pathway mapping.

GO Term Pathways	FDR
TOR signaling pathway	0.003
Insulin signaling pathway	0.004
Chronic myeloid leukemia	0.026
JAK-STAT signaling pathway	0.026
Neurotrophin signaling pathway	0.034

Only pathways with an FDR of $p < 0.05$ are listed

Table 4-5: ENCODE ChIP-Seq Significance Tool profile for enriched transcription factors [TFs] within the Nmp4 target core gene list

Factor	Q-value*	Factor	Q-value
Nmp4	0.00E+00	Max	0.00E+00
CHD2	0.00E+00	Mxi1	0.00E+00
CTCF	0.00E+00	NELFe	0.00E+00
GCN5	0.00E+00	Pol2	0.00E+00
HCFC1	0.00E+00	SIN3A	0.00E+00
MAZ	0.00E+00	TBP	0.00E+00
p300	0.00E+00	c-Myc	7.352e-317

* Hypergeometric test; Benjamini-Hochberg; (select TFs from 72 entries).

CHAPTER 5

Summary

We have been able to improve the efficacy of intermittent parathyroid in a mouse model of post-menopausal osteoporosis using a global knockout for the transcription factor *Nmp4*. The KO mice treated with anabolic doses of PTH did show enhanced response to hormone after 4 and 8 weeks as measured by uCT. This recapitulates the phenotype seen with healthy *Nmp4*-K mice after 3 and 7 weeks of therapy. Bone marrow from these mice showed a nearly 4-fold increase for frequency of CD146+/Nestin+ osteoprogenitors and CD8+ T-cell. However, these increased pools of cells did not confer protection from bone loss associated with estrogen loss due to ovx. This is in contrast to male mice which are null for *Nmp4/CIZ* and protected from osteopenia associated with hind limb suspension. We and others have also shown both *in vitro* and *in vivo* that *Nmp4* restricts multiple anabolic stimuli in what appears to be a limited set of cells based on the unremarkable phenotype of the *Nmp4* global knockout animal. A genome wide ChIP-seq approach using vehicle and PTH treated osteoblasts has confirmed *Nmp4* binding to a homopolymeric consensus sequence and also its PTH-sensitive DNA occupancy. This discovery driven technique also suggests biochemical pathways and biological processes which may contribute to the *Nmp4*-KO phenotype. The data included herein however leaves some questions unanswered. In particular the role, if any, that CD8+ T-cells play in enhancing the PTH response is unknown. Though enhanced responses to IGF1, BMP2 and fluid shear stress have been shown *in vitro*, their contribution to the baseline differences in osteoprogenitors, proliferation and pool size, has yet to be experimentally shown. Also *Nmp4* acts as an architectural transcription factor and GO analysis of its core target genes suggests control over chromatin organization. How this protein may affect genomic super structure and change genetic expression is still largely undescribed. The future research into how *Nmp4* restricts bone gain in response to anabolic stimuli will should include the cell type contributions of osteoprogenitors, T-cells, and osteoclast progenitors. Also the difficult question of understanding how loss of *Nmp4* appears to affect only a select number of progenitor cell types should be addressed. The discussion will summarize these findings, open questions and future directions for research.

Enhanced response to PTH

Previous work published in the Bidwell lab looked at wild type and *Nmp4*-KO mice treated with PTH (30µg/kg/day) or vehicle for 7 weeks. As predicted the KO mice experienced a significantly enhanced response to hormone. This was consistent with other work using *Bmp2* which showed a similar response. Importantly, the PTH demonstrated the enhanced response to a second anabolic agonist. Moreover, intermittent PTH is the only FDA approved anabolic therapy to treat osteoporosis, a devastating and costly disease. Work included in this thesis went on to characterize this phenotype further. After 2 weeks of PTH therapy estrogen replete WT and *Nmp4*-KO female mice responded equally to PTH. By 3 weeks of treatment the KO mice had begun to pull away with more bone anabolism. BMP2 injected directly on calvaria resulted in enhanced bone gain in the KO mice after 10 days. The results are not directly comparable because of different treatment regimens (systemic PTH vs. local BMP2 delivery), but it remains possible that the enhanced BMP2 response is upstream of and contributes to PTH hypersensitivity. This concept is consistent with CHIP-seq analysis which predicts *Nmp4* restricts biological processes which control *Bmp2* signaling, potentially by limiting the unfolded protein response. Additionally, PTH engaging the PTHR1 receptor induces internalization of the complex as well as BMP2 inhibitors such as Noggin thus potentiating BMP2 signals. Whether crosstalk between these two pathways contributes to the enhanced response to PTH remains unclear. Nevertheless, by 7 weeks of PTH treatment the KO mice continued to increase cancellous bone production. The formation marker osteocalcin was also still increasing at the end of this treatment period as well after WT levels began to decline. This suggests the anabolic window for increased bone production has been extended in the KO mice. OVX *Nmp4*-KO mice have a similar pattern of enhanced response. At 4 weeks and 8 weeks of treatment the KO mice still have enhanced bone in the distal femur and L5 vertebra as evidenced by a significant genotype x treatment interaction for BV/TV from microCT. The magnitude of the difference was less, but still significant. Contrary to the intact mice, the formation marker P1NP was used to monitor bone formation in the OVX study. This marker revealed a significant treatment effect, but not a difference between WT and *Nmp4*-KO animals. The reasons for this are unclear, but the easiest explanation is that the magnitude difference seen between PTH treated WT and *Nmp4*-KO mice is captured in the intact mice, but not in the OVX group with a smaller magnitude difference. That said, other factors may contribute to this difference as well such as osteoclast activity which releases matrix bound osteocalcin. Because the KO phenotype

includes modest increases in osteoclast numbers and activity, the difference in markers may be the result of that increase. Vehicle treated OVX Nmp4-KO mice did experience increased bone loss 8 weeks post-OVX which was statistically significant in the L5 and nearly so in the distal femur which would support the argument that osteoclast activity increased the osteocalcin in the serum. However, this was only true in the OVX group and Tukey's HSD post-hoc tests did not reveal a difference in the vehicle treated animals indicating the osteoclast phenotype was not a dominant effect. Another reason for the discordant serum formation markers is the hypersensitivity to Bmp2, which induces expression of osteocalcin directly. The Nmp4-KO mice would be expected to increase expression of this marker if indeed PTH treatment potentiates Bmp2 signaling. P1NP on the other hand is a biochemical byproduct matrix deposition and not *directly* regulated by Bmp2 (or PTH).

Differences in in BM cells

One of the most striking aspect of this work is the discovery that the *Nmp4*-KO baseline phenotype includes an increase in the number of CD146+/Nestin+ osteoprogenitors. These cells contain a large fraction of the CFU-F population in the bone marrow which ultimately go on to form matrix producing osteoblasts [REF]. Their detection by FACS counting matches results from independent CFU-Ob and CFU-F^{alk phos+} clonogenic assays, and the increase is independent of PTH therapy. Expanded cultures of heterogeneous mesenchymal bone marrow stem and progenitors (MSPCs) from single animals demonstrated that *Nmp4* acts to attenuate proliferation to a mild degree. These cultures also revealed that KO MSPCs have an accelerated differentiation based on alkaline phosphatase activity and mineralization assays. In the untreated KO animal these characteristics likely counterbalance the increased osteoclastogenic potential to yield an unremarkable phenotype which varies between indistinct from wild type to a modest increase in bone mass. This cell type expansion also renders the KO animals capable of an enhanced response when challenged with anabolic agents that result in progenitor recruitment and bone anabolism such as PTH and BMP2 (Yu, Zhao et al. 2012). Underpinning the MSPC expansion is potentially the hypersensitivity to growth factors such as IGF1. This is consistent with the dependence upon Igf1/Akt signaling seen with intermittent PTH treatment. Future studies to link IGF1 signaling with the expanded KO MPSCs and delineate cell stage specific sensitivity, as exists with BMP2, will confirm this hypothesis (Alvarez, Childress et al. 2012).

A largely unexplored, but potentially important observation is the increase of CD8⁺ T-cells in the *Nmp4*-KO bone marrow. This increase is not consistently seen in the peripheral blood of these animals. Parathyroid hormone is pleiotropic and directly affects CD8⁺ T-cells inducing the release of Wnt10b, a secreted glycoprotein which causes progenitor differentiation to osteoblasts. Work in Pacifici's laboratory has demonstrated the reliance of the intermittent PTH response on this interaction with T-cells (Terauchi, Li et al. 2009, Bedi, Li et al. 2012), and it would be important to evaluate if the increased numbers participate in the enhanced KO response. Based on the cell autonomous behavior seen in MSPC cultures, it is unclear if more T-cells in the marrow are required, dispensable, or contribute in part to the hyper response to hormone.

The paradoxical observation that *Nmp4*-KO bone marrow contains more CFU-GM osteoclast progenitors, gives more osteoclasts *in vitro*, and these cells have a greater resorption capacity on dentin slices is again incompletely understood. These results are consistent with the transient increase in bone loss seen after OVX in the *Nmp4*-KO mice where osteoclast activity is the predominant effector. It has been suggested that osteoclastic bone resorption is required for the PTH anabolic response [REF], though this hypothesis is controversial [REF]. Regardless of whether osteoclasts participate in the enhanced PTH response, the fact that at baseline the *Nmp4*-KO animal is not osteopenic and we have observed no baseline differences in bone formation rate implies an increase in bone remodeling unit activation frequency. This remains to be experimentally determined, but could represent a higher 'idling' state in the KO marrow which is capable of greater response to anabolics.

Differences in histomorphometry

Dynamic histomorphometry in healthy female mice after 7 weeks of PTH treatment and OVX mice after 4 weeks of PTH did not reveal any differences in mineral apposition or bone formation rate despite seeing clear treatment effects for both parameters. This was unexpected and has not been resolved. Perhaps the most likely reason is that these parameters showed differences earlier in the treatment period. It also remains possible that the differences are subtle and cannot be distinguished by these measurements. The enhanced response to PTH shows a steady progression whereby the KO mice respond equally as the WT to hormone then begin to put on more bone as a function of

time. So, the aggregate bone mass may be the result of small differences in formation rate that only reveal themselves after a period of time into the treatment regime.

Discussion of ChIP-seq results

Nmp4 is a nucleocytoplasmic shuttling transcription factor therefore its genomic binding occupancy can be interrogated with chromosome immunoprecipitation followed by high throughput sequencing. We choose the MC3T3 osteoblast-like cell model for this experiments. This model is widely used and supported by decades of literature. Importantly MC3T3-E1 cells can be differentiated in culture using ascorbic acid and beta-glycerophosphate to approximate the maturation of pre-osteoblast to a mature, bone matrix synthesizing cell. These cells are a spontaneously immortal line originally cultured from newborn mouse calvaria (Sudo, Kodama et al. 1983). Our studies utilized subclone 4, selected for its high alkaline phosphatase activity and robust response to PTH (Wang, Christensen et al. 1999). The cells were grown in osteogenic media for 14 days prior to harvest to represent a committed osteoblast that was producing matrix and experienced significant increases in the mature bone marker osteocalcin (Bglap). Gene ontology (GO) analysis of Nmp4 'core' target genes predicted, and we have confirmed that cells lacking Nmp4 are hyper-responsive to IGF1 stimulation. Additionally, our GO results suggest potential mechanisms for hyper-sensitivity to BMP2 by identifying *Tob2* and *Smad7* as Nmp4 target genes; both of these gene products are endogenous inhibitors of Bmp2 signaling. Further, *Gadd34* is another core target gene which is involved in the unfolded protein response and contributes to down regulation of translation in professional secretory cells. Disrupting the unfolded protein response confers hypersensitivity to BMP2. Over 20 genes identified as core target genes are also involved in the chromatin remodeling which is central to mesenchymal stem cell differentiation (Chen and Dent 2014).

Conclusion

This thesis presents evidence to show that Nmp4 acts to attenuate bone anabolic signals through a variety of possible cellular and molecular mechanisms. Bone marrow from the KO animal appears to be primed for anabolic signals which intermittent PTH exploits with the end result being more bone added to the skeleton. Though not completely described, the molecular mechanism for this attenuation involves the level of phosphorylated Akt which participates in many cellular processes such as proliferation

and differentiation. Nmp4 is a transcription factor which binds regulatory regions of several genes involved in these processes as well, thus the mechanism of action may be at the level of signal transduction and/or genetic expression. The protein itself is expressed in most tissues and is highly conserved at the nucleic acid and protein sequence levels implying conserved function. Despite its wide expression pattern however, mice without a functional copy of the gene have almost not baseline phenotype and no observed deleterious effects beyond sporadic spermatogenic defects. Thus Nmp4 or the pathways which it regulates may be an effective target for interventions to treat diseases of low bone mass.

Appendix

A.

0610031O16Rik	2410022M11Rik	9030624J02Rik	Acyp1
0610043K17Rik	2500002B13Rik	9430008C03Rik	Adam17
1110001J03Rik	2500004C02Rik	9430041J12Rik	Adamts1
1110002J07Rik	2510009E07Rik	9430083A17Rik	Adamts10
1110002L01Rik	2610301B20Rik	9530026F06Rik	Adamts6
1110037F02Rik	2610507B11Rik	9530027J09Rik	Adamtsl4
1110038B12Rik	2700029M09Rik	9530068E07Rik	Adat1
1110051M20Rik	2700050L05Rik	9630014M24Rik	Adc
1190002F15Rik	2700060E02Rik	A330017A19Rik	Adcy3
1600002K03Rik	2810403A07Rik	A330050B17Rik	Adcy7
1600020E01Rik	2810403D21Rik	A330069E16Rik	Adk
1700001G11Rik	2810404F17Rik	A430018G15Rik	Ado
1700007K13Rik	2810408M09Rik	A630072M18Ri	Adora2b
1700007L15Rik	2810428I15Rik	k	Adpgk
1700013F07Rik	2810454H06Rik	A730036I17Rik	Adrbk1
1700016C15Rik	3010003L21Rik	A830031A19Rik	Adss
1700018L02Rik	3110009E18Rik	A830035A12Rik	AF357374
1700018M17Rik	3110067C02Rik	A930001C03Rik	AF357376
1700021A07Rik	3110082J24Rik	A930007I19Rik	Afap1I1
1700022K14Rik	4732471J01Rik	AA387883	Aff1
1700023H06Rik	4921530L18Rik	AA415398	Aff4
1700030C12Rik	4921531C22Rik	AA465934	Afmid
1700034H15Rik	4930402F06Rik	Aaas	Aftph
1700052N19Rik	4930404I05Rik	Aarsd1	Aga
1700063D05Rik	4930412O13Rik	AB041803	Agbl5
1700064E03Rik	4930432B10Rik	Abcb6	Agpat1
1700067K01Rik	4930447C04Rik	Abcc10	Agt
1700095J07Rik	4930503L19Rik	Abcc3	Ahcyl2
1700101I11Rik	4930509E16Rik	Abcf3	Ahsa2
1700110C19Rik	4930529M08Rik	Abcg2	AI118078
1700112E06Rik	4930546H06Rik	Abhd16a	AI450353
1700120B22Rik	4930552N02Rik	Abi1	AI462493
1810013L24Rik	4931406C07Rik	Abl1	AI597468
1810019N24Rik	4933411K20Rik	Ablim1	Aicda
1810059C17Rik	4933433G15Rik	Abr	Aifm1
2010204K13Rik	4933434E20Rik	Acaca	AK006189
2210016F16Rik	5031434O11Rik	Acad11	AK006245
2210408F21Rik	5330430P22Rik	Acat1	AK007083
2210417K05Rik	5530601H04Rik	Acot8	AK013187
2310011J03Rik	5730405O15Rik	Acp6	AK015545
2310034G01Rik	5730420D15Rik	Acsl4	AK016837
2310068J16Rik	5730455P16Rik	Actb	AK018891
2410002F23Rik	5730508B09Rik	Actr8	AK018967

AK019250	AK204212	Arl6ip5	Bach2
AK019365	AK212603	Arpc3	Banf1
AK031165	AK212710	Arrb2	Baz2b
AK035829	Ak3	Arrdc3	BB019430
AK037159	Akap1	Arvcf	Bbc3
AK038627	Akap13	Asap1	BC004004
AK040752	Akirin1	Asb4	BC024582
AK042136	Akirin2	Ash2l	BC025920
AK043789	Akt2	Asl	BC030867
AK043804	Aldoa	Asun	BC055111
AK043846	Alg5	Asxl1	BC055823
AK043958	Alkbh5	Asxl2	BC065397
AK044354	Aloxe3	Atad2	BC099561
AK044623	Ambra1	Atat1	BC126883
AK045700	Ammecr1	Atf7ip	Bcar1
AK047520	Anapc1	Atg16l1	Bcas2
AK048941	Anapc5	Atg16l2	Bcas3
AK051804	Ang	Atg2a	Bcl11a
AK053136	Ank3	Atg2b	Bcl2l1
AK053772	Ankrd24	Atl3	Bcl7a
AK054042	Ankrd40	Atp13a1	Bdp1
AK078466	Ankrd52	Atp1b2	Bend3
AK079699	Ankrd54	Atp2b1	Bgn
AK079730	Antxr1	Atp5a1	Birc6
AK079777	Anxa2	Atp5b	Blcap
AK085438	Anxa7	Atp6v0a1	Blmh
AK087382	Ap1g1	Atp6v1a	Bloc1s4
AK089118	Ap1s2	Atp6v1b2	Bola2
AK131831	Ap3m1	Atp6v1e1	Bptf
AK132720	Ap4s1	Atpaf2	Brat1
AK134933	Aph1c	Atpif1	Brca1
AK140370	Appl1	Atraid	Brd3
AK141659	Arf3	Atrnl1	Brf1
AK142999	Arfgap1	Atxn2	Bri3
AK154275	Arhgap12	Atxn3	Brwd3
AK155149	Arhgap18	Atxn7l1	Bscl2
AK155592	Arhgap21	Atxn7l3	Btaf1
AK156477	Arhgap26	Avl9	Btd
AK158379	Arhgap4	AW209491	Btf3l4
AK162774	Arhgef10l	AW495222	C030013C21Rik
AK163160	Arhgef25	B230217C12Rik	C030034L19Rik
AK164218	Arhgef7	B230325K18Rik	C030037D09Rik
AK165329	Arid1b	B330016D10Rik	C1ra
AK166079	Arl15	B3gnt2	C1rb
AK167137	Arl2bp	B930003M22Ri	C1rl
AK172386	Arl3	k	C2
AK188991	Arl5a	B930082K07Rik	C2cd2l

C2cd5	Cdc25a	Clptm1	Ctnnd1
C330006A16Rik	Cdc26	Clspn	Ctsa
C330007P06Rik	Cdc6	Clta	Ctse
Cabin1	Cdc73	Cltc	Ctsl
Cacna1f	Cdca5	Cmah	Ctnn
Cad	Cdh12	Cmip	Cuedc1
Cage1	Cdh16	Cnn2	Cux1
Calm2	Cdk11b	Cnot3	Cwc15
Camk2d	Cdk17	Cnot6	Cyb5
Capn8	Cdk2ap1	Cnot6l	Cyb5d1
Capn9	Cdk5rap3	Cnppd1	Cyb5r1
Capns1	Cdkal1	Cnpy3	Cyp2t4
Car12	Cdkl3	Cnpy4	Cyth1
Carhsp1	Cdkl5	Cog4	D030025P21Rik
Cask	Cdkn1b	Col8a2	D030028A08Rik
Caskin2	Cdkn2c	Commd1	D14Abb1e
Casp8	Cdv3	Commd7	D17Wsu104e
Cat	Celf1	Commd8	D630003M21Ri
Catsper2	Cep128	Comt	k
Catsperg1	Cfdp1	Cops7a	D6Wsu163e
Cbfb	Cfi	Cops8	D830025C05Rik
Cbr1	Cflar	Copz2	Dapk2
Cbx4	Chd2	Coq10a	Dbi
Cbx7	Chd3	Coq5	Dbp
Ccdc116	Chek1	Cox7b	Dbr1
Ccdc136	Chfr	Cpeb3	Dcaf17
Ccdc14	Chrac1	Cpm	Dcakd
Ccdc146	Chrna1	Cpt1c	Dck
Ccdc176	Chrn4	Cradd	Ddb2
Ccdc22	Chst11	Creb3	Ddit4
Ccdc65	Chst3	Crebbp	Ddx20
Ccdc77	Chsy1	Crebl2	Deb1
Ccdc84	Cic	Creld1	Def8
Ccdc92	Cirbp	Crem	Dennd1b
Ccdc93	Cisd3	Crk	Des
Ccnd2	Ciz1	Crlf3	Desi1
Ccnh	Ckap5	Crnk1	Dgat1
Ccnk	Clasp1	Crocc	Dgcr14
Ccser2	Clca1	Cryl1	Dgka
Cct6a	Clcf1	Cryz1	Dhodh
Cd164	Clcn2	Cse1l	Dhrs3
Cd164l2	Clcn5	Csgalnact2	Dhx38
Cd247	Cldn14	Csnk1a1	Dhx57
Cd276	Clic4	Csnk1g3	Dhx58
Cd2ap	Clint1	Cspp1	Dhx8
Cd300lh	Clip1	Csrnp1	Dlat
Cdc14b	Clk3	Ctnna3	Dleu2

Dmtf1	Dusp13	Ercc6l	Fgfr1op2
Dmtn	Dusp16	Ergic1	Fhl3
Dnajb14	Dynll1	Erlin2	Fhl4
Dnajc25	Dynll2	Ern1	Fig4
Dnajc3	Dyrk1a	Esyt2	Figf
Dnajc8	Dzip3	Ets2	Figl1
Dnm1	E030042O20Rik	Etv5	Fis1
Dnmt1	E130102H24Rik	Evi5	Fkbp10
Dnttip2	E130304I02Rik	Ewsr1	Fkbp14
Dopey2	E2f2	Exd2	Fkbp1a
Dpagt1	E530001K10Rik	Exosc8	Fkbp5
Dpcd	Eapp	Extl2	Fkbp7
Dpep1	Ebf1	Eya3	Fkbp8
Dpep2	Ece1	F420014N23Rik	Flna
Dph3	Ech1	Fam111a	Fmnl2
Dpy30	Ecsit	Fam117a	Fnbp1
Dpysl2	Edem1	Fam129b	Fndc3a
Dpysl5	Eed	Fam131a	Fndc7
DQ544183	Eef1b2	Fam134a	Fnip1
DQ548101	Eef2k	Fam136a	Fosl2
DQ552992	Efcab2	Fam185a	Foxh1
DQ553098	Ehbp1	Fam188a	Foxj3
DQ565977	Ehmt2	Fam19a2	Foxn2
DQ566768	Eid1	Fam214b	Foxn3
DQ692659	Eif1ad	Fam216a	Foxo1
DQ694768	Eif3c	Fam35a	Foxp1
DQ695092	Eif3d	Fam49b	Frat1
DQ695356	Eif3k	Fam57b	Frat2
DQ703023	Eif3l	Fam63b	Frg1
DQ704415	Eif4e	Fam73b	Frmd4a
DQ704975	Eif4ebp2	Fam98a	Frs2
DQ705542	Eif4g3	Fanca	Fry
DQ712916	Eif4h	Fancc	Fstl1
DQ713407	Eif5a	Fance	Fus
DQ716966	Eif5b	Fancg	Fut8
DQ725849	Elk3	Fars2	Fxr2
Dr1	Elk4	Fbxl16	Fytd1
Drg1	Ell	Fbxl20	Fzd7
Drg2	Elmsan1	Fbxo30	G730013B05Rik
Drp2	Emp1	Fbxo36	Gabarapl1
Dscr3	Entpd5	Fbxo42	Gabarapl2
Dtd2	Epb4.1	Fbxo47	Gabpb1
Dtnb	Epb4.111	Fbxo9	Gabpb2
Dtx3	Epc1	Fchsd2	Gadd45b
Dus1l	Ephb4	Fdps	Gadd45g
Dus2l	Epo	Fes	Gadd45gip1
Dus3l	Erbb2	Fgd2	Gak

Gapdh	Gm11602	Gm13936	Gm5258
Gapvd1	Gm11612	Gm14005	Gm5428
Gareml	Gm11619	Gm14167	Gm5432
Gast	Gm11627	Gm14216	Gm5464
Gata3	Gm11630	Gm14455	Gm5512
Gatad2a	Gm11680	Gm14634	Gm608
Gatc	Gm11696	Gm15411	Gm6225
Gbas	Gm11715	Gm15420	Gm6297
Gbp3	Gm11827	Gm15454	Gm6444
Gcc2	Gm12035	Gm15688	Gm6471
Gclc	Gm12054	Gm15747	Gm6525
Gdf9	Gm12057	Gm15760	Gm7598
Gdi2	Gm12060	Gm15787	Gm9812
Gemin2	Gm12063	Gm15831	Gm9850
Gemin6	Gm12245	Gm15860	Gm9900
Gfpt2	Gm12257	Gm15892	Gm9959
Gga2	Gm12279	Gm15903	Gm9985
Ggnbp2	Gm12308	Gm15927	Gna13
Ggt5	Gm12309	Gm15962	Gnb2
Gimap8	Gm12314	Gm16023	Gnb2l1
Gins1	Gm12358	Gm16185	Gnl3
Git2	Gm12396	Gm16196	Golga3
Glg1	Gm12795	Gm16197	Got2
Glipr1	Gm12951	Gm16230	Gpbar1
Glo1	Gm12974	Gm16274	Gpn3
Glud1	Gm12981	Gm16540	Gpr19
Gm10433	Gm13054	Gm16557	Gpr35
Gm10463	Gm13182	Gm16580	Gpr82
Gm10610	Gm13201	Gm16740	Gpr85
Gm10642	Gm13256	Gm16880	Gramd1a
Gm10653	Gm13297	Gm17077	Grb2
Gm10655	Gm13334	Gm17098	Grcc10
Gm10657	Gm13363	Gm17112	Grik4
Gm10658	Gm13375	Gm17138	Gse1
Gm10762	Gm13398	Gm17157	Gskip
Gm10837	Gm13447	Gm17300	Gstt3
Gm11184	Gm13548	Gm17617	Gtf2h2
Gm11206	Gm13559	Gm17661	Gtf2i
Gm11292	Gm13564	Gm17705	Gtf2ird2
Gm11335	Gm13626	Gm19705	Gyk
Gm11336	Gm13630	Gm20257	Gypc
Gm11437	Gm13657	Gm20748	Gys1
Gm11453	Gm13705	Gm4221	Gzmm
Gm11464	Gm13770	Gm4673	H1f0
Gm11474	Gm13830	Gm4978	H2afz
Gm11491	Gm13836	Gm5069	H2-D1
Gm11521	Gm13855	Gm5134	H2-DMb1

H2-DMb2	Hsp90ab1	Kbtbd7	Lphn1
H2-L	Hspa13	Kcnh3	Lpin2
Hacl1	Hspa4	Kctd19	Lpxn
Hbp1	Hspb9	Kctd20	Lrch1
Hdac7	I830077J02Rik	Kdm3a	Lrg1
Hdgfrp2	Ica1	Kdm4d	Lrig2
Heatr5a	Icam1	Kdm5a	Lrp2bp
Helb	Id3	Kif11	Lrrc1
Helz	Ifi35	Kif23	Lrrc16a
Herc4	Ift80	Kif24	Lrrc16b
Hes1	Igf1r	Kif5b	Lrrc46
Hes7	Igfbp6	Klc1	Lrrc49
Hexim2	Ik	Klhdc10	Lrrc58
Hic1	Il1rap	Klh11	Lrrk1
Hic2	Il3ra	Klh18	Lrsam1
Hif1a	Ilf2	Kmt2d	Lsmd1
Hint2	Ilf3	Kntc1	Luc7l
Hip1r	Ilk	Kpna2	Luc7l2
Hira	Immt	Kpnb1	Luc7l3
Hirip3	Impdh1	Krt222	Luzp1
Hist1h2ac	Ing1	L3mbtl2	Ly6g6f
Hist1h2af	Ing3	L3mbtl3	Lym4
Hist1h2bb	Ing4	Lamp2	Lym7
Hist1h2bc	Inip	Lamtor3	Lysmd3
Hist1h3c	Ino80	Larp4	Lyzl6
Hivep1	Ino80d	Lars2	Mad2l1
Hlcs	Ino80e	Las1l	Mad2l1bp
Hlx	Inpp5b	Lck	Madd
Hmbs	Ints8	Lctl	Maea
Hmg20b	Ipo11	Ldb1	Magt1
Hmox2	Iqce	Leo1	Malat1
Hnrnpf	Iqcg	Leprel4	Maml2
Hnrnph1	Irf2bp2	Leprotl1	Manea
Hnrnph3	Irf2bpl	Letm2	Map2k6
Hnrnpk	Irs3	Lhb	Map2k7
Hnrnpl	Itfg2	Lias	Map3k12
Hnrnpu	Itgb2	Lipe	Map3k3
Hnrnpul1	Itgb5	Lmf2	Map4k1
Hnrnpul2	Itm2b	Lmna	Map4k2
Homer1	Itpkb	Lmo2	Map4k3
Hoxb6	Izumo4	Lmo4	Mapk6
Hoxb8	Jarid2	Lmtk2	Mapkbp1
Hoxc5	Kalrn	Lnx2	Mapt
Hoxd10	Kansl1	LOC100504608	March5
Hoxd3	Kars	LOC100504703	March6
Hps3	Kat2a	Loxl3	March7
Hsd17b12	Kat2b	Lpar5	March8

Mark2	Mir702	Mxra7	Nfic
Marveld1	Mir92-1	Myadm	Nfil3
Mast4	Mir99b	Myc	Nfix
Mbnl2	Mirlet7e	Myg1	Nfkbia
Mbnl3	Mitd1	Myh9	Nfx1
Mbtps2	Mkks	My112b	Nfxl1
Mccc1	Mlec	My1pf	Nhlrc2
Mcm3	Mlf2	Myo1g	Nhp2
Mcm3ap	Mlit10	Myo1h	Nipbl
Mcm9	Mlxip	Myo9a	Nkrf
Mcts1	Mmp25	Mzf1	Nktr
Mdp1	Mms19	N4bp2	Nlk
Med13	Mob1a	N4bp2l2	Nol7
Med14	Mob3a	Naa16	Nono
Med18	Morc3	Naa20	Nop58
Med6	Morf4l1	Naa25	Notch3
Melk	Morf4l2	Naa50	Npepps
Memo1	Morn1	Nadk	Nphp1
Mettl1	Morn2	Nagk	Nploc4
Mettl14	Morn3	Nap1l1	Nppa
Mettl17	Mpnd	Napa	Nptn
Mettl8	Mpp6	Nasp	Nqo2
Mga	Mpv17	Nat10	Nr2f6
Mical3	Mrc2	Nat2	Nr3c1
Midn	Mrfap1	Nbeal1	Nr4a2
Mif4gd	Mrpl10	Nbeal2	n-R5s79
Mir125a	Mrpl14	Nbr1	Nrf1
Mir132	Mrpl30	Ncaph2	Nrg4
Mir152	Mrpl32	Nck1	Nt5c2
Mir15b	Mrpl40	Ncoa3	Ntf5
Mir17	Mrpl45	Ncoa4	Nub1
Mir17hg	Mrpl48	Ncor1	Nubp2
Mir18	Mrpl52	Ncor2	Nufip2
Mir1931	Mrpl9	Ncrna00085	Numa1
Mir1956	Mrps2	Ndfip2	Nup133
Mir199b	Mrps36	Ndrp4	Nup153
Mir19a	Mrps6	Ndufaf4	Nup205
Mir19b-1	Mrs2	Ndufs7	Nup98
Mir20a	Ms4a10	Necap1	Nyx
Mir212	Msh5	Nedd4	Oas1b
Mir3058	Msl1	Nek10	Oas1c
Mir3109	Msrp3	Nek8	Oas2
Mir5122	Mtf2	Nek9	Ocr1
Mir5135	Mtif3	Neu1	Ogt
Mir615	Mtmt3	Neurl2	Olfr1414
Mir670	Muc6	Nf2	Oma1
Mir677	Mxi1	Nfat5	Opn1sw

Orai2	Pgam1	Plekhg2	Prkrip1
Orc1	Pgap2	Plekhg3	Prpf19
Orc2	Pgd	Plin3	Prpf3
Osbpl3	Phactr4	Plk1s1	Prpf38a
Osbpl7	Phc1	Plod3	Prpf38b
Osbpl8	Phc3	Plxna2	Prpf39
Otub1	Phf12	Plxnd1	Prpf4
Otud4	Phf15	Pml	Prpf4b
Ovol1	Phf20	Pmm2	Prpsap1
Oxnad1	Phf21a	Pnpla8	Prpsap2
Oxsr1	Phf6	Poc1a	Prr12
P2rx4	Phf8	Poldip2	Prr13
P4ha1	Phgdh	Pole2	Prr14l
Pacsin2	Phip	Polg	Prrc2a
Palld	Phospho1	Polg2	Prrg2
Pan3	Phyhd1	Poll	Psap
Papd4	Pias4	Polr2h	Psma1
Papss1	Picalm	Polr2i	Psma2
Papss2	Pif1	Polr3c	Psma3
Paqr8	Pigl	Polrmt	Psmb3
Parl	Pigp	Pop4	Psmb6
Patz1	Pigv	Pou2f1	Psmc1
Pax2	Pik3c3	Pou4f3	Psmd14
Pax6	Pik3ca	Pou6f1	Psmd7
Pbld2	Pik3cb	Ppard	Pspc1
Pbrm1	Pik3cd	Ppcdc	Psph
Pcbd2	Pik3r1	Ppfia3	Ptbp3
Pcbp1	Pik3r3	Ppil1	Ptch1
Pcbp2	Pim1	Ppm1b	Ptp4a1
Pcca	Pisd	Ppm1h	Ptp4a2
Pccb	Pisd-ps1	Ppm1k	Ptplad2
Pcgf2	Pisd-ps2	Ppp1r12a	Ptpmt1
Pcm1	Pitpnc1	Ppp1r15a	Ptpn11
Pcnxl2	Pitpnm2	Ppp1r16a	Ptpn6
Pcsk4	Pja1	Ppp1r3f	Ptprj
Pde4d	Pkd2l1	Ppp1r8	Ptrh2
Pdia3	Pkig	Ppp2cb	Pttg1
Pdia6	Pkn3	Ppp2r5c	Pum1
Pdk1	Pknox1	Ppp6r2	Pycard
Pdpk1	Pla2g6	Prdm1	Pycr2
Pdxdc1	Plbd2	Prex1	Pygl
Peg13	Plcg1	Prickle1	Qk
Peli1	Plcl2	Prkaa1	Qrich1
Pes1	Plekha3	Prkag1	Qsox2
Pex19	Plekha4	Prkag2	R3hdm2
Pfkm	Plekha8	Prkar1a	Rab1
Pfn2	Plekhf2	Prkcg	Rab21

Rab28	Riok1	Rtfdc1	Setd2
Rab3gap2	Rlim	Rtn4rl2	Setd3
Rab42	Rmi1	Rufy3	Setd4
Rab5b	Rmnd1	Rundc3a	Setd5
Rab6a	Rnase4	Runx1	Setd7
Rab7	Rnf10	Rybp	Setd8
Rad51ap1	Rnf121	S100pbp	Sfmbt1
Rad51c	Rnf13	Sacm1l	Sfpq
Rad9b	Rnf146	Sae1	Sfxn2
Ralbp1	Rnf157	Samd1	Sgk1
Ralgapa1	Rnf167	Samd8	Sgk2
Ralgps1	Rnf2	Samd9l	Sgk3
Rap1b	Rnf34	Samhd1	Sgms2
Rap2a	Rnf5	Sap30	Sh2b3
Rapgef6	Rnft1	Sapcd2	Sh3bgrl
Rarg	Rp9	Sarm1	Sh3bp5l
Rasal2	Rpa1	Sbds	Sh3glb2
Rasd1	Rpa2	Sbf1	Sh3kbp1
Rb1	Rpl10	Sbno2	Shc4
Rbbp5	Rpl10-ps2	Scamp3	Shisa5
Rbbp6	Rpl12	Scara5	Shmt1
Rbck1	Rpl24	Scarb1	Shroom3
Rbm12b2	Rpl27	Scgb1a1	Siae
Rbm27	Rpl30-ps5	Schip1	Sigmar1
Rbms1	Rpl35a	Scmh1	Sin3a
Rcc1	Rpl35a-ps2	Scn1a	Sirt1
Rcc2	Rpl38	Scn3a	Sit1
Rccd1	Rpl41	Scpep1	Six6
Rcor1	Rpl5	Sec14l1	Skil
Rdh10	Rpl6	Sec22c	Slain2
Rdm1	Rpl7	Sec23a	Slc16a1
Rell1	Rpl9	Sec24b	Slc18a1
Reps2	Rpp21	Sec24c	Slc23a2
Rere	Rprd2	Sec31a	Slc25a11
Rexo2	Rps10	Sec31b	Slc25a14
Rffl	Rps15a	Sec61a1	Slc25a3
Rft1	Rps26	Seh1l	Slc25a35
Rftn2	Rps6ka1	Selt	Slc25a36
Rfwd3	Rps6kb1	Sema3c	Slc25a38
Rfx2	Rps8	Sephs1	Slc25a39
Rfx3	Rptor	Sept5	Slc25a43
Rhbdd2	Rreb1	Sept8	Slc25a51
Rhbg	Rrm1	Serf1	Slc26a10
Rhob	Rrm2b	Serpinb9	Slc30a1
Rhobtb2	Rrp8	Sertad1	Slc30a7
Rhot1	Rsb1l	Sertad2	Slc31a2
Rilpl2	Rsrc2	Sesn2	Slc32a1

Slc35b1	Snrnp70	Stam	Tbcb
Slc35b4	Sntb2	Stam2	Tbcc
Slc38a10	Snupn	Stard6	Tbl1xr1
Slc38a2	Snx10	Stard9	Tbx15
Slc39a2	Snx27	Stat2	Tcam1
Slc3a2	Snx29	Stim2	Tceanc2
Slc43a2	Snx30	Stip1	Tcf12
Slc5a3	Soat1	Stk25	Tcf4
Slc5a6	Socs1	Stk30	Tcf7l2
Slc7a7	Socs2	Stk38	Tcof1
Slc9a1	Socs3	Stk38l	TCR-alpha
Slc9a8	Socs7	Stoml1	chain
Slu7	Sod1	Strada	Tctn1
Slx1b	Sorbs1	Strn3	Tdrd3
Slx4ip	Sos2	Stx11	Tead2
Smad6	Sp1	Stx16	Tecr
Smad7	Sp3	Styk1	Terf2
Smap1	Spa17	Suco	Terf2ip
Smarca2	Spag8	Sumo1	Tet2
Smarcc2	Specc1	Sun1	Tex14
Smarcd2	Spg11	Suz12	Tex30
Smc4	Spin1	Swsap1	Tfap4
Smg7	Spp1	Syne1	Tfdp2
Smim13	Sppl2a	Syng1	Tfg
Smndc1	Spred1	Syng3	Tfrc
Smpd1	Spred2	Syng4	Tgif1
Smyd4	Spry4	Synj1	Thrap3
Snai1	Spryd3	Synj2	Tia1
Snf8	Spryd4	Tacc1	Tial1
Snhg1	Spsb3	Tacc2	Ticam1
Snhg12	Sptan1	Taco1	Timm13
Snhg5	Sptlc2	Taf1	Timm8a2
Snora16a	Sqrdl	Taf1c	Timm9
Snora44	Srek1	Taf1d	Timmdc1
Snora61	Srgap3	Taf3	Tipin
Snora70	Srrm1	Taf4a	Tjap1
Snord19	Srrm2	Taf6	Tjp3
Snord21	Srsf1	Tagln2	Tle2
Snord38a	Srsf3	Tango2	Tle3
Snord52	Ssb	Tango6	Tle6
Snord55	Ssbp3	Taok2	Tlk2
Snord7	Ssbp4	Taok3	Tln1
Snord88a	Ssh2	Tarbp2	Tm2d2
Snord88c	St13	Tatdn2	Tm9sf4
Snord96a	St6galnac2	Tbc1d1	Tmbim1
Snord99	Stac2	Tbc1d10a	Tmcc2
Snrnp35	Stag2	Tbc1d10b	Tmem100

Tmem106a	Trap1	Uba1	Vgll4
Tmem120b	Trdv5	Uba5	Vhl
Tmem143	Trerf1	Uba52	Vmp1
Tmem156	Triap1	Ubald1	Vprbp
Tmem164	Trib1	Ubap2l	Vps13d
Tmem18	Trib2	Ubb	Vps29
Tmem180	Trim35	Ubc	Vps37b
Tmem186	Trim37	Ube2b	Vps53
Tmem192	Trim59	Ube2e3	Vps54
Tmem194	Trim7	Ube2f	Vtn
Tmem199	Trim8	Ube2h	Wbscr16
Tmem231	Triobp	Ube2v1	Wdfy2
Tmem242	Trip12	Ublcp1	Wdpcp
Tmem259	Trmt12	Ubn2	Wdr1
Tmem29	Trpc2	Ubr2	Wdr34
Tmem33	Trpv2	Ubt2d	Wdr37
Tmem5	Trpv4	Ubtf	Wdr47
Tmem59	Trub2	Ubxn1	Wdr5
Tmem67	Tsc22d3	Ubxn4	Wdr6
Tmem82	Tsen54	Ubxn7	Wdr63
Tmem88	Tspan10	Uchl4	Wdr75
Tmpo	Tspan14	Ulk2	Wee1
Tnfaip8	Tspan17	Umodl1	Whsc1
Tnfrsf9	Tspan31	Unc119	Whsc111
Tnk2	Ttc17	Uqcrq	Wibg
Tnp2	Ttc19	Urgcp	Wipf1
Tnpo2	Ttc28	Urm1	Wrnip1
Tnpo3	Ttc3	Usb1	Wtap
Tnrc18	Ttc7	Usf2	Wwp1
Tnrc6a	Ttc9c	Usp1	Wwp2
Tob1	Tuba1a	Usp10	Xbp1
Tob2	Tuba1c	Usp15	Xiap
Tom111	Tubb5	Usp2	Xpnpep3
Top1	Tubd1	Usp20	Xpot
Top2a	Tulp1	Usp28	Yars
Tor1aip1	Tulp3	Usp3	Ybey
Tor1aip2	Txlna	Usp32	Ydjc
Tpm1	Txn2	Usp34	Yipf2
Tprgl	Txndc12	Usp45	Yipf4
Tpt1	Txndc9	Usp48	Ypel2
Tpx2	Txnl4b	Usp49	Ywhag
Tra2b	Txnrd1	Utp14a	Yy2
Traf6	Txnrd2	Vac14	Zan
Trafd1	Tyw1	Vcp	Zbtb1
Traj58	U05342	Vdac1	Zbtb24
Traj59	U3	VeZF1	Zbtb25
Tram1	U7	VeZt	Zbtb38

Zbtb45	Zfp207	Zfp52	Zfp1
Zbtb7a	Zfp217	Zfp553	Zfx
Zc3h10	Zfp251	Zfp592	Zkscan17
Zc3h6	Zfp27	Zfp606	Zkscan3
Zc3hav1	Zfp280b	Zfp607	Zmat1
Zc3hc1	Zfp319	Zfp608	Zmiz2
Zcchc8	Zfp324	Zfp64	Zmym5
Zdhhc17	Zfp361	Zfp646	Zmynd11
Zdhhc5	Zfp383	Zfp664	Zmynd8
Zer1	Zfp384	Zfp668	Znhit1
Zfand3	Zfp39	Zfp672	Znhit3
Zfat	Zfp395	Zfp703	Zscan25
Zfp1	Zfp40	Zfp719	Zswim7
Zfp101	Zfp428	Zfp809	Zufsp
Zfp106	Zfp438	Zfp866	Zw10
Zfp182	Zfp507	Zfp91	
Zfp184	Zfp512	Zfp948	

B.**Ingenuity Canonical Pathways**

	-log(p-val)
Insulin Receptor Signaling	5.74E00
Glucocorticoid Receptor Signaling	5.48E00
Prolactin Signaling	5.47E00
Hereditary Breast Cancer Signaling	5.42E00
FAK Signaling	5.42E00
Integrin Signaling	5.16E00
Huntington's Disease Signaling	5.15E00
IGF-1 Signaling	5.03E00
Melanocyte Development and Pigmentation Signaling	5.03E00
JAK/Stat Signaling	4.97E00
p53 Signaling	4.95E00
Protein Ubiquitination Pathway	4.94E00
Leptin Signaling in Obesity	4.88E00
IL-4 Signaling	4.88E00
Erythropoietin Signaling	4.86E00
Neurotrophin/TRK Signaling	4.86E00
AMPK Signaling	4.47E00
B Cell Receptor Signaling	4.43E00
Molecular Mechanisms of Cancer	4.4E00
EIF2 Signaling	4.38E00
Prostate Cancer Signaling	4.28E00
mTOR Signaling	4.26E00
ErbB2-ErbB3 Signaling	4.13E00
Growth Hormone Signaling	4.1E00
Telomerase Signaling	4.1E00
Acute Myeloid Leukemia Signaling	4.07E00
FLT3 Signaling in Hematopoietic Progenitor Cells	3.94E00
NGF Signaling	3.9E00
PI3K/AKT Signaling	3.88E00
CTLA4 Signaling in Cytotoxic T Lymphocytes	3.76E00
GM-CSF Signaling	3.59E00
RAR Activation	3.58E00
Gap Junction Signaling	3.5E00
Chronic Myeloid Leukemia Signaling	3.43E00
CREB Signaling in Neurons	3.4E00
Non-Small Cell Lung Cancer Signaling	3.36E00
Endometrial Cancer Signaling	3.34E00
P2Y Purigenic Receptor Signaling Pathway	3.22E00
Virus Entry via Endocytic Pathways	3.16E00
HER-2 Signaling in Breast Cancer	3.07E00
Renal Cell Carcinoma Signaling	3.07E00
Cardiac Hypertrophy Signaling	3.02E00
PDGF Signaling	3.01E00
Axonal Guidance Signaling	3E00
Hypoxia Signaling in the Cardiovascular System	3E00
ErbB Signaling	2.96E00
FGF Signaling	2.96E00
Natural Killer Cell Signaling	2.94E00

Small Cell Lung Cancer Signaling	2.93E00
SAPK/JNK Signaling	2.93E00
14-3-3-mediated Signaling	2.93E00
Neuregulin Signaling	2.9E00
Fc Epsilon RI Signaling	2.89E00
Glioma Signaling	2.87E00
Myc Mediated Apoptosis Signaling	2.86E00
ErbB4 Signaling	2.86E00
p70S6K Signaling	2.83E00
Role of Oct4 in Mammalian Embryonic Stem Cell Pluripotency	2.82E00
Clathrin-mediated Endocytosis Signaling	2.8E00
Role of NFAT in Cardiac Hypertrophy	2.78E00
Docosahexaenoic Acid (DHA) Signaling	2.78E00
Acute Phase Response Signaling	2.77E00
VEGF Signaling	2.73E00
ERK/MAPK Signaling	2.72E00
IL-2 Signaling	2.72E00
Glioblastoma Multiforme Signaling	2.7E00
Lymphotoxin β Receptor Signaling	2.65E00
Type II Diabetes Mellitus Signaling	2.64E00
Biotin-carboxyl Carrier Protein Assembly	2.59E00
Sphingosine-1-phosphate Signaling	2.55E00
Role of p14/p19ARF in Tumor Suppression	2.54E00
Cell Cycle: G1/S Checkpoint Regulation	2.52E00
EGF Signaling	2.51E00
Regulation of eIF4 and p70S6K Signaling	2.49E00
Mouse Embryonic Stem Cell Pluripotency	2.47E00
PTEN Signaling	2.46E00
eNOS Signaling	2.44E00
Estrogen Receptor Signaling	2.43E00
iCOS-iCOSL Signaling in T Helper Cells	2.42E00
Thrombin Signaling	2.39E00
Angiopoietin Signaling	2.39E00
HGF Signaling	2.37E00
Role of JAK2 in Hormone-like Cytokine Signaling	2.25E00
Antiproliferative Role of Somatostatin Receptor 2	2.25E00
Superpathway of Inositol Phosphate Compounds	2.24E00
Paxillin Signaling	2.23E00
Role of BRCA1 in DNA Damage Response	2.19E00
TR/RXR Activation	2.14E00
Estrogen-Dependent Breast Cancer Signaling	2.13E00
Sulfate Activation for Sulfonation	2.11E00
Thrombopoietin Signaling	2.1E00
IL-9 Signaling	2.08E00
3-phosphoinositide Degradation	2.08E00
PEDF Signaling	2.06E00
3-phosphoinositide Biosynthesis	2.03E00
ILK Signaling	2.03E00
Breast Cancer Regulation by Stathmin1	2.03E00
CNTF Signaling	2.02E00

Cell Cycle: G2/M DNA Damage Checkpoint Regulation	2.02E00
CD28 Signaling in T Helper Cells	1.99E00
PKC θ Signaling in T Lymphocytes	1.99E00
Ovarian Cancer Signaling	1.99E00
Germ Cell-Sertoli Cell Junction Signaling	1.99E00
Glioma Invasiveness Signaling	1.99E00
PPAR α /RXR α Activation	1.98E00
Protein Kinase A Signaling	1.98E00
Amyotrophic Lateral Sclerosis Signaling	1.97E00
Sonic Hedgehog Signaling	1.94E00
Pancreatic Adenocarcinoma Signaling	1.94E00
NRF2-mediated Oxidative Stress Response	1.89E00
ATM Signaling	1.88E00
Aldosterone Signaling in Epithelial Cells	1.87E00
Renin-Angiotensin Signaling	1.86E00
Role of JAK1 and JAK3 in γ c Cytokine Signaling	1.82E00
VEGF Family Ligand-Receptor Interactions	1.82E00
MSP-RON Signaling Pathway	1.75E00
RANK Signaling in Osteoclasts	1.74E00
Superpathway of Serine and Glycine Biosynthesis I	1.74E00
UVA-Induced MAPK Signaling	1.7E00
IL-3 Signaling	1.68E00
Mitotic Roles of Polo-Like Kinase	1.67E00
ERK5 Signaling	1.67E00
1D-myo-inositol Hexakisphosphate Biosynthesis II (Mammalian)	1.66E00
D-myo-inositol (1,3,4)-trisphosphate Biosynthesis	1.66E00
Apoptosis Signaling	1.66E00
CD40 Signaling	1.63E00
CXCR4 Signaling	1.6E00
Fc γ RIIB Signaling in B Lymphocytes	1.6E00
NF- κ B Activation by Viruses	1.59E00
Role of Tissue Factor in Cancer	1.59E00
IL-6 Signaling	1.58E00
Cell Cycle Control of Chromosomal Replication	1.56E00
IL-1 Signaling	1.54E00
Melanoma Signaling	1.54E00
Assembly of RNA Polymerase II Complex	1.53E00
Amyloid Processing	1.53E00
GNRH Signaling	1.51E00
IL-8 Signaling	1.48E00
Endoplasmic Reticulum Stress Pathway	1.48E00
Leukocyte Extravasation Signaling	1.47E00
Melatonin Signaling	1.45E00
GDNF Family Ligand-Receptor Interactions	1.45E00
Macropinocytosis Signaling	1.45E00
Cyclins and Cell Cycle Regulation	1.43E00
Nitric Oxide Signaling in the Cardiovascular System	1.4E00
Role of PI3K/AKT Signaling in the Pathogenesis of Influenza	1.39E00
UVB-Induced MAPK Signaling	1.38E00
Methylmalonyl Pathway	1.38E00

Role of IL-17A in Arthritis	1.34E00
RAN Signaling	1.33E00
Neuropathic Pain Signaling In Dorsal Horn Neurons	1.28E00
Colorectal Cancer Metastasis Signaling	1.27E00
Estrogen-mediated S-phase Entry	1.26E00
Superpathway of D-myo-inositol (1,4,5)-trisphosphate Metabolism	1.26E00
Actin Nucleation by ARP-WASP Complex	1.25E00
HMGB1 Signaling	1.25E00
Ephrin A Signaling	1.24E00
Neuroprotective Role of THOP1 in Alzheimer's Disease	1.23E00
D-myo-inositol (1,4,5,6)-Tetrakisphosphate Biosynthesis	1.22E00
D-myo-inositol (3,4,5,6)-tetrakisphosphate Biosynthesis	1.22E00
Role of NFAT in Regulation of the Immune Response	1.22E00
Androgen Signaling	1.22E00
HIF1 α Signaling	1.22E00
IL-15 Signaling	1.2E00
Remodeling of Epithelial Adherens Junctions	1.2E00
Serine Biosynthesis	1.19E00
2-oxobutanoate Degradation I	1.19E00
Endothelin-1 Signaling	1.18E00
D-myo-inositol (1,4,5)-trisphosphate Degradation	1.16E00
α -Adrenergic Signaling	1.15E00
Systemic Lupus Erythematosus Signaling	1.15E00
Production of Nitric Oxide and Reactive Oxygen Species in Macrophages	1.15E00
Relaxin Signaling	1.13E00
VDR/RXR Activation	1.12E00
T Cell Receptor Signaling	1.1E00
GADD45 Signaling	1.09E00
Ephrin Receptor Signaling	1.09E00
Type I Diabetes Mellitus Signaling	1.08E00
Nucleotide Excision Repair Pathway	1.08E00
G Beta Gamma Signaling	1.06E00
PAK Signaling	1.06E00
D-myo-inositol-5-phosphate Metabolism	1.06E00
Reelin Signaling in Neurons	1.06E00
Adenine and Adenosine Salvage VI	1.05E00
Sertoli Cell-Sertoli Cell Junction Signaling	1.05E00
G α q Signaling	1.05E00
G α 12/13 Signaling	1.04E00
Arginine Biosynthesis IV	1.04E00
Chondroitin and Dermatan Biosynthesis	1.04E00
Thioredoxin Pathway	1.04E00
Superoxide Radicals Degradation	1.04E00
DNA Methylation and Transcriptional Repression Signaling	1.03E00
Wnt/ β -catenin Signaling	1.02E00
Pyridoxal 5'-phosphate Salvage Pathway	9.94E-01
STAT3 Pathway	9.65E-01
Role of CHK Proteins in Cell Cycle Checkpoint Control	9.61E-01
IL-17A Signaling in Airway Cells	9.61E-01
Fc γ Receptor-mediated Phagocytosis in Macrophages and Monocytes	9.28E-01

DNA Double-Strand Break Repair by Homologous Recombination	9.19E-01
Leukotriene Biosynthesis	9.19E-01
Vitamin-C Transport	9.19E-01
Regulation of the Epithelial-Mesenchymal Transition Pathway	9.01E-01
Netrin Signaling	9E-01
PI3K Signaling in B Lymphocytes	8.99E-01
Epithelial Adherens Junction Signaling	8.9E-01
Signaling by Rho Family GTPases	8.89E-01
G Protein Signaling Mediated by Tubby	8.73E-01
TGF- β Signaling	8.4E-01
Tec Kinase Signaling	8.32E-01
fMLP Signaling in Neutrophils	8.25E-01
Sphingomyelin Metabolism	8.15E-01
Tumoricidal Function of Hepatic Natural Killer Cells	8.03E-01
Glycolysis I	8.03E-01
CD27 Signaling in Lymphocytes	7.94E-01
Actin Cytoskeleton Signaling	7.76E-01
Lipoate Biosynthesis and Incorporation II	7.72E-01
L-DOPA Degradation	7.72E-01
Uridine-5'-phosphate Biosynthesis	7.72E-01
Cardiolipin Biosynthesis II	7.72E-01
Putrescine Biosynthesis III	7.72E-01
Glycine Biosynthesis I	7.72E-01
Glutamate Biosynthesis II	7.72E-01
Glutamate Degradation X	7.72E-01
Human Embryonic Stem Cell Pluripotency	7.41E-01
IL-17 Signaling	7.36E-01
Assembly of RNA Polymerase I Complex	7.31E-01
PXR/RXR Activation	7.2E-01
Role of Macrophages, Fibroblasts and Endothelial Cells in Rheumatoid Arthritis	7.17E-01
Antiproliferative Role of TOB in T Cell Signaling	7.13E-01
LPS-stimulated MAPK Signaling	7.12E-01
Cellular Effects of Sildenafil (Viagra)	6.86E-01
Regulation of Cellular Mechanics by Calpain Protease	6.77E-01
nNOS Signaling in Neurons	6.61E-01
NAD Phosphorylation and Dephosphorylation	6.59E-01
Dolichyl-diphosphooligosaccharide Biosynthesis	6.59E-01
Synaptic Long Term Potentiation	6.49E-01
Dopamine-DARPP32 Feedback in cAMP Signaling	6.48E-01
Notch Signaling	6.46E-01
Phospholipase C Signaling	6.34E-01
TNFR1 Signaling	6.33E-01
Dendritic Cell Maturation	6.25E-01
NF- κ B Signaling	6.25E-01
Regulation of Actin-based Motility by Rho	6.23E-01
Agrin Interactions at Neuromuscular Junction	6.23E-01
Dopamine Receptor Signaling	6.22E-01
NADH Repair	6.15E-01
Methylglyoxal Degradation I	6.15E-01
Coenzyme A Biosynthesis	6.15E-01

Glutathione Biosynthesis	6.15E-01
Glutathione Redox Reactions II	6.15E-01
D-glucuronate Degradation I	6.15E-01
Hypusine Biosynthesis	6.15E-01
Glutamate Degradation II	6.15E-01
Tyrosine Biosynthesis IV	6.15E-01
Aspartate Biosynthesis	6.15E-01
Corticotropin Releasing Hormone Signaling	6.1E-01
Purine Nucleotides De Novo Biosynthesis II	5.96E-01
Role of Osteoblasts, Osteoclasts and Chondrocytes in Rheumatoid Arthritis	5.85E-01
RhoGDI Signaling	5.84E-01
Induction of Apoptosis by HIV1	5.78E-01
PPAR Signaling	5.66E-01
Ceramide Signaling	5.62E-01
Cholecystokinin/Gastrin-mediated Signaling	5.54E-01
Death Receptor Signaling	5.48E-01
Assembly of RNA Polymerase III Complex	5.41E-01
Superpathway of Methionine Degradation	5.34E-01
Salvage Pathways of Pyrimidine Ribonucleotides	5.31E-01
Role of RIG1-like Receptors in Antiviral Innate Immunity	5.3E-01
CCR3 Signaling in Eosinophils	5.28E-01
Sperm Motility	5.28E-01
Uracil Degradation II (Reductive)	5.09E-01
Pentose Phosphate Pathway (Oxidative Branch)	5.09E-01
Heme Degradation	5.09E-01
Thymine Degradation	5.09E-01
Geranylgeranyldiphosphate Biosynthesis	5.09E-01
Proline Biosynthesis I	5.09E-01
Trans, trans-farnesyl Diphosphate Biosynthesis	5.09E-01
Rapoport-Luebering Glycolytic Shunt	5.09E-01
L-cysteine Degradation I	5.09E-01
N-acetylglucosamine Degradation II	5.09E-01
Phenylalanine Degradation I (Aerobic)	5.09E-01
Semaphorin Signaling in Neurons	5.08E-01
NAD biosynthesis II (from tryptophan)	4.93E-01
BMP signaling pathway	4.81E-01
p38 MAPK Signaling	4.7E-01
nNOS Signaling in Skeletal Muscle Cells	4.5E-01
Urate Biosynthesis/Inosine 5'-phosphate Degradation	4.5E-01
γ-glutamyl Cycle	4.5E-01
Role of JAK1, JAK2 and TYK2 in Interferon Signaling	4.46E-01
CDK5 Signaling	4.36E-01
Ceramide Biosynthesis	4.31E-01
Tetrapyrrole Biosynthesis II	4.31E-01
CMP-N-acetylneuraminate Biosynthesis I (Eukaryotes)	4.31E-01
dTMP De Novo Biosynthesis	4.31E-01
Folate Polyglutamylation	4.31E-01
RhoA Signaling	4.29E-01
Role of JAK family kinases in IL-6-type Cytokine Signaling	4.17E-01
Gluconeogenesis I	4.17E-01

Cardiac β -adrenergic Signaling	4.15E-01
Regulation of IL-2 Expression in Activated and Anergic T Lymphocytes	4.14E-01
Mitochondrial Dysfunction	4.11E-01
Telomere Extension by Telomerase	4.11E-01
The Visual Cycle	4.11E-01
Interferon Signaling	4.03E-01
G-Protein Coupled Receptor Signaling	4E-01
Calcium-induced T Lymphocyte Apoptosis	3.9E-01
Antigen Presentation Pathway	3.81E-01
Aryl Hydrocarbon Receptor Signaling	3.8E-01
Granzyme B Signaling	3.77E-01
Superpathway of Geranylgeranyldiphosphate Biosynthesis I (via Mevalonate)	3.77E-01
NAD Biosynthesis from 2-amino-3-carboxymuconate Semialdehyde	3.7E-01
Proline Biosynthesis II (from Arginine)	3.7E-01
Urea Cycle	3.7E-01
Arginine Degradation VI (Arginase 2 Pathway)	3.7E-01
Acetyl-CoA Biosynthesis I (Pyruvate Dehydrogenase Complex)	3.7E-01
Selenocysteine Biosynthesis II (Archaea and Eukaryotes)	3.7E-01
UDP-N-acetyl-D-glucosamine Biosynthesis II	3.7E-01
Glycogen Biosynthesis II (from UDP-D-Glucose)	3.7E-01
Citrulline-Nitric Oxide Cycle	3.7E-01
Pregnenolone Biosynthesis	3.7E-01
GDP-mannose Biosynthesis	3.7E-01
Rac Signaling	3.69E-01
April Mediated Signaling	3.6E-01
tRNA Charging	3.6E-01
Granzyme A Signaling	3.46E-01
γ -linolenate Biosynthesis II (Animals)	3.46E-01
Phosphatidylglycerol Biosynthesis II (Non-plastidic)	3.46E-01
Mitochondrial L-carnitine Shuttle Pathway	3.46E-01
Antioxidant Action of Vitamin C	3.44E-01
Caveolar-mediated Endocytosis Signaling	3.42E-01
Thyroid Cancer Signaling	3.4E-01
Role of Wnt/GSK-3 β Signaling in the Pathogenesis of Influenza	3.28E-01
Ephrin B Signaling	3.28E-01
Nur77 Signaling in T Lymphocytes	3.24E-01
Role of PKR in Interferon Induction and Antiviral Response	3.22E-01
B Cell Activating Factor Signaling	3.22E-01
Tryptophan Degradation to 2-amino-3-carboxymuconate Semialdehyde	3.21E-01
Ketolysis	3.21E-01
Aspartate Degradation II	3.21E-01
Gas Signaling	3.11E-01
Mechanisms of Viral Exit from Host Cells	3.04E-01
Role of IL-17F in Allergic Inflammatory Airway Diseases	3.04E-01
Role of NANOG in Mammalian Embryonic Stem Cell Pluripotency	3.01E-01
Xenobiotic Metabolism Signaling	3.01E-01
Retinol Biosynthesis	2.99E-01
Tight Junction Signaling	2.97E-01
Cardiomyocyte Differentiation via BMP Receptors	2.92E-01
Purine Nucleotides Degradation II (Aerobic)	2.92E-01

Tryptophan Degradation III (Eukaryotic)	2.92E-01
DNA damage-induced 14-3-3 σ Signaling	2.92E-01
Sucrose Degradation V (Mammalian)	2.81E-01
Salvage Pathways of Pyrimidine Deoxyribonucleotides	2.81E-01
Cytotoxic T Lymphocyte-mediated Apoptosis of Target Cells	2.8E-01
OX40 Signaling Pathway	2.79E-01
Phospholipases	2.79E-01
Complement System	2.62E-01
CCR5 Signaling in Macrophages	2.6E-01
Chondroitin Sulfate Biosynthesis (Late Stages)	2.57E-01
Calcium Transport I	2.48E-01
Glycogen Degradation II	2.48E-01
Leucine Degradation I	2.48E-01
Heme Biosynthesis II	2.48E-01
Histidine Degradation VI	2.48E-01
Folate Transformations I	2.48E-01
NAD Salvage Pathway II	2.48E-01
Pyrimidine Deoxyribonucleotides De Novo Biosynthesis I	2.48E-01
TWEAK Signaling	2.45E-01
MIF-mediated Glucocorticoid Regulation	2.45E-01
Triacylglycerol Biosynthesis	2.45E-01
Polyamine Regulation in Colon Cancer	2.28E-01
Ketogenesis	2.19E-01
Oleate Biosynthesis II (Animals)	2.19E-01
Pentose Phosphate Pathway	2.19E-01
Glycine Betaine Degradation	2.19E-01
Glutaryl-CoA Degradation	1.95E-01
Acyl-CoA Hydrolysis	1.95E-01
Glycogen Degradation III	1.95E-01

REFERENCES

(2012). "Adipose Tissue Inflammation and Reduced Insulin Sensitivity in Ovariectomized Mice Occurs in the Absence of Increased Adiposity." Endocrinology **153**(9): 4266-4277.

Aguirre, J. I., L. I. Plotkin, S. A. Stewart, R. S. Weinstein, A. M. Parfitt, S. C. Manolagas and T. Bellido (2006). "Osteocyte apoptosis is induced by weightlessness in mice and precedes osteoclast recruitment and bone loss." J Bone Miner Res **21**(4): 605-615.

Ahlstrom, M. and C. Lamberg-Allardt (1997). "Rapid protein kinase A--mediated activation of cyclic AMP-phosphodiesterase by parathyroid hormone in UMR-106 osteoblast-like cells." J Bone Miner Res **12**(2): 172-178.

Allen, M. and D. Burr (2006). "Parathyroid hormone and bone biomechanics." Clinical Reviews in Bone and Mineral Metabolism **4**(4): 259-268.

Alvarez, M., R. Shah, S. J. Rhodes and J. P. Bidwell (2005). "Two promoters control the mouse Nmp4/CIZ transcription factor gene." Gene **347**(1): 43-54.

Alvarez, M., P. Thunyakitpisal, P. Morrison, J. Onyia, J. Hock and J. P. Bidwell (1998). "PTH-responsive osteoblast nuclear matrix architectural transcription factor binds to the rat type I collagen promoter." J Cell Biochem **69**(3): 336-352.

Alvarez, M. B., P. Childress, B. K. Philip, R. Gerard-O'Riley, M. Hanlon, B.-S. Herbert, A. G. Robling, F. M. Pavalko and J. P. Bidwell (2012). "Immortalization and characterization of osteoblast cell lines generated from wild-type and Nmp4-null mouse bone marrow stromal cells using murine telomerase reverse transcriptase (mTERT)." J Cell Physiol **227**(5): 1873-1882.

Alvarez, M. B., P. Childress, B. K. Philip, R. Gerard-O'Riley, M. Hanlon, B. S. Herbert, A. G. Robling, F. M. Pavalko and J. P. Bidwell (2012). "Immortalization and characterization of osteoblast cell lines generated from wild-type and Nmp4-null mouse bone marrow stromal cells using murine telomerase reverse transcriptase (mTERT)." J Cell Physiol **227**(5): 1873-1882.

Auerbach, R. K., B. Chen and A. J. Butte (2013). "Relating genes to function: identifying enriched transcription factors using the ENCODE ChIP-Seq significance tool." Bioinformatics **29**(15): 1922-1924.

Baron, R. and E. Hesse (2012). "Update on bone anabolics in osteoporosis treatment: rationale, current status, and perspectives." J Clin Endocrinol Metab **97**(2): 311-325.

Bauer, W., J. C. Aub and F. Albright (1929). "STUDIES OF CALCIUM AND PHOSPHORUS METABOLISM : V. A STUDY OF THE BONE TRABECULAE AS A READILY AVAILABLE RESERVE SUPPLY OF CALCIUM." J Exp Med **49**(1): 145-162.

Becker, T. C., S. M. Coley, E. J. Wherry and R. Ahmed (2005). "Bone marrow is a preferred site for homeostatic proliferation of memory CD8 T cells." J Immunol **174**(3): 1269-1273.

Bedi, B., J. Y. Li, H. Tawfeek, K. H. Baek, J. Adams, S. S. Vangara, M. K. Chang, M. Kneissel, M. N. Weitzmann and R. Pacifici (2012). "Silencing of parathyroid hormone (PTH) receptor 1 in T cells blunts the bone anabolic activity of PTH." Proc Natl Acad Sci U S A **109**(12): 5.

Bellido, T. (2006). "Downregulation of SOST/sclerostin by PTH: a novel mechanism of hormonal control of bone formation mediated by osteocytes." Journal of Musculoskeletal and Neuronal Interactions **6**(4): 358.

Bellido, T., A. A. Ali, L. I. Plotkin, Q. Fu, I. Gubrij, P. K. Roberson, R. S. Weinstein, C. A. O'Brien, S. C. Manolagas and R. L. Jilka (2003). "Proteasomal degradation of Runx2 shortens parathyroid hormone-induced anti-apoptotic signaling in osteoblasts. A putative explanation for why intermittent administration is needed for bone anabolism." J Biol Chem **278**(50): 50259-50272.

Bennett, C. N., H. Ouyang, Y. L. Ma, Q. Zeng, I. Gerin, K. M. Sousa, T. F. Lane, V. Krishnan, K. D. Hankenson and O. A. MacDougald (2007). "Wnt10b increases postnatal bone formation by enhancing osteoblast differentiation." J Bone Miner Res **22**(12): 1924-1932.

Bergman, R. J., D. Gazit, A. J. Kahn, H. Gruber, S. McDougall and T. J. Hahn (1996). "Age-related changes in osteogenic stem cells in mice." J Bone Miner Res **11**(5): 568-577.

Bidwell, J. P., M. B. Alvarez, M. Hood, Jr. and P. Childress (2013). "Functional impairment of bone formation in the pathogenesis of osteoporosis: the bone marrow regenerative competence." Curr Osteoporos Rep **11**(2): 117-125.

Bidwell, J. P., P. Childress, M. B. Alvarez, M. Hood, Jr., Y. He, F. M. Pavalko, M. A. Kacena and F. C. Yang (2012). "Nmp4/CIZ closes the parathyroid hormone anabolic window." Crit Rev Eukaryot Gene Expr **22**(3): 205-218.

Bikle, D. D., T. Sakata, C. Leary, H. Elalieh, D. Ginzinger, C. J. Rosen, W. Beamer, S. Majumdar and B. P. Halloran (2002). "Insulin-like growth factor I is required for the anabolic actions of parathyroid hormone on mouse bone." J Bone Miner Res **17**(9): 1570-1578.

Bikle, D. D. and Y. Wang (2012). "Insulin like growth factor-I: a critical mediator of the skeletal response to parathyroid hormone." Curr Mol Pharmacol **5**(2): 135-142.

Bilezikian, J. P. (2008). "Combination anabolic and antiresorptive therapy for osteoporosis: opening the anabolic window." Curr Osteoporos Rep **6**(1): 24-30.

Black, D. M., S. L. Greenspan, K. E. Ensrud, L. Palermo, J. A. McGowan, T. F. Lang, P. Garnero, M. L. Bouxsein, J. P. Bilezikian, C. J. Rosen and P. S. Investigators (2003). "The effects of parathyroid hormone and alendronate alone or in combination in postmenopausal osteoporosis." N Engl J Med **349**(13): 1207-1215.

Boonen, S., S. Ferrari, P. D. Miller, E. F. Eriksen, P. N. Sambrook, J. Compston, I. R. Reid, D. Vanderschueren and F. Cosman (2012). "Postmenopausal osteoporosis treatment with antiresorptives: effects of discontinuation or long-term continuation on bone turnover and fracture risk--a perspective." J Bone Miner Res **27**(5): 963-974.

Bord, S., A. Horner, S. Beavan and J. Compston (2001). "Estrogen Receptors α and β Are Differentially Expressed in Developing Human Bone." The Journal of Clinical Endocrinology & Metabolism **86**(5): 2309-2314.

Bouxsein, M. L., D. D. Pierroz, V. Glatt, D. S. Goddard, F. Cavat, R. Rizzoli and S. L. Ferrari (2005). "beta-Arrestin2 regulates the differential response of cortical and trabecular bone to intermittent PTH in female mice." J Bone Miner Res **20**(4): 635-643.

Boyle, W. J., W. S. Simonet and D. L. Lacey (2003). "Osteoclast differentiation and activation." Nature **423**(6937): 337-342.

Bozec, A., L. Bakiri, A. Hoebertz, R. Eferl, A. F. Schilling, V. Komnenovic, H. Scheuch, M. Priemel, C. L. Stewart, M. Amling and E. F. Wagner (2008). "Osteoclast size is controlled by Fra-2 through LIF/LIF-receptor signalling and hypoxia." Nature **454**(7201): 221-225.

Burge, R., B. Dawson-Hughes, D. H. Solomon, J. B. Wong, A. King and A. Tosteson (2007). "Incidence and economic burden of osteoporosis-related fractures in the United States, 2005-2025." J Bone Miner Res **22**(3): 465-475.

Cary, L. A., D. C. Han, T. R. Polte, S. K. Hanks and J. L. Guan (1998). "Identification of p130Cas as a mediator of focal adhesion kinase-promoted cell migration." J Cell Biol **140**(1): 211-221.

Cenci, S., M. N. Weitzmann, C. Roggia, N. Namba, D. Novack, J. Woodring and R. Pacifici (2000). "Estrogen deficiency induces bone loss by enhancing T-cell production of TNF- α ." The Journal of Clinical Investigation **106**(10): 1229-1237.

Chen, T. and S. Y. R. Dent (2014). "Chromatin modifiers and remodellers: regulators of cellular differentiation." Nat Rev Genet **15**(2): 93-106.

Chen, T. L. (2004). "Inhibition of growth and differentiation of osteoprogenitors in mouse bone marrow stromal cell cultures by increased donor age and glucocorticoid treatment." Bone **35**(1): 83-95.

Cheng, S., S. Sipilä, D. R. Taaffe, J. Puolakka and H. Suominen (2002). "Change in bone mass distribution induced by hormone replacement therapy and high-impact physical exercise in post-menopausal women." Bone **31**(1): 126-135.

Childress, P., B. Philip, A. Robling, A. Bruzzaniti, M. Kacena, N. Bivi, L. Plotkin, A. Heller and J. Bidwell (2011). "Nmp4/CIZ Suppresses the Response of Bone to Anabolic Parathyroid Hormone by Regulating Both Osteoblasts and Osteoclasts." Calcified Tissue International **89**(1): 74-89.

Childress, P., B. K. Philip, A. G. Robling, A. Bruzzaniti, M. A. Kacena, N. Bivi, L. I. Plotkin, A. Heller and J. P. Bidwell (2011). "Nmp4/CIZ suppresses the response of bone to anabolic parathyroid hormone by regulating both osteoblasts and osteoclasts." Calcif Tissue Int **89**(1): 74-89.

Childress, P., A. G. Robling and J. P. Bidwell Nmp4/CIZ: road block at the intersection of PTH and load, Bone. 2010 Feb;46(2):259-66. doi: 10.1016/j.bone.2009.09.014. Epub 2009 Sep 18.

Christakos, S. (2012). "Mechanism of action of 1,25-dihydroxyvitamin D3 on intestinal calcium absorption." Rev Endocr Metab Disord **13**(1): 39-44.

Chung, D. J., C. H. Castro, M. Watkins, J. P. Stains, M. Y. Chung, V. L. Szejnfeld, K. Willecke, M. Theis and R. Civitelli (2006). "Low peak bone mass and attenuated anabolic response to parathyroid hormone in mice with an osteoblast-specific deletion of connexin43." J Cell Sci **119**(Pt 20): 4187-4198.

Cipriani, C., C. Capriani, D. Irani and J. P. Bilezikian (2012). "Safety of osteoanabolic therapy: a decade of experience." J Bone Miner Res **27**(12): 2419-2428.

Consortium, M. E., J. A. Stamatoyannopoulos, M. Snyder, R. Hardison, B. Ren, T. Gingeras, D. M. Gilbert, M. Groudine, M. Bender, R. Kaul, T. Canfield, E. Giste, A. Johnson, M. Zhang, G. Balasundaram, R. Byron, V. Roach, P. J. Sabo, R. Sandstrom, A. S. Stehling, R. E. Thurman, S. M. Weissman, P. Cayting, M. Hariharan, J. Lian, Y. Cheng, S. G. Landt, Z. Ma, B. J. Wold, J. Dekker, G. E. Crawford, C. A. Keller, W. Wu, C. Morrissey, S. A. Kumar, T. Mishra, D. Jain, M. Byrska-Bishop, D. Blankenberg, B. R. Lajoie1, G. Jain, A. Sanyal, K.-B. Chen, O. Denas, J. Taylor, G. A. Blobel, M. J. Weiss, M.

Pimkin, W. Deng, G. K. Marinov, B. A. Williams, K. I. Fisher-Aylor, G. Desalvo, A. Kiralusha, D. Trout, H. Amrhein, A. Mortazavi, L. Edsall, D. McCleary, S. Kuan, Y. Shen, F. Yue, Z. Ye, C. A. Davis, C. Zaleski, S. Jha, C. Xue, A. Dobin, W. Lin, M. Fastuca, H. Wang, R. Guigo, S. Djebali, J. Lagarde, T. Ryba, T. Sasaki, V. S. Malladi, M. S. Cline, V. M. Kirkup, K. Learned, K. R. Rosenbloom, W. J. Kent, E. A. Feingold, P. J. Good, M. Pazin, R. F. Lowdon and L. B. Adams (2012). "An encyclopedia of mouse DNA elements (Mouse ENCODE)." Genome Biol **13**(8): 418.

Cosman, F., E. F. Eriksen, C. Recknor, P. D. Miller, N. Guanabens, C. Kasperk, P. Papanastasiou, A. Readie, H. Rao, J. A. Gasser, C. Bucci-Rechtweg and S. Boonen (2011). "Effects of intravenous zoledronic acid plus subcutaneous teriparatide [rhPTH(1-34)] in postmenopausal osteoporosis." J Bone Miner Res **26**(3): 503-511.

Cusano, N. E. and J. P. Bilezikian Combination antiresorptive and osteoanabolic therapy for osteoporosis: we are not there yet, Curr Med Res Opin. 2011 Sep;27(9):1705-7. doi: 10.1185/03007995.2011.599837. Epub 2011 Jul 11.

Cusano, N. E. and J. P. Bilezikian (2010). "Teriparatide: Variations on the theme of a 2-year therapeutic course." IBMS BoneKEy **7**(2): 84-87.

D'Alonzo, R. C., N. Selvamurugan, G. Karsenty and N. C. Partridge (2002). "Physical interaction of the activator protein-1 factors c-Fos and c-Jun with Cbfa1 for collagenase-3 promoter activation." J Biol Chem **277**(1): 816-822.

Delmas, P. D., A. A. Licata, J. Y. Reginster, G. G. Crans, P. Chen, D. A. Misurski, R. B. Wagman and B. H. Mitlak (2006). "Fracture risk reduction during treatment with teriparatide is independent of pretreatment bone turnover." Bone **39**(2): 237-243.

Dempster, D. W., J. E. Compston, M. K. Drezner, F. H. Glorieux, J. A. Kanis, H. Malluche, P. J. Meunier, S. M. Ott, R. R. Recker and A. M. Parfitt (2013). "Standardized nomenclature, symbols, and units for bone histomorphometry: A 2012 update of the report of the ASBMR Histomorphometry Nomenclature Committee." Journal of Bone and Mineral Research **28**(1): 2-17.

Dhillon, R. S., C. Xie, W. Tyler, L. M. Calvi, H. A. Awad, M. J. Zuscik, R. J. O'Keefe and E. M. Schwarz (2013). "PTH-enhanced structural allograft healing is associated with decreased angiopoietin-2-mediated arteriogenesis, mast cell accumulation, and fibrosis." J Bone Miner Res **28**(3): 586-597.

Di Gregorio, G. B., M. Yamamoto, A. A. Ali, E. Abe, P. Roberson, S. C. Manolagas and R. L. Jilka (2001). "Attenuation of the self-renewal of transit-amplifying osteoblast progenitors in the murine bone marrow by 17 beta-estradiol." J Clin Invest **107**(7): 803-812.

Ding, M. and I. Hvid (2000). "Quantification of age-related changes in the structure model type and trabecular thickness of human tibial cancellous bone." Bone **26**(3): 291-295.

Dobnig, H. and R. T. Turner (1995). "Evidence that intermittent treatment with parathyroid hormone increases bone formation in adult rats by activation of bone lining cells." Endocrinology **136**(8): 3632-3638.

Eijken, M., M. Koedam, M. van Driel, C. J. Buurman, H. A. P. Pols and J. P. T. M. van Leeuwen (2006). "The essential role of glucocorticoids for proper human osteoblast differentiation and matrix mineralization." Molecular and Cellular Endocrinology **248**(1-2): 87-93.

Elis, S., H. W. Courtland, Y. Wu, J. C. Fritton, H. Sun, C. J. Rosen and S. Yakar (2010). "Elevated serum IGF-1 levels synergize PTH action on the skeleton only when the tissue IGF-1 axis is intact." J Bone Miner Res **25**(9): 2051-2058.

Feister, H. A., K. Torrungruang, P. Thunyakitpisal, G. E. Parker, S. J. Rhodes and J. P. Bidwell (2000). "NP/NMP4 transcription factors have distinct osteoblast nuclear matrix subdomains." J Cell Biochem **79**(3): 506-517.

Finkelstein, J. S., J. J. Wyland, H. Lee and R. M. Neer (2010). "Effects of teriparatide, alendronate, or both in women with postmenopausal osteoporosis." J Clin Endocrinol Metab **95**(4): 1838-1845.

Fu, Q., R. L. Jilka, S. C. Manolagas and C. A. O'Brien (2002). "Parathyroid hormone stimulates receptor activator of NFkappa B ligand and inhibits osteoprotegerin expression via protein kinase A activation of cAMP-response element-binding protein." J Biol Chem **277**(50): 48868-48875.

Galli, C., Q. Fu, W. Wang, B. R. Olsen, S. C. Manolagas, R. L. Jilka and C. A. O'Brien (2009). "Commitment to the osteoblast lineage is not required for RANKL gene expression." J Biol Chem **284**(19): 12654-12662.

Gao, B., Q. Huang, Y.-S. Lin, B.-Y. Wei, Y.-S. Guo, Z. Sun, L. Wang, J. Fan, H.-Y. Zhang, Y.-H. Han, X.-J. Li, J. Shi, J. Liu, L. Yang and Z.-J. Luo (2014). "Dose-dependent effect of estrogen suppresses the osteo-adipogenic transdifferentiation of osteoblasts via canonical Wnt signaling pathway." PLoS One **9**(6): e99137.

Garnero, P., E. Sornay-Rendu, M.-C. Chapuy and P. D. Delmas (1996). "Increased bone turnover in late postmenopausal women is a major determinant of osteoporosis." Journal of Bone and Mineral Research **11**(3): 337-349.

Girasole, G., R. L. Jilka, G. Passeri, S. Boswell, G. Boder, D. C. Williams and S. C. Manolagas (1992). "17 beta-estradiol inhibits interleukin-6 production by bone marrow-derived stromal cells and osteoblasts in vitro: a potential mechanism for the antiosteoporotic effect of estrogens." J Clin Invest **89**(3): 883-891.

Goltzman, D. (2008). "Studies on the mechanisms of the skeletal anabolic action of endogenous and exogenous parathyroid hormone." Archives of Biochemistry and Biophysics **473**(2): 218-224.

Goossens, K., M. Van Poucke, A. Van Soom, J. Vandesompele, A. Van Zeveren and L. J. Peelman (2005). "Selection of reference genes for quantitative real-time PCR in bovine preimplantation embryos." BMC Dev Biol **5**: 27.

Guo, Y., S. Mahony and D. K. Gifford (2012). "High resolution genome wide binding event finding and motif discovery reveals transcription factor spatial binding constraints." PLoS Comput Biol **8**(8): e1002638.

Haÿ E, D. F., Marty C, Marie P (2013). "N-cadherin governs age-related osteoprogenitor cell determination in mice through modulation of Wnt5a and Wnt10b." Presented at the European Calcified Tissue Society Congress, Lisbon, Portugal **1**(PP180).

Hall, J. M. and D. P. McDonnell (1999). "The Estrogen Receptor β -Isoform (ER β) of the Human Estrogen Receptor Modulates ER α Transcriptional Activity and Is a Key Regulator of the Cellular Response to Estrogens and Antiestrogens." Endocrinology **140**(12): 5566-5578.

Hamidouche, Z., E. Haÿ, P. Vaudin, P. Charbord, R. Schüle, P. J. Marie and O. Fromigüé (2008). "FHL2 mediates dexamethasone-induced mesenchymal cell differentiation into osteoblasts by activating Wnt/ β -catenin signaling-dependent Runx2 expression." The FASEB Journal **22**(11): 3813-3822.

Harada A, O. S., Konno D, Odawara, Yoshimi T, Yoshimura S, Kumamaru H, Saiwai H, Tsubota T, Kurumizaka H, Akashi K, Tachibana T, Imbalzano A, Ohkawa Y (2012). "Chd2 interacts with H3.3 to determine myogenic cell fate." EMBO J **31**(13): 2994-3007.

He, Y., P. Childress, M. Hood, Jr., M. Alvarez, M. A. Kacena, M. Hanlon, B. McKee, J. P. Bidwell and F. C. Yang (2013). "Nmp4/CIZ suppresses the parathyroid hormone anabolic window by restricting mesenchymal stem cell and osteoprogenitor frequency." Stem Cells Dev **22**(3): 492-500.

Herndler-Brandstetter, D., K. Landgraf, B. Jenewein, A. Tzankov, R. Brunauer, S. Brunner, W. Parson, F. Kloss, R. Gassner, G. Lepperdinger and B. Grubeck-Loebenstein (2011).

"Human bone marrow hosts polyfunctional memory CD4+ and CD8+ T cells with close contact to IL-15-producing cells." J Immunol **186**(12): 6965-6971.

Hino, K., T. Nakamoto, A. Nifuji, M. Morinobu, H. Yamamoto, Y. Ezura and M. Noda (2007). "Deficiency of Clz, a nucleocytoplasmic shuttling protein, prevents unloading-induced bone loss through the enhancement of osteoblastic bone formation in vivo." Bone **40**(4): 852-860.

Hodge, J. M., M. A. Kirkland, C. J. Aitken, C. M. Waugh, D. E. Myers, C. M. Lopez, B. E. Adams and G. C. Nicholson (2004). "Osteoclastic potential of human CFU-GM: biphasic effect of GM-CSF." J Bone Miner Res **19**(2): 190-199.

Hodsman, A. B. B., Douglas C; Dempster David W; Dian, Larry; Hanley, David A; Harris, Steven T; Kendler David L; McClung, Michael R; Miller, Paul D; Olszynski Wojciech P; Orwoll, Eric; Yen, Chui Kin (2005). "Parathyroid Hormone and Teriparatide for the Treatment of Osteoporosis: A Review of the Evidence and Suggested Guidelines for Its Use." Endocr Rev **26**(5): 688-703.

Hofbauer, L. C., S. Khosla, C. R. Dunstan, D. L. Lacey, T. C. Spelsberg and B. L. Riggs (1999). "Estrogen Stimulates Gene Expression and Protein Production of Osteoprotegerin in Human Osteoblastic Cells*." Endocrinology **140**(9): 4367-4370.

Hruska, K. A., D. Moskowitz, P. Esbrit, R. Civitelli, S. Westbrook and M. Huskey (1987). "Stimulation of inositol trisphosphate and diacylglycerol production in renal tubular cells by parathyroid hormone." J Clin Invest **79**(1): 230-239.

Huang, D. W., B. T. Sherman and R. A. Lempicki (2009). "Systematic and integrative analysis of large gene lists using DAVID bioinformatics resources." Nat Protoc **4**(1): 44-57.

Iida-Klein, A., H. Zhou, S. S. Lu, L. R. Levine, M. Ducayen-Knowles, D. W. Dempster, J. Nieves and R. Lindsay (2002). "Anabolic action of parathyroid hormone is skeletal site specific at the tissue and cellular levels in mice." J Bone Miner Res **17**(5): 808-816.

Isern, J., B. Martín-Antonio, R. Ghazanfari, Ana M. Martín, Juan A. López, R. del Toro, A. Sánchez-Aguilera, L. Arranz, D. Martín-Pérez, M. Suárez-Lledó, P. Marín, M. Van Pel, Willem E. Fibbe, J. Vázquez, S. Scheduling, Á. Urbano-Ispizúa and S. Méndez-Ferrer "Self-Renewing Human Bone Marrow Mesenspheres Promote Hematopoietic Stem Cell Expansion." Cell Reports **3**(5): 1714-1724.

Isogai, Y., T. Akatsu, T. Ishizuya, A. Yamaguchi, M. Hori, N. Takahashi and T. Suda (1996). "Parathyroid hormone regulates osteoblast differentiation positively or negatively depending on the differentiation stages." J Bone Miner Res **11**(10): 1384-1393.

Jiang, Y., J. J. Zhao, B. H. Mitlak, O. Wang, H. K. Genant and E. F. Eriksen (2003). "Recombinant human parathyroid hormone (1-34) [teriparatide] improves both cortical and cancellous bone structure." J Bone Miner Res **18**(11): 1932-1941.

Jilka, R. L. (2007). "Molecular and cellular mechanisms of the anabolic effect of intermittent PTH." Bone **40**(6): 1434-1446.

Jilka, R. L., R. S. Weinstein, T. Bellido, P. Roberson, A. M. Parfitt and S. C. Manolagas (1999). "Increased bone formation by prevention of osteoblast apoptosis with parathyroid hormone." J Clin Invest **104**(4): 439-446.

Jimi, E., I. Nakamura, T. Ikebe, S. Akiyama, N. Takahashi and T. Suda (1998). "Activation of NF- κ B Is Involved in the Survival of Osteoclasts Promoted by Interleukin-1." Journal of Biological Chemistry **273**(15): 8799-8805.

Juppner, H., A. B. Abou-Samra, M. Freeman, X. F. Kong, E. Schipani, J. Richards, L. F. Kolakowski, Jr., J. Hock, J. T. Potts, Jr., H. M. Kronenberg and et al. (1991). "A G protein-linked receptor for parathyroid hormone and parathyroid hormone-related peptide." Science **254**(5034): 1024-1026.

Kameda, T., H. Mano, T. Yuasa, Y. Mori, K. Miyazawa, M. Shiokawa, Y. Nakamaru, E. Hiroi, K. Hiura, A. Kameda, N. N. Yang, Y. Hakeda and M. Kumegawa (1997). "Estrogen inhibits bone resorption by directly inducing apoptosis of the bone-resorbing osteoclasts." J Exp Med **186**(4): 489-495.

Karreth, F., A. Hoebertz, H. Scheuch, R. Eferl and E. F. Wagner (2004). "The AP1 transcription factor Fra2 is required for efficient cartilage development." Development **131**(22): 5717-5725.

Keaveny, T. M., P. F. Hoffmann, M. Singh, L. Palermo, J. P. Bilezikian, S. L. Greenspan and D. M. Black (2008). "Femoral bone strength and its relation to cortical and trabecular changes after treatment with PTH, alendronate, and their combination as assessed by finite element analysis of quantitative CT scans." J Bone Miner Res **23**(12): 1974-1982.

Keller, H. and M. Kneissel (2005). "SOST is a target gene for PTH in bone." Bone **37**(2): 148-158.

Koh, A. J., B. Demiralp, K. G. Neiva, J. Hooten, R. M. Nohutcu, H. Shim, N. S. Datta, R. S. Taichman and L. K. McCauley (2005). "Cells of the osteoclast lineage as mediators of the anabolic actions of parathyroid hormone in bone." Endocrinology **146**(11): 4584-4596.

Kousteni, S., T. Bellido, L. I. Plotkin, C. A. O'Brien, D. L. Bodenner, L. Han, K. Han, G. B. DiGregorio, J. A. Katzenellenbogen, B. S. Katzenellenbogen, P. K. Roberson, R. S. Weinstein, R. L. Jilka and S. C. Manolagas (2001). "Nongenotropic, Sex-Nonspecific Signaling through the Estrogen or Androgen Receptors: Dissociation from Transcriptional Activity." Cell **104**(5): 719-730.

Kousteni, S., J.-R. Chen, T. Bellido, L. Han, A. A. Ali, C. A. O'Brien, L. Plotkin, Q. Fu, A. T. Mancino, Y. Wen, A. M. Vertino, C. C. Powers, S. A. Stewart, R. Ebert, A. M. Parfitt, R. S. Weinstein, R. L. Jilka and S. C. Manolagas (2002). "Reversal of Bone Loss in Mice by Nongenotropic Signaling of Sex Steroids." Science **298**(5594): 843-846.

Kraenzlin, M. E. and C. Meier (2011). "Parathyroid hormone analogues in the treatment of osteoporosis." Nat Rev Endocrinol **7**(11): 647-656.

Kramer, I., G. G. Loots, A. Studer, H. Keller and M. Kneissel (2010). "Parathyroid hormone (PTH)-induced bone gain is blunted in SOST overexpressing and deficient mice." J Bone Miner Res **25**(2): 178-189.

Krane, S. M. (2005). "Identifying genes that regulate bone remodeling as potential therapeutic targets." J Exp Med **201**(6): 841-843.

Krum, S. A., G. A. Miranda-Carboni, P. V. Hauschka, J. S. Carroll, T. F. Lane, L. P. Freedman and M. Brown (2008). "Estrogen protects bone by inducing Fas ligand in osteoblasts to regulate osteoclast survival." EMBO J **27**(3): 535-545.

Kular, J., J. Tickner, S. M. Chim and J. Xu (2012). "An overview of the regulation of bone remodelling at the cellular level." Clin Biochem **45**(12): 863-873.

Kusumbe, A. P., S. K. Ramasamy and R. H. Adams (2014). "Coupling of angiogenesis and osteogenesis by a specific vessel subtype in bone." Nature **507**(7492): 323-328.

Langenbach, F. and J. Handschel (2013). "Effects of dexamethasone, ascorbic acid and beta-glycerophosphate on the osteogenic differentiation of stem cells in vitro." Stem Cell Research & Therapy **4**(5): 117.

Li, H. and R. Durbin (2009). "Fast and accurate short read alignment with Burrows-Wheeler transform." Bioinformatics **25**(14): 1754-1760.

Li, H. and R. Durbin (2010). "Fast and accurate long-read alignment with Burrows-Wheeler transform." Bioinformatics **26**(5): 589-595.

Li, J.-Y., L. D. Walker, A. M. Tyagi, J. Adams, M. N. Weitzmann and R. Pacifici (2014). "The sclerostin-independent bone anabolic activity of intermittent PTH treatment is mediated by T-cell-produced Wnt10b." J Bone Miner Res **29**(1): 43-54.

Li, X., L. Qin, M. Bergenstock, L. M. Bevelock, D. V. Novack and N. C. Partridge (2007). "Parathyroid hormone stimulates osteoblastic expression of MCP-1 to recruit and increase the fusion of pre/osteoclasts." J Biol Chem **282**(45): 33098-33106.

Liang, J. D., J. M. Hock, G. E. Sandusky, R. F. Santerre and J. E. Onyia (1999). "Immunohistochemical localization of selected early response genes expressed in trabecular bone of young rats given hPTH 1-34." Calcif Tissue Int **65**(5): 369-373.

Lin, W., G. Srajer, Y. A. Evrard, H. M. Phan, Y. Furuta and S. Y. R. Dent (2007). "Developmental potential of Gcn5^{-/-} embryonic stem cells in vivo and in vitro." Developmental Dynamics **236**(6): 1547-1557.

Liu, H., K. Michaud, S. Nayak, D. B. Karpf, D. K. Owens and A. M. Garber (2006). "The cost-effectiveness of therapy with teriparatide and alendronate in women with severe osteoporosis." Arch Intern Med **166**(11): 1209-1217.

Luiz de Freitas, P. H., M. Li, T. Ninomiya, M. Nakamura, S. Ubaidus, K. Oda, N. Udagawa, T. Maeda, R. Takagi and N. Amizuka (2009). "Intermittent PTH administration stimulates pre-osteoblastic proliferation without leading to enhanced bone formation in osteoclast-less c-fos^(-/-) mice." J Bone Miner Res **24**(9): 1586-1597.

Ma, Y. L., Q. Q. Zeng, A. Y. Chiang, D. Burr, J. Li, H. Dobnig, A. Fahrleitner-Pammer, D. Michalská, F. Marin, I. Pavo and J. J. Stepan (2014). "Effects of teriparatide on cortical histomorphometric variables in postmenopausal women with or without prior alendronate treatment." Bone **59**: 139-147.

Marie, P. J. (2008). "Transcription factors controlling osteoblastogenesis." Arch Biochem Biophys **473**(2): 98-105.

Mazo, I. B., M. Honczarenko, H. Leung, L. L. Cavanagh, R. Bonasio, W. Weninger, K. Engelke, L. Xia, R. P. McEver, P. A. Koni, L. E. Silberstein and U. H. von Andrian (2005). "Bone marrow is a major reservoir and site of recruitment for central memory CD8⁺ T cells." Immunity **22**(2): 259-270.

McClung, M. R., A. Grauer, S. Boonen, M. A. Bolognese, J. P. Brown, A. Diez-Perez, B. L. Langdahl, J.-Y. Reginster, J. R. Zanchetta, S. M. Wasserman, L. Katz, J. Maddox, Y.-C. Yang, C. Libanati and H. G. Bone (2014). "Romosozumab in Postmenopausal Women with Low Bone Mineral Density." New England Journal of Medicine **370**(5): 412-420.

Menea, C., N. Kurihara and G. D. Roodman (2000). "CFU-GM-Derived Cells Form Osteoclasts at a Very High Efficiency." Biochemical and Biophysical Research Communications **267**(3): 943-946.

Menea, C., N. Kurihara and G. D. Roodman (2000). "CFU-GM-derived cells form osteoclasts at a very high efficiency." Biochem Biophys Res Commun **267**(3): 943-946.

Méndez-Ferrer, S., T. V. Michurina, F. Ferraro, A. R. Mazloom, B. D. Macarthur, S. A. Lira, D. T. Scadden, A. Ma'ayan, G. N. Enikolopov and P. S. Frenette (2010). "Mesenchymal and haematopoietic stem cells form a unique bone marrow niche." Nature **466**(7308): 829-834.

Mitlak, B. H. (2002). "Parathyroid hormone as a therapeutic agent." Curr Opin Pharmacol **2**(6): 694-699.

Mizoguchi, T., S. Pinho, J. Ahmed, Y. Kunisaki, M. Hanoun, A. Mendelson, N. Ono, H. M. Kronenberg and P. S. Frenette (2014). "Osterix marks distinct waves of primitive and definitive stromal progenitors during bone marrow development." Dev Cell **29**(3): 340-349.

Morinobu, M., T. Nakamoto, K. Hino, K. Tsuji, Z. J. Shen, K. Nakashima, A. Nifuji, H. Yamamoto, H. Hirai and M. Noda (2005). "The nucleocytoplasmic shuttling protein CIZ reduces adult bone mass by inhibiting bone morphogenetic protein-induced bone formation." J Exp Med **201**(6): 961-970.

Mukherjee, A., E. M. Wilson and P. Rotwein (2010). "Selective signaling by Akt2 promotes bone morphogenetic protein 2-mediated osteoblast differentiation." Mol Cell Biol **30**(4): 1018-1027.

Murray, T. M., L. G. Rao, P. Divieti and F. R. Bringhurst (2005). "Parathyroid hormone secretion and action: evidence for discrete receptors for the carboxyl-terminal region and related biological actions of carboxyl-terminal ligands." Endocr Rev **26**(1): 78-113.

Nakamoto, T., A. Shiratsuchi, H. Oda, K. Inoue, T. Matsumura, M. Ichikawa, T. Saito, S. Seo, K. Maki, T. Asai, T. Suzuki, A. Hangaishi, T. Yamagata, S. Aizawa, M. Noda, Y. Nakanishi and H. Hirai (2004). "Impaired spermatogenesis and male fertility defects in CIZ/Nmp4-disrupted mice." Genes Cells **9**(6): 575-589.

Nakamoto, T., T. Yamagata, R. Sakai, S. Ogawa, H. Honda, H. Ueno, N. Hirano, Y. Yazaki and H. Hirai (2000). "CIZ, a zinc finger protein that interacts with p130(cas) and activates the expression of matrix metalloproteinases." Mol Cell Biol **20**(5): 1649-1658.

Nascimento, E. M., C. L. Cox, S. MacArthur, S. Hussain, M. Trotter, S. Blanco, M. Suraj, J. Nichols, B. Kubler, S. A. Benitah, B. Hendrich, D. T. Odom and M. Frye (2011). "The opposing transcriptional functions of Sin3a and c-Myc are required to maintain tissue homeostasis." Nat Cell Biol **13**(12): 1395-1405.

Negishi-Koga, T. and H. Takayanagi (2009). "Ca²⁺-NFATc1 signaling is an essential axis of osteoclast differentiation." Immunol Rev **231**(1): 241-256.

Nervina, J. M., C. E. Magyar, F. Q. Pirih and S. Tetradis (2006). "PGC-1alpha is induced by parathyroid hormone and coactivates Nurr1-mediated promoter activity in osteoblasts." Bone **39**(5): 1018-1025.

Nishida, S., N. Endo, H. Yamagiwa, T. Tanizawa and H. E. Takahashi (1999). "Number of osteoprogenitor cells in human bone marrow markedly decreases after skeletal maturation." J Bone Miner Metab **17**(3): 171-177.

Nishida, S., A. Yamaguchi, T. Tanizawa, N. Endo, T. Mashiba, Y. Uchiyama, T. Suda, S. Yoshiki and H. E. Takahashi (1994). "Increased bone formation by intermittent parathyroid hormone administration is due to the stimulation of proliferation and differentiation of osteoprogenitor cells in bone marrow." Bone **15**(6): 717-723.

Niziolek, P. J., S. Murthy, S. N. Ellis, K. B. Sukhija, T. A. Hornberger, C. H. Turner and A. G. Robling (2009). "Rapamycin impairs trabecular bone acquisition from high-dose but not low-dose intermittent parathyroid hormone treatment." J Cell Physiol **221**(3): 579-585.

O'Brien, C. A., L. I. Plotkin, C. Galli, J. J. Goellner, A. R. Gortazar, M. R. Allen, A. G. Robling, M. Bouxsein, E. Schipani, C. H. Turner, R. L. Jilka, R. S. Weinstein, S. C. Manolagas and T. Bellido (2008). "Control of bone mass and remodeling by PTH receptor signaling in osteocytes." PLoS One **3**(8): e2942.

Okazaki, R., D. Inoue, M. Shibata, M. Saika, S. Kido, H. Ooka, H. Tomiyama, Y. Sakamoto and T. Matsumoto (2002). "Estrogen promotes early osteoblast differentiation and inhibits adipocyte differentiation in mouse bone marrow stromal cell lines that express estrogen receptor (ER) alpha or beta." Endocrinology **143**(6): 2349-2356.

Onyia, J. E., B. Miller, J. Hulman, J. Liang, R. Galvin, C. Frolik, S. Chandrasekhar, A. K. Harvey, J. Bidwell, J. Herring and J. M. Hock (1997). "Proliferating cells in the primary spongiosa express osteoblastic phenotype in vitro." Bone **20**(2): 93-100.

Owen, M. and A. J. Friedenstein (1988). "Stromal stem cells: marrow-derived osteogenic precursors." Ciba Found Symp **136**: 42-60.

Pacifici, R. (1996). "Estrogen, cytokines, and pathogenesis of postmenopausal osteoporosis." J Bone Miner Res **11**(8): 1043-1051.

Pacifici, R. (2010). "The immune system and bone." Arch Biochem Biophys **503**(1): 41-53.

Padhi, D., G. Jang, B. Stouch, L. Fang and E. Posvar (2011). "Single-dose, placebo-controlled, randomized study of AMG 785, a sclerostin monoclonal antibody." Journal of Bone and Mineral Research **26**(1): 19-26.

Park, D., J. A. Spencer, B. I. Koh, T. Kobayashi, J. Fujisaki, T. L. Clemens, C. P. Lin, H. M. Kronenberg and D. T. Scadden (2012). "Endogenous bone marrow MSCs are dynamic, fate-restricted participants in bone maintenance and regeneration." Cell Stem Cell **10**(3): 259-272.

Pei, W., C. G. Bellows, Y. Jia and J. N. M. Heersche (2006). "Effect of age on progesterone receptor expression, and osteoprogenitor proliferation and differentiation in female rat vertebral cell populations." Journal of Endocrinology **190**(2): 261-270.

Philip, B. K., P. J. Childress, A. G. Robling, A. Heller, P. P. Nawroth, A. Bierhaus and J. P. Bidwell (2010). "RAGE supports parathyroid hormone-induced gains in femoral trabecular bone." Am J Physiol Endocrinol Metab **298**(3): E714-725.

Pignolo, R. J. and M. Kassem (2011). "Circulating osteogenic cells: implications for injury, repair, and regeneration." J Bone Miner Res **26**(8): 1685-1693.

Pirro, M., C. Leli, G. Fabbriciani, M. R. Manfredelli, L. Callarelli, F. Bagaglia, A. M. Scarponi and E. Mannarino (2010). "Association between circulating osteoprogenitor cell numbers and bone mineral density in postmenopausal osteoporosis." Osteoporos Int **21**(2): 297-306.

Qin, L., X. Li, J.-K. Ko and N. C. Partridge (2005). "Parathyroid hormone uses multiple mechanisms to arrest the cell cycle progression of osteoblastic cells from G1 to S phase." J Biol Chem **280**(4): 3104-3111.

Qin, L., L. J. Raggatt and N. C. Partridge (2004). "Parathyroid hormone: a double-edged sword for bone metabolism." Trends Endocrinol Metab **15**(2): 60-65.

Qin, L., J. Tamasi, L. Raggatt, X. Li, J. H. M. Feyen, D. C. Lee, E. Dicicco-Bloom and N. C. Partridge (2005). "Amphiregulin is a novel growth factor involved in normal bone development and in the cellular response to parathyroid hormone stimulation." J Biol Chem **280**(5): 3974-3981.

Rhee, Y., E.-Y. Lee, V. Lezcano, A. C. Ronda, K. W. Condon, M. R. Allen, L. I. Plotkin and T. Bellido (2013). "Resorption controls bone anabolism driven by parathyroid hormone (PTH) receptor signaling in osteocytes." J Biol Chem **288**(41): 29809-29820.

Riggs, B. L. and A. M. Parfitt (2005). "Drugs used to treat osteoporosis: the critical need for a uniform nomenclature based on their action on bone remodeling." J Bone Miner Res **20**(2): 177-184.

Robling, A. G., P. Childress, J. Yu, J. Cotte, A. Heller, B. K. Philip and J. P. Bidwell (2009). "Nmp4/CIZ suppresses parathyroid hormone-induced increases in trabecular bone." J Cell Physiol **219**(3): 734-743.

Saag, K. G., J. R. Zanchetta, J. P. Devogelaer, R. A. Adler, R. Eastell, K. See, J. H. Krege, K. Krohn and M. R. Warner (2009). "Effects of teriparatide versus alendronate for treating glucocorticoid-induced osteoporosis: thirty-six-month results of a randomized, double-blind, controlled trial." Arthritis Rheum **60**(11): 3346-3355.

Sacchetti, B., A. Funari, S. Michienzi, S. Di Cesare, S. Piersanti, I. Saggio, E. Tagliafico, S. Ferrari, P. G. Robey, M. Riminucci and P. Bianco (2007). "Self-renewing osteoprogenitors in bone marrow sinusoids can organize a hematopoietic microenvironment." Cell **131**(2): 324-336.

Saini, V., D. A. Marengi, K. J. Barry, K. S. Fulzele, E. Heiden, X. Liu, C. Dedic, A. Maeda, S. Lotinun, R. Baron and P. D. Pajevic (2013). "Parathyroid hormone (PTH)/PTH-related peptide type 1 receptor (PPR) signaling in osteocytes regulates anabolic and catabolic skeletal responses to PTH." J Biol Chem **288**(28): 20122-20134.

Satija, N. K., G. U. Gurudutta, S. Sharma, F. Afrin, P. Gupta, Y. K. Verma, V. K. Singh and R. P. Tripathi (2007). "Mesenchymal stem cells: molecular targets for tissue engineering." Stem Cells Dev **16**(1): 7-23.

Selye, H. (1932). "ON THE STIMULATION OF NEW BONE-FORMATION WITH PARATHYROID EXTRACT AND IRRADIATED ERGOSTEROL." Endocrinology **16**(5): 547-558.

Sethe, S., A. Scutt and A. Stolzing (2006). "Aging of mesenchymal stem cells." Ageing Res Rev **5**(1): 91-116.

Shah, R., M. Alvarez, D. R. Jones, K. Torrungruang, A. J. Watt, N. Selvamurugan, N. C. Partridge, C. O. Quinn, F. M. Pavalko, S. J. Rhodes and J. P. Bidwell (2004). "Nmp4/CIZ regulation of matrix metalloproteinase 13 (MMP-13) response to parathyroid hormone in osteoblasts." Am J Physiol Endocrinol Metab **287**(2): 16.

Shah, R., M. Alvarez, D. R. Jones, K. Torrungruang, A. J. Watt, N. Selvamurugan, N. C. Partridge, C. O. Quinn, F. M. Pavalko, S. J. Rhodes and J. P. Bidwell (2004). "Nmp4/CIZ regulation of matrix metalloproteinase 13 (MMP-13) response to parathyroid hormone in osteoblasts." Am J Physiol Endocrinol Metab **287**(2): E289-296.

Shen, Z.-J., T. Nakamoto, K. Tsuji, A. Nifuji, K. Miyazono, T. Komori, H. Hirai and M. Noda (2002). "Negative regulation of bone morphogenetic protein/Smad signaling by Cas-interacting zinc finger protein in osteoblasts." J Biol Chem **277**(33): 29840-29846.

Shen, Z. J., T. Nakamoto, K. Tsuji, A. Nifuji, K. Miyazono, T. Komori, H. Hirai and M. Noda (2002). "Negative regulation of bone morphogenetic protein/Smad signaling by Cas-interacting zinc finger protein in osteoblasts." J Biol Chem **277**(33): 29840-29846.

Silverman, S. and C. Christiansen (2012). "Individualizing osteoporosis therapy." Osteoporos Int **23**(3): 797-809.

Stein, B. and M. X. Yang (1995). "Repression of the interleukin-6 promoter by estrogen receptor is mediated by NF-kappa B and C/EBP beta." Mol Cell Biol **15**(9): 4971-4979.

Stroup, J., M. P. Kane and A. M. Abu-Baker (2008). "Teriparatide in the treatment of osteoporosis." Am J Health Syst Pharm **65**(6): 532-539.

Sudo, H., H. A. Kodama, Y. Amagai, S. Yamamoto and S. Kasai (1983). "In vitro differentiation and calcification in a new clonal osteogenic cell line derived from newborn mouse calvaria." J Cell Biol **96**(1): 191-198.

Sun, H., J. K. Kim, R. Mortensen, L. P. Mutyaba, K. D. Hankenson and P. H. Krebsbach (2013). "Osteoblast-targeted suppression of PPAR γ increases osteogenesis through activation of mTOR signaling." Stem Cells **31**(10): 2183-2192.

Supek, F., M. Bošnjak, N. Škunca and T. Šmuc (2011). "REVIGO summarizes and visualizes long lists of gene ontology terms." PLoS One **6**(7): e21800.

Syed, F. A., M. J. Oursler, T. E. Hefferan, J. M. Peterson, B. L. Riggs and S. Khosla (2008). "Effects of estrogen therapy on bone marrow adipocytes in postmenopausal osteoporotic women." Osteoporos Int **19**(9): 1323-1330.

Tahimic, C. G. T., Y. Wang and D. D. Bikle (2013). "Anabolic effects of IGF-1 signaling on the skeleton." Front Endocrinol (Lausanne) **4**: 6.

Takayanagi, H. (2007). "The role of NFAT in osteoclast formation." Ann N Y Acad Sci **1116**: 227-237.

Takayanagi, H., S. Kim, K. Matsuo, H. Suzuki, T. Suzuki, K. Sato, T. Yokochi, H. Oda, K. Nakamura, N. Ida, E. F. Wagner and T. Taniguchi (2002). "RANKL maintains bone homeostasis through c-Fos-dependent induction of interferon-beta." Nature **416**(6882): 744-749.

Tanaka, S., M. Amling, L. Neff, A. Peyman, E. Uhlmann, J. B. Levy and R. Baron (1996). "c-Cbl is downstream of c-Src in a signalling pathway necessary for bone resorption." Nature **383**(6600): 528-531.

Tella, S. H. and J. C. Gallagher (2014). "Prevention and treatment of postmenopausal osteoporosis." J Steroid Biochem Mol Biol **142**: 155-170.

Terauchi, M., J. Y. Li, B. Bedi, K. H. Baek, H. Tawfeek, S. Galley, L. Gilbert, M. S. Nanes, M. Zayzafoon, R. Guldborg, D. L. Lamar, M. A. Singer, T. F. Lane, H. M. Kronenberg, M. N. Weitzmann and R. Pacifici (2009). "T lymphocytes amplify the anabolic activity of parathyroid hormone through Wnt10b signaling." Cell Metab **10**(3): 229-240.

Thunyakitpisal, P., M. Alvarez, K. Tokunaga, J. E. Onyia, J. Hock, N. Ohashi, H. Feister, S. J. Rhodes and J. P. Bidwell (2001). "Cloning and functional analysis of a family of nuclear matrix transcription factors (NP/NMP4) that regulate type I collagen expression in osteoblasts." J Bone Miner Res **16**(1): 10-23.

Tobimatsu, T., H. Kaji, H. Sowa, J. Naito, L. Canaff, G. N. Hendy, T. Sugimoto and K. Chihara (2006). "Parathyroid hormone increases beta-catenin levels through Smad3 in mouse osteoblastic cells." Endocrinology **147**(5): 2583-2590.

Torrunguang, K., M. Alvarez, R. Shah, J. E. Onyia, S. J. Rhodes and J. P. Bidwell (2002). "DNA binding and gene activation properties of the Nmp4 nuclear matrix transcription factors." J Biol Chem **277**(18): 16153-16159.

Trivedi, R., R. Goswami and N. Chattopadhyay (2010). "Investigational anabolic therapies for osteoporosis." Expert Opin Investig Drugs **19**(8): 995-1005.

Turner, R. T., J. J. Vandersteenhoven and N. H. Bell (1987). "The effects of ovariectomy and 17 β -estradiol on cortical bone histomorphometry in growing rats." Journal of Bone and Mineral Research **2**(2): 115-122.

Udagawa, N., N. Takahashi, E. Jimi, K. Matsuzaki, T. Tsurukai, K. Itoh, N. Nakagawa, H. Yasuda, M. Goto, E. Tsuda, K. Higashio, M. T. Gillespie, T. J. Martin and T. Suda (1999).

"Osteoblasts/stromal cells stimulate osteoclast activation through expression of osteoclast differentiation factor/RANKL but not macrophage colony-stimulating factor: receptor activator of NF-kappa B ligand." Bone **25**(5): 517-523.

Vieira Potter, V. J., Strissel KJ, Xie C, Chang E, Bennett G, Defuria J, Obin MS, Greenberg AS (2012). "Adipose Tissue Inflammation and Reduced Insulin Sensitivity in Ovariectomized Mice Occurs in the Absence of Increased Adiposity." Endocrinology **153**(9): 4266-4277.

Wagner, E. F. (2010). "Bone development and inflammatory disease is regulated by AP-1 (Fos/Jun)." Ann Rheum Dis **69** **Suppl 1**: i86-88.

Wang, D., K. Christensen, K. Chawla, G. Xiao, P. H. Krebsbach and R. T. Franceschi (1999). "Isolation and characterization of MC3T3-E1 preosteoblast subclones with distinct in vitro and in vivo differentiation/mineralization potential." J Bone Miner Res **14**(6): 893-903.

Wang, L., Y. Zhao and S. Shi (2012). "Interplay between mesenchymal stem cells and lymphocytes: implications for immunotherapy and tissue regeneration." J Dent Res **91**(11): 1003-1010.

Wang, Y.-H., Y. Liu, K. Buhl and D. W. Rowe (2005). "Comparison of the action of transient and continuous PTH on primary osteoblast cultures expressing differentiation stage-specific GFP." J Bone Miner Res **20**(1): 5-14.

Wang, Y.-H., Y. Liu and D. W. Rowe (2007). "Effects of transient PTH on early proliferation, apoptosis, and subsequent differentiation of osteoblast in primary osteoblast cultures." Am J Physiol Endocrinol Metab **292**(2): E594-603.

Wu, X., L. Pang, W. Lei, W. Lu, J. Li, Z. Li, F. J. Frassica, X. Chen, M. Wan and X. Cao (2010). "Inhibition of Sca-1-Positive Skeletal Stem Cell Recruitment by Alendronate Blunts the Anabolic Effects of Parathyroid Hormone on Bone Remodeling." Cell Stem Cell **7**(5): 571-580.

Yang, F. C., S. Watanabe, K. Tsuji, M. J. Xu, A. Kaneko, Y. Ebihara and T. Nakahata (1998). "Human granulocyte colony-stimulating factor (G-CSF) stimulates the in vitro and in vivo development but not commitment of primitive multipotential progenitors from transgenic mice expressing the human G-CSF receptor." Blood **92**(12): 4632-4640.

Yang, Z., J. P. Bidwell, S. R. Young, R. Gerard-O'Riley, H. Wang and F. M. Pavalko (2010). "Nmp4/CIZ inhibits mechanically induced beta-catenin signaling activity in osteoblasts." J Cell Physiol **223**(2): 435-441.

Yasuda, H., N. Shima, N. Nakagawa, K. Yamaguchi, M. Kinosaki, S. Mochizuki, A. Tomoyasu, K. Yano, M. Goto, A. Murakami, E. Tsuda, T. Morinaga, K. Higashio, N. Udagawa, N. Takahashi and T. Suda (1998). "Osteoclast differentiation factor is a ligand for osteoprotegerin/osteoclastogenesis-inhibitory factor and is identical to TRANCE/RANKL." Proc Natl Acad Sci U S A **95**(7): 3597-3602.

Yu, B., X. Zhao, C. Yang, J. Crane, L. Xian, W. Lu, M. Wan and X. Cao (2012). "Parathyroid hormone induces differentiation of mesenchymal stromal/stem cells by enhancing bone morphogenetic protein signaling." J Bone Miner Res **27**(9): 2001-2014.

Yu, E. W., R. M. Neer, H. Lee, J. J. Wyland, A. V. de la Paz, M. C. Davis, M. Okazaki and J. S. Finkelstein (2011). "Time-dependent changes in skeletal response to teriparatide: escalating vs. constant dose teriparatide (PTH 1-34) in osteoporotic women." Bone **48**(4): 713-719.

Zangari, M., E. Terpos, F. Zhan and G. Tricot (2012). "Impact of bortezomib on bone health in myeloma: a review of current evidence." Cancer Treat Rev **38**(8): 968-980.

Zhang, X., L. Ding and A. J. Sandford (2005). "Selection of reference genes for gene expression studies in human neutrophils by real-time PCR." BMC Mol Biol **6**: 4.

Zhao, C., N. Irie, Y. Takada, K. Shimoda, T. Miyamoto, T. Nishiwaki, T. Suda and K. Matsuo (2006). "Bidirectional ephrinB2-EphB4 signaling controls bone homeostasis." Cell Metab **4**(2): 111-121.

Curriculum Vitae

Paul Jeffrey Childress

Education:

2010- 2014	Ph.D.	Indiana University Department of Anatomy and Cell Biology Indianapolis, IN 46202
2002-2005	MS	Indiana University Bioinformatics Indianapolis, IN 46202

Professional Experience

2014	Post-doctoral Researcher	Indiana University School of Medicine Department of Orthopaedic Surgery Indianapolis, IN 46202
2000-2011	Tissue Donor Coordinator	American Tissue Services Foundation Oklahoma City, OK 73132
1993-2000	Supervisor	American Red Cross Tissue Services Fort Wayne, IN 46201

Conferences Attended

American Society for Bone and Mineral Research Annual Meeting
Minneapolis MN – Oral Presentation, 2012
Baltimore MD – Poster Presentation, 2013
Houston TX – Poster Presentation, 2014

Clinical and Translational Science Predoctoral Meeting, 2013
Rochester, MN - Poster Presentation

Association for Clinical and Translational Science Annual Meeting, 2014
Washington DC – Poster Presentation

Publications

1. Disabling Nmp4 Amplifies PTH Skeletal Restoration Therapy Following Ovariectomy: a ChIP-Seq Defined Genome-Wide Map of Nmp4 Occupancy Reveals Pathways associated with its role in suppressing bone anabolism. (Manuscript submitted).
2. Bidwell JP, Alvarez MB, Hood M Jr, Childress P. Functional impairment of bone formation in the pathogenesis of osteoporosis: the bone marrow regenerative competence. *Curr Osteoporos Rep.* 2013 Jun;11(2):117-25. doi: 10.1007/s11914-013-0139-2. Review. PubMed PMID: 23471774.
3. He Y*, Childress P*, Hood M Jr, Alvarez M, Kacena MA, Hanlon M, McKee B, Bidwell JP, Yang FC. Nmp4/CIZ suppresses the parathyroid hormone anabolic window by restricting mesenchymal stem cell and osteoprogenitor frequency. *Stem Cells Dev.* 2013 Feb 1;22(3):492-500. doi: 10.1089/scd.2012.0308. Epub 2012 Sep 14. PubMed PMID: 22873745; PubMed Central PMCID: PMC3549622
4. Dirks RC, Galley MR, Childress PJ, Fearon AM, Scott A, Koch LG, Britton SL, Warden SJ. Uphill running does not exacerbate collagenase-induced pathological changes in the Achilles tendon of rats selectively bred for high-capacity running. *Connect Tissue Res.* 2013;54(6):386-93. doi: 10.3109/03008207.2013.848201. PubMed PMID: 24060053.
5. Alvarez MB, Childress P, Philip BK, Gerard-O'Riley R, Hanlon M, Herbert BS, Robling AG, Pavalko FM, Bidwell JP. Immortalization and characterization of osteoblast cell lines generated from wild-type and Nmp4-null mouse bone marrow stromal cells using murine telomerase reverse transcriptase (mTERT). *J Cell Physiol.* 2012 May;227(5):1873-82. doi: 10.1002/jcp.22915. PubMed PMID: 21732358; PubMed Central PMCID: PMC3209493.
6. Bidwell JP, Childress P, Alvarez MB, Hood M Jr, He Y, Pavalko FM, Kacena MA, Yang FC. Nmp4/CIZ closes the parathyroid hormone anabolic window. *Crit Rev Eukaryot Gene Expr.* 2012;22(3):205-18. Review. PubMed PMID: 23140162; PubMed Central PMCID: PMC3586259.
7. Robling AG, Kedlaya R, Ellis SN, Childress PJ, Bidwell JP, Bellido T, Turner CH. Anabolic and catabolic regimens of human parathyroid hormone 1-34 elicit bone- and envelope-specific attenuation of skeletal effects in Sost-deficient mice. *Endocrinology.* 2011 Aug;152(8):2963-75. doi: 10.1210/en.2011-0049. Epub 2011 Jun 7. PubMed PMID: 21652726; PubMed Central PMCID: PMC3138236.
8. Childress P, Philip BK, Robling AG, Bruzzaniti A, Kacena MA, Bivi N, Plotkin LI, Heller A, Bidwell JP. Nmp4/CIZ suppresses the response of bone to anabolic parathyroid hormone by regulating both osteoblasts and osteoclasts. *Calcif Tissue Int.* 2011 Jul;89(1):74-89. doi: 10.1007/s00223-011-9496-y. Epub 2011 May 24. PubMed PMID: 21607813; PubMed Central PMCID: PMC3200195.
9. Philip BK, Childress PJ, Robling AG, Heller A, Nawroth PP, Bierhaus A, Bidwell JP. RAGE supports parathyroid hormone-induced gains in femoral trabecular bone. *Am J Physiol Endocrinol Metab.* 2010 Mar;298(3):E714-25. doi: 10.1152/ajpendo.00564.2009. Epub 2009 Dec 22. PubMed PMID: 20028966; PubMed Central PMCID: PMC2838526.
10. Childress P, Robling AG, Bidwell JP. Nmp4/CIZ: road block at the intersection of PTH and load. *Bone.* 2010 Feb;46(2):259-66. doi: 10.1016/j.bone.2009.09.014. Epub 2009 Sep 18. PubMed PMID: 19766748; PubMed Central PMCID: PMC2818167.
11. Robling AG*, Childress P*, Yu J, Cotte J, Heller A, Philip BK, Bidwell JP. Nmp4/CIZ suppresses parathyroid hormone-induced increases in trabecular

bone. *J Cell Physiol.* 2009 Jun;219(3):734-43. doi: 10.1002/jcp.21717. PubMed PMID: 19189321; PubMed Central PMCID: PMC2746029.

12. Childress PJ, Fletcher RL, Perumal NB. LymphTF-DB: a database of transcription factors involved in lymphocyte development. *Genes Immun.* 2007 Jun;8(4):360-5. Epub 2007 Mar 15. PubMed PMID: 17361201.

(* co-first author)